Discontinuous Space-Time Dependent Nodal Synthesis Method for Reactor Analysis

by

Chi H. Kang

B.S. in Nuclear Engineering
University of Maryland at College Park, May 1991

S.M. in Nuclear Engineering
Massachusetts Institute of Technology, June 1993

Submitted to the Department of Nuclear Engineering
in partial fulfillment of the requirements for the degree of

DOCTOR OF SCIENCE

at the

MASSACHUSETTS INSTITUTE OF TECHNOLOGY

June 1996

Author _____
Department of Nuclear Engineering
May 16, 1996

Certified by _____
Professor Allan F. Henry
Thesis Supervisor

Certified by _____
Professor John E. Meyer
Thesis Reader

Accepted by _____
Professor Jeffrey P. Friedberg
Chairman, Departmental Committee on Graduate Students

Discontinuous Space-Time Dependent Nodal Synthesis Method for Reactor Analysis

by

Chi H. Kang

Submitted to the Department of Nuclear Engineering
on May 16, 1996, in partial fulfillment of the
requirements for the degree of
DOCTOR OF SCIENCE

ABSTRACT

The accuracy and efficiency of a nodal synthesis method for steady-state and transient reactor analysis are investigated using DISCOVER (**DI**scontinuous **S**ynthesis **CO**de for **VER**ification) computer code developed by the author. A three dimensional neutron flux shape of a reactor is approximated as a linear combination of predetermined two dimensional expansion functions. One dimensional mixing coefficients are computed using synthesis equations. The governing synthesis equations are derived by applying a variational principle. Discontinuous trial functions are allowed in both space and time. Two different approaches for updating Coarse Mesh Finite Difference (CMFD) discontinuity factors are incorporated in DISCOVER. One approach is a discontinuity factor synthesis scheme in which discontinuity factors are approximated as the weighted average of precomputed values. The other approach is a non-linear iteration scheme which forces the synthesis solution to match a quartic polynomial solution. Both flux and adjoint weight functions are edited from three dimensional steady-state CONQUEST calculations.

A few benchmark problems with and without feedback effects are tested using DISCOVER. For most cases, average nodal power errors are observed to be less than five percent of the reference solution, and eigenvalues are usually consistent up to three to four significant digits. In steady-state cases, there is about a five to tenfold reduction in computing time, compared with that of CONQUEST if the discontinuity factor synthesis scheme is applied. There is no reduction in execution time, however, if the non-linear iteration scheme is applied. This is attributed to the slow convergence rate of the synthesis solution method. In transient cases, even with the discontinuity factor synthesis scheme, the reduction in computing time is less than for steady-state cases. In fact, if the non-linear iteration scheme is applied, the execution time may even increase. The time-consuming matrix multiplication routine is the main cause of the increase in execution time. Still, a two to threefold reduction is possible if the discontinuity factor synthesis scheme is utilized. Also, real-time calculations are feasible for some slow transients.

Thesis Supervisor: Professor Allan F. Henry

Thesis Reader: Professor John E. Meyer

ACKNOWLEDGMENTS

I would like to express my sincere gratitude to Professor Allan F. Henry, my thesis supervisor, for his guidance, encouragement and enduring patience. From the inception of the research idea to the completion of this thesis, he provided unending support and guidance and sometimes endured undue delays due to my incapability. It has been an honor and a pleasure to work with him throughout my years at Massachusetts Institute of Technology. I have nothing but a sincere admiration for his expertise and insights.

Thanks are also due to Professor John E. Meyer for his valuable advice on the incorporation of the thermal hydraulic model and for serving as my thesis reader. In addition, I would like to thank my friends at MIT for their friendship; Sangman for that somewhat disastrous fishing trip we took together for an elusive 2-foot-20-pound cod; Changhee for those occasional poker games; Changwoo for those drinking explorations through Boston bars. My stay at MIT was not only professionally enriching but also enjoyable because of their support and company.

Last, but not the least by any means, I owe my deepest gratitude to my wife, Seung, for her love and understanding. I would not be what I am without her unending encouragement and sacrifice. Thanks are also due to my parents and parent-in-laws for their love and support.

TABLE OF CONTENTS

ABSTRACT **2**

ACKNOWLEDGMENTS **3**

LIST OF FIGURES **7**

LIST OF TABLES **8**

CHAPTER 1 INTRODUCTION **9**

1.1 Overview 9
1.2 Background 11
1.3 Research Objectives 12
1.4 Thesis Contributions 13
1.5 Thesis Organization 14

CHAPTER 2 STEADY-STATE NODAL SYNTHESIS METHOD **15**

2.1 Introduction 15
2.2 Nodal Balance Equation 16
2.3 Finite Difference Nodal Coupling Equations 18
2.3.1 Boundary Conditions 21
2.3.2 Evaluation of CMFD Discontinuity Factors 22
2.4 Discontinuous Synthesis Equation 23
2.5 CMFD Discontinuity Factor Updating Schemes 27
2.5.1 CMFD Discontinuity Factor Synthesis Scheme 27
2.5.2 Non-Linear Iteration Scheme 28
2.5.2.a Transverse-Integration Procedure 28
2.5.2.b Polynomial Expansion 29
2.5.2.c Weighted Residual Procedure 31
2.5.2.d Expansion Coefficient Solution 34
2.5.2.e Boundary Conditions 36
2.5.2.f Non-Linear Iteration Procedure 37
2.6 Summary 39

CHAPTER 3 TRANSIENT NODAL SYNTHESIS METHOD **40**

3.1 Introduction 40
3.2 Time-Dependent, Finite-Difference Nodal Equation 41
3.3 Discontinuous, Time-Dependent Synthesis Equation 43
3.4 CMFD Discontinuity Factor Updating Schemes 50
3.4.1 CMFD Discontinuity Factor Synthesis Scheme 51
3.4.2 Non-Linear Iteration Scheme 51
3.5 Time-Integration of the Synthesis Equation 53
3.6 Thermal Hydraulic and Cross Section Feedback Models 54

3.6.1 WIGL Thermal Hydraulic Model....55
3.6.2 Cross Section Feedback....56
3.7 Control Rod Cusping Correction....57
3.8 Summary....58

CHAPTER 4 NUMERICAL SOLUTION METHODS....60

4.1 Introduction....60
4.2 Steady-State Solution Methods....61
4.2.1 Numerical Properties....61
4.2.2 CMFD Discontinuity Factor Iterations....62
4.2.3 Outer Iterations....63
4.2.4 LU Factorization....67
4.2.5 Steady-State Iteration Strategy....69
4.3 Transient Solution Methods....70
4.3.1 Numerical Properties....71
4.3.2 Dynamic Frequency Estimation....72
4.3.3 Transient Solution Procedure....72
4.4 Summary....73

CHAPTER 5 APPLICATION OF SYNTHESIS METHOD....75

5.1 Introduction....75
5.2 Prelude to Synthesis Results....76
5.2.1 Computer Code....76
5.2.2 Transverse Leakage Approximations....77
5.2.3 Power Distribution Errors....77
5.2.4 Execution Times....78
5.3 The Three-Dimensional LMW Reactor....79
5.3.1 The Three-Dimensional LMW Problem Without Feedback....79
5.3.2 The Three-Dimensional LMW Problem With Feedback....89
5.4 The PWR Operational Transient....94
5.5 The PWR Coolant Inlet Temperature Transient....100
5.6 Summary....103

CHAPTER 6 CONCLUSIONS AND RECOMMENDATIONS....105

6.1 Overview and Conclusions....105
6.2 Recommendations for Future Work....107
6.2.1 A Code Allowing Different Number of Expansion Functions Axially....107
6.2.2 Further Investigation of Discontinuity Factor Updating Procedures....108
6.2.3 Non-Iterative Discontinuity Factor Updating During Transient....108
6.2.4 A Quasi-Static Method Using Synthesis As Shape Update....108

REFERENCES....110

APPENDIX A THE QUADRATIC TRANSVERSE LEAKAGE MOMENTS AND COEFFICIENTS....113

A.1 The Quadratic Transverse Leakage Approximation....114
A.2 LHS-Biased Quadratic Transverse Leakage Approximation....116
A.3 RHS-Biased Quadratic Transverse Leakage Approximation....117
A.4 Flat Transverse Leakage Approximation....119

APPENDIX B NUMERICAL STUDY OF THERMAL HYDRAULIC MODELS....120

APPENDIX C PROBLEM SPECIFICATIONS....126

C.1 The LMW LWR Transient Problem....126
C.2 The PWR Transient Problems....130

LIST OF FIGURES

Figure 2.1 Diagram indicating Interface and node labeling conventions. 19
Figure 2.2 Non-linear iteration flow diagram....38
Figure 3.1 Diagram showing the subdivision of time steps in synthesis method....55
Figure 5.1 Core power vs. time for the LMW transient without feedback. (3 Cont. Expan. Functions: CR Out, Bank 1 In, Bank 2 In) 82
Figure 5.2 Core power vs. time for the LMW transient without feedback. (DF Synthesis Scheme with different time steps) 84
Figure 5.3 Core Power vs. time for the LMW transient without feedback. (Non-Linear Iteration Scheme with different time steps) 84
Figure 5.4 Core power vs. time for the LMW transient without feedback demonstrating the cusping correction. 85
Figure 5.5 Core power vs. time for the LMW transient without feedback. (2 Discontinuous Expansion Functions) 87
Figure 5.6 Core power vs. time for the LMW transient without feedback. (3 Discontinuous Expansion Functions) 88
Figure 5.7 Core power vs. time for the LMW transient with feedback. 91
Figure 5.8 Core power vs. time for the LMW transient with feedback. (DF Synthesis Scheme with several different time steps)....92
Figure 5.9 Core power vs. time for the LMW transient with feedback. (Non-Linear Iteration Scheme with several different time steps)....93
Figure 5.10 Core power vs. time for the LMW transient with feedback demonstrating the effects of cusping correction. 93
Figure 5.11 Core power vs. time for the PWR operational transient. 96
Figure 5.12 Axial power shape for the PWR operational transient. (t = 0 s) 98
Figure 5.13 Axial power shape for the PWR operational transient. (t = 60 s) 98
Figure 5.14 Axial power shape for the PWR operational transient. (t = 120 s) 99
Figure 5.15 Core power vs. time for the LMW transient with feedback. (Control rod group 1 withdrawal) 100
Figure 5.16 Core power vs. time for the PWR coolant inlet temperature transient....102
Figure B.1 Space-time discretization used for IDC model....121
Figure B.2 Space-time discretization used for WIGL model....121
Figure B.3 Two-node problem used to test thermal hydraulic models....123
Figure B.4 Average enthalpy vs. time steps for r = 0.1....123
Figure B.5 Average enthalpy vs. time steps for r = 0.5....124
Figure B.6 Average enthalpy vs. time steps for r = 1.0....124
Figure B.7 Average enthalpy vs. time steps for r = 5.0....125

LIST OF TABLES

Table 5.1 Convergence criteria used in DISCOVER and CONQUEST. 79
Table 5.2 Expansion functions for the LMW steady-state problem without feedback. (3 Expansion functions)....81
Table 5.3 A summary of the results for the LMW steady-state problem without feedback. (3 Expansion Functions). 81
Table 5.4 A comparison of errors for the LMW transient without feedback.....82
Table 5.5 A summary of execution times for the LMW transient without feedback. 83
Table 5.6 Expansion functions for the LMW steady-state problem without feedback. (2 Expansion Functions)....85
Table 5.7 A summary of the results for the LMW steady-state problem without feedback. (2 Expansion Functions) 86
Table 5.8 Changes in expansion functions for the LMW transient problem without feedback. (2 Expansion Functions)....87
Table 5.9 Changes in expansion function for the LMW transient problem without feedback. (3 Expansion Functions)....88
Table 5.10 Expansion functions for the LMW steady-state problem with feedback. (All expansion functions generated at 184.8 MW_{th})....90
Table 5.11 A summary of the results for the LMW steady-state problem with feedback. 90
Table 5.12 A comparison of errors for the LMW transient with feedback. 91
Table 5.13 A summary of execution times for the LMW transient with feedback. 92
Table 5.14 Expansion functions for the PWR steady-state and transient problems. (All expansion functions generated at 667.6 MW_{th}) 95
Table 5.15 A summary of the results for the PWR steady-state problem with feedback. 96
Table 5.16 A summary of execution times for the PWR operational transient.....97
Table 5.17 Expansion functions for the PWR inlet coolant temperature transient. 101
Table 5.18 A summary of the results for the PWR steady-state problem....102
Table 5.19 A summary of execution times for the PWR coolant inlet temperature transient. 103

CHAPTER 1

INTRODUCTION

1.1 Overview

One of the most fundamental quantities that pervades every aspect of nuclear reactor core design and operation is the neutron flux. Ever since the beginning of the nuclear era, great efforts by many bright minds have been devoted to answering the seemingly simple question of how neutrons are distributed in a reactor core. The difficulties in answering this question do not lie in lack of understanding of the physical phenomena or in inadequate modeling. The governing neutron balance equation, the Boltzmann Transport Equation, is well understood, and basic nuclear data are readily available. The problem stems from the enormous difficulties in solving the Boltzmann Transport Equation. It takes seven independent variables to describe the directional neutron flux. And, even with the super computers of today, it is a formidable task to carry all those variables in their discretized forms when a very accurate reference solution is mandated. It is impractical to solve the Boltzmann Transport Equation repeatedly for a particular reactor design or fuel loading optimization. Fortunately, for Light Water Reactors (LWR), in which high-order transport effects are negligible, it is also unnecessary.

Diffusion theory, which assumes a first order directional dependence of neutron flux, has been shown to be sufficient for LWR's. This diffusion theory approximation eases some of the difficulties associated with solving the Boltzmann Transport Equation, and has been the basis of design and safety calculations associated with LWR's. Yet, three dimensional spatial discretization of the neutron diffusion equation still retains the problem of having to calculate millions of fine-mesh neutron fluxes. Because of this limitation, most computer codes employing a fine-mesh representation of the neutron diffusion equation resort to either one- or two-dimensional analysis taking advantage of symmetry conditions.

Over the last twenty years, considerable research effort has been directed toward developing nodal diffusion theory, which allows a much more coarse spatial discretization (i.e., assembly size mesh). With the introduction of equivalence parameters (usually called discontinuity factors), which account for homogenization, discretization and even diffusion theory errors, the solution of the nodal diffusion equation can replicate a reference solution obtained by either a fine-mesh diffusion calculation or even a transport calculation. The nodal diffusion equation, therefore, reduces the number of spatial fluxes by orders of magnitude and makes three dimensional analysis feasible on desk-top computers.

The nodal theory greatly reduces the computing efforts associated with reactor analysis and, thereby, serves as an excellent tool for a nuclear analyst to optimize a particular reactor design or a fuel loading pattern without an undue burden of long waiting time between each computation. Furthermore, the realization of a real-time calculation, at least for some slow transients not requiring very small temporal steps, is within reach with adequate computers. The natural progression in research efforts, therefore, is to combine an efficient nodal code into an automatic controller to regulate steady-state and transient behavior of a nuclear reactor on a real-time basis. Accomplishing this ambitious goal, however, requires a further reduction in computing time without sacrificing the computational accuracy. This goal can be realized in part by faster computers, but it will also require further refinements in nodal theory and development of more efficient computer codes.

This thesis concentrates on the development of a nodal **synthesis** method which can be used for steady-state and transient reactor analysis. The primary goal is to reduce further the computing efforts without unduly compromising the accuracy of neutron flux determination.

1.2 Background

The synthesis method in reactor analysis approximates the neutron flux shape of interest as a linear combination of predetermined expansion functions (sometimes called trial functions). These expansion functions are, in fact, educated guesses of an actual neutron flux shape. Although, little theoretical justification exists for deciding which expansion functions to select, previous numerical studies [Y-1,Y-2,Y-3] indicate no significant problem in choosing expansion functions based on physical intuition and past experience. On the contrary, there is a firm theoretical ground for obtaining the mixing coefficients, the parameters which specify how given expansion functions should be combined to replicate the actual neutron flux shape as closely as possible. Both a weighted residual method and a variational principle are used to derive synthesis equations having mixing coefficients as the unknowns. The most attractive feature of the synthesis method stems from the fact that the number of mixing coefficients is orders of magnitude less than the number of discretized flux values. Thus, computational requirements can be greatly reduced with proper application of the scheme.

The synthesis method in reactor analysis was first applied to a fine-mesh representation of the neutron diffusion equation. Because of the enormous computational requirements associated with a fine-mesh discretization, the synthesis method was the only practical approach to calculate three-dimensional neutron fluxes. Earlier studies by Yasinsky and Kaplan [Y-1,Y-2,Y-3] showed that space-dependent synthesis employing discontinuous sets of axial and temporal expansion functions was capable of constructing accurate space-time neutron fluxes. Yet, no mention of computational speed was given in these studies. Furthermore, all the numerical tests were performed for either one- or two-dimensional reactors.

Recently, there have been several attempts to apply the synthesis method to the nodal diffusion equation. K. Lee studied a point synthesis method, which utilized three-dimensional expansion functions, based on an analytical nodal diffusion theory model [L-5]. The point synthesis model produced satisfactory results involving homogeneous changes in reactor conditions. However, because of the inherent limitation of using three-dimensional expansion functions, heterogeneous changes in reactor conditions (i.e., control rod motions) were not tested. Moreover, the computational speed did not improve relative to the reference QUANDRY [S-2] calculations.

W. Kuo investigated the point synthesis method based on a finite difference nodal diffusion theory [K-1]. He suggested a synthesis scheme to update the Coarse Mesh Finite Difference (CMFD) discontinuity factors. The results were encouraging as

far as accuracy was concerned, but the computational speed again was not satisfactory. He indicated the additional matrix multiplication steps needed in the synthesis method as the main cause of inefficiency. Moreover, his study was limited to one-dimensional reactors which would not exhibit the complexities associated with multi-dimensional analysis.

R. Jacqmin investigated a semi-experimental instrumented nodal synthesis method in which the synthesized neutron fluxes were force to match, in a least-squares sense, neutron detector readings [J-1]. It was semi-experimental in that the detector readings were generated by simulated transients rather than by actual experiments. Although there were some concerns about measurement noise, the number and positions of detectors, and detector characteristics, his study showed that nodal fluxes could be reconstructed in real-time with maximum errors of a few percent.

J. Hughes applied an instrumented nodal flux synthesis method to analysis of the Massachusetts Institute of Technology Reactor, MITR-II [H-1]. Detector measurements were collected using fission chambers placed around the core. The experimental results indicated that the instrumented synthesis accurately reflected the changes in reactor conditions in real-time, though they did not replicate the reference solutions with acceptable accuracy.

1.3 Research Objectives

The objective of this study is the development of an efficient (fast and accurate) discontinuous space-time dependent nodal synthesis method for the solution of the three-dimensional, few group, steady-state and transient neutron diffusion equations. No restriction is placed on the number of energy groups, and neutron upscattering is allowed. The synthesis method permits both spatially and temporally discontinuous flux expansion functions while maintaining initial adjoint weight functions. Although different flux expansion functions may be adopted at different axial planes and different time steps, their total number is kept constant. The CONQUEST code, developed by J. Gehin [G-1], is used to generate two-dimensional flux expansion functions and adjoint weight functions. A three-dimensional CONQUEST calculation rather than a series of two-dimensional calculations is performed for the generation of expansion functions.

Two different discontinuity factor updating approaches are incorporated to test their accuracy and speed. A non-linear iteration scheme, where finite difference nodal

fluxes are forced to match a quartic polynomial nodal solution, is one way to update CMFD discontinuity factors. This scheme is successfully implemented in the CONQUEST code, and results obtained from it indicate excellent accuracy [G-1]. However, one of the shortcomings of this non-linear iteration scheme is its computational burden: Preliminary analysis indicates that more than half of the total computing time is spent in updating CMFD discontinuity factors. This shows that if significant reduction in computing effort is to be realized, a more efficient updating scheme should be considered. A discontinuity factor synthesis scheme suggested by W. Kuo [K-1] is another approach. Though this scheme lacks the theoretical basis that the non-linear iteration scheme possesses, the results obtained are encouraging [K-1]. Furthermore, the discontinuity factor synthesis scheme requires much less computational efforts than the non-linear iteration scheme.

Direct inversion of matrices, rather than iterative inversion, is adopted in the synthesis solution procedure for two reasons. First, the number of unknowns are on the order of tens to hundreds and, thereby, makes the direct inversion practical. Second, the matrix to be inverted lacks the structure that guarantees that the iterative inversion techniques converges. A simultaneous group solution is adopted and the band structure is exploited in the direct inversion procedure.

Finally, a simple, one-dimensional thermal hydraulic WIGL model [V-1] is adopted to allow feedback effects. This model is selected for its simplicity and comparison purpose because the CONQUEST code adopts the same model.

1.4 Thesis Contributions

The space-time synthesis method was applied years ago to a fine-mesh representation of the neutron diffusion equation, but has not been previously attempted for a nodal method. Thus, the main contribution of this thesis is the development of a computer code which can serve as a tool to test the accuracy and efficiency of the discontinuous space-time nodal synthesis method. Another contribution is the identification of the numerical properties of the synthesis method and the subsequent development of numerical solution methods consistent with them. The implications of discontinuous usage of expansion functions are identified variationally. Also, an eigenvalue iteration strategy which maximizes the computational speed is tested for its effectiveness.

1.5 Thesis Organization

Chapter 2 presents the complete mathematical derivation of a steady-state nodal synthesis method. First, a finite difference method which incorporates CMFD discontinuity factors is developed. Then, a nodal synthesis method is derived by applying a variational principle to the finite difference nodal equation. Two different discontinuity factor updating approaches (a discontinuity factor synthesis scheme and a non-linear iteration scheme) are presented next. For the non-linear iteration scheme, a polynomial nodal method is discussed in great detail.

Chapter 3 offers a similar derivation of a transient nodal synthesis method. Although not implemented in this thesis, the implications of using a different number of expansion functions at different time steps and of allowing flux and adjoint expansion functions to change at the same time are discussed in light of the variational principle. The thermal hydraulic and cross section feedback models as well as a cusping correction model are also presented.

Chapter 4 presents the numerical solution methods for the steady state and transient nodal synthesis method. The eigenvalue iteration procedure and the direct matrix inversion technique are discussed. Also, a temporal solution advancing strategy is presented.

In Chapter 5, the results from several steady state and transient benchmark problems with and without cross section feedback effects are presented.

Finally, Chapter 6 presents the summary and conclusion of this study. Some recommendations for future research are also made.

CHAPTER 2

STEADY-STATE NODAL SYNTHESIS METHOD

2.1 Introduction

This chapter presents the derivation of a steady-state nodal synthesis equation from the few-group diffusion equations. First, the finite-difference nodal equation, which is mathematically rigorous with the introduction of CMFD discontinuity factors, is derived in Cartesian geometry. With appropriate CMFD discontinuity factors, the finite-difference nodal equation can reproduce any reference solution. Second, a discontinuous nodal synthesis equation is derived by applying a variational principle to the finite-difference nodal equation. Next, two different discontinuity factor updating schemes, a discontinuity factor synthesis scheme and a non-linear iteration scheme, are introduced. A polynomial nodal method, which produces accurate results even when assembly-size spatial discretization is employed, is discussed in great detail. The non-linear iteration scheme results when the synthesis solution is forced to match the polynomial nodal solution. Although it lacks the theoretical basis of the non-linear iteration scheme, the discontinuity factor synthesis scheme is introduced for its computational simplicity and efficiency.

2.2 Nodal Balance Equation

The derivation of the nodal balance equation starts from the few-group, steady-state diffusion equation in P_1 form without an extraneous neutron source [H-2]

$$\nabla \cdot J_g(r) + \Sigma_{tg}(r)\phi_g(r) = \sum_{g'=1}^{G}\left[\frac{1}{\lambda}\chi_g \upsilon\Sigma_{fg'}(r) + \Sigma_{gg'}(r)\right]\phi_{g'}(r), \qquad (2.1a)$$

$$J_g(r) = -D_g(r)\nabla\phi_g(r) \qquad g = 1,2,...,G. \qquad (2.1b)$$

Where

$J_g(r)$ = neutron current for group g,
$\phi_g(r)$ = scalar neutron flux for group g,
$\Sigma_{tg}(r)$ = macroscopic total cross section for group g,
$\Sigma_{fg}(r)$ = macroscopic fission cross section for group g,
$\Sigma_{gg'}(r)$ = macroscopic scattering cross section from group g' to g,
$D_g(r)$ = diffusion coefficient for group g,
χ_g = fission spectrum for group g,
λ = reactor eigenvalue,
υ = mean number of neutron emitted per fission,
G = total number of energy groups.

It is a bit of a misnomer to call Eqs. (2.1a) and (2.1b) the few-group diffusion equation because the multi-group diffusion equation assumes the exact same form. The methods by which the group parameters (cross sections and diffusion coefficients) are obtained distinguish one from the other. The few-group diffusion equation uses the neutron energy spectrum obtained by a separate calculation to determine the group parameters while the multi-group diffusion equations uses an arbitrarily assumed energy shape (i.e., Maxwellian distribution in the thermal range). Note that, according to this distinction, group parameters obtained by averaging over a detailed energy spectrum are "few-group constants" even though the number of groups may be hundreds. With the number of "few-groups" this large, however, the distinction is generally abandoned and the model is referred to as a multi-group scheme [H-2].

The few-group diffusion equation in its spatially discretized form has been the basis of most safety and fuel depletion calculations for LWR's, and many utilities still perform reactor analyses using computer codes adopting this scheme. The solution of the fine-mesh, few-group diffusion equation in its three-dimensional form, however,

requires an prohibitively large computing time. Thus, the repeated use of the fine-mesh diffusion equation is undesirable in fuel loading, depletion and reactor safety calculations which are inherently iterative in nature. This difficulty is somewhat alleviated by exploiting symmetry conditions and the axially homogenous geometry that exists in most LWR's, but even a two-dimensional analysis requires a formidable computing effort, and furthermore, some of the reactor systems do mandate three-dimensional analyses.

The nodal diffusion equation makes three-dimensional analyses feasible by employing much more coarse spatial discretizations (i.e., assembly-size nodes). However, it requires additional equivalence parameters, called discontinuity factors, to replicate the reference solutions obtained from either the Boltzmann Transport Equation or the fine-mesh diffusion equation. The physical meaning of discontinuity factors will be discussed in Section 2.3. In Cartesian geometry, Eqs. (2.1a) and (2.1b) are

$$\begin{aligned}\frac{\partial}{\partial x}J_{gx}(x,y,z)+\frac{\partial}{\partial y}J_{gy}(x,y,z)+\frac{\partial}{\partial z}J_{gz}(x,y,z)+\Sigma_{tg}(x,y,z)\phi_g(x,y,z)\\ =\sum_{g'=1}^{G}\left[\frac{1}{\lambda}\chi_g\upsilon\Sigma_{fg'}(x,y,z)+\Sigma_{gg'}(x,y,z)\right]\phi_{g'}(x,y,z),\end{aligned} \tag{2.2a}$$

$$J_{gu}(x,y,z)=-D_g(x,y,z)\frac{\partial}{\partial u}\phi_g(x,y,z) \qquad u = x,y,z. \tag{2.2b}$$

The node (i,j,k) and its widths are defined by

$$\begin{aligned} x\in[x_i,x_{i+1}] \quad & h_x^i\equiv x_{i+1}-x_i,\\ y\in[y_j,y_{j+1}] \quad & h_y^j\equiv y_{j+1}-y_j,\\ z\in[z_k,z_{k+1}] \quad & h_z^k\equiv z_{k+1}-z_k,\end{aligned} \tag{2.3}$$

and the node volume is

$$V^{ijk}\equiv h_x^i h_y^j h_z^k. \tag{2.4}$$

The nodal balance equation is obtained by integrating Eq. (2.2a) over the volume of node (i,j,k) and then diving by V^{ijk}

$$\begin{aligned}\frac{1}{h_x^i}\left[J_{gx}^{jk}(x_{i+1})-J_{gx}^{jk}(x_i)\right]+\frac{1}{h_y^j}\left[J_{gy}^{ik}(y_{j+1})-J_{gy}^{ik}(y_j)\right]+\frac{1}{h_z^k}\left[J_{gz}^{ij}(z_{k+1})-J_{gz}^{ij}(z_k)\right]\\ +\Sigma_{tg}^{ijk}\bar{\phi}_g^{ijk}=\sum_{g'=1}^{G}\left[\frac{1}{\lambda}\chi_g\upsilon\Sigma_{fg'}^{ijk}+\Sigma_{gg'}^{ijk}\right]\bar{\phi}_{g'}^{ijk},\end{aligned} \tag{2.5}$$

where the node-averaged flux and the surface-averaged current are defined by

$$\bar{\phi}_g^{ijk} \equiv \frac{1}{V^{ijk}} \int_{x_i}^{x_{i+1}} dx \int_{y_j}^{y_{j+1}} dy \int_{z_k}^{z_{k+1}} dz \, \phi_g(x,y,z), \tag{2.6}$$

$$J_{gu}^{mn}(u) \equiv \frac{1}{h_v^m h_w^n} \int_{v_m}^{v_{m+1}} dv \int_{w_n}^{w_{n+1}} dw \, J_{gu}(u,v,w), \quad u \equiv x,y,z, \; v \neq u, \; w \neq u,v. \tag{2.7}$$

The group parameters within node (*i,j,k*) are assumed to be constant.

Although derived without any approximation, Eq. (2.5) is not complete by itself because it contains both node-averaged fluxes and surface-averaged currents as the unknowns. Therefore, additional equations relating node-averaged fluxes and surface-averaged currents must be provided. These additional equations are called **nodal coupling equations** and discussed in the following section.

2.3 Finite Difference Nodal Coupling Equations

The finite-difference nodal coupling equations are derived by integrating the second P_1 equation, Eq. (2.2b), over a surface and diving by its widths

$$J_{gu}^{mn}(u) = -D_g^{lmn} \frac{d}{du} \phi_{gu}^{mn}(u), \tag{2.8}$$

where the surface-averaged flux is defined by

$$\phi_{gu}^{mn}(u) \equiv \frac{1}{h_v^m h_w^n} \int_{v_m}^{v_{m+1}} dv \int_{w_n}^{w_{n+1}} dw \, \phi_g(u,v,w), \tag{2.9}$$

and by approximating the spatial derivative as a simple first-order difference

$$J_{gu}^{mn}(u_l) \approx -D_g^{lmn} \frac{\bar{\phi}_g^{lmn} - \phi_{gu}^{mn}(u_l^+)}{h_u^l/2}, \tag{2.10}$$

where u_l^+ indicates the positive side of the interface shown in Figure 2.1. Similarly, the same surface-averaged current at the interface u_l can be approximated for node *l-1*

$$J_{gu}^{mn}(u_l) \approx -D_g^{l-1,mn} \frac{\phi_{gu}^{mn}(u_l^-) - \bar{\phi}_g^{l-1,mn}}{h_u^{l-1}/2}, \tag{2.11}$$

where u_l^- indicates the negative side of the interface shown in Figure 2.1.

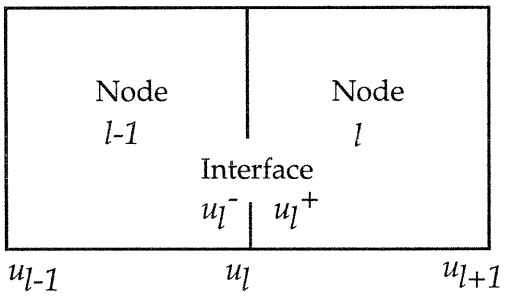

Figure 2.1: Diagram indicating Interface and node labeling conventions.

Eqs. (2.10) and (2.11) are incomplete because they are valid only when a very fine-mesh spacing is considered. When assembly-size nodes are used, which is the very goal of a nodal theory, a large error will result. The assumption of a linearly varying flux is more often than not invalid for assembly-size nodes.

This difficulty is overcome by the use of correction factors, first introduced by Smith [S-1], to force Eqs. (2.10) and (2.11) mathematically rigorous. The correction factors, $f_{gu+}^{l-1,mn}$ and f_{gu-}^{lmn}, for the opposite sides of the interface between node (*l-1,m,n*) and (*l,m,n*) are defined by

$$\begin{aligned} f_{gu+}^{l-1,mn} &\equiv \frac{\phi_{gu}^{mn}(u_l)}{\phi_{gu}^{mn}(u_l^-)}, \\ f_{gu-}^{lmn} &\equiv \frac{\phi_{gu}^{mn}(u_l)}{\phi_{gu}^{mn}(u_l^+)}, \end{aligned} \tag{2.12}$$

where $\phi_{gu}^{mn}(u_l)$ is the true surface-averaged flux. Examination of Eq. (2.12) shows that the correction factors have the effect of making the surface-averaged flux discontinuous if $f_{gu+}^{l-1,mn}$ and f_{gu-}^{lmn} are not identical. For this reason, the correction factors are called discontinuity factors [H-3]. Inserting the discontinuity factors given in Eq. (2.12) into Eqs. (2.10) and (2.11) results in the following equation

$$\begin{aligned} J_{gu}^{mn}(u_l) &= -D_g^{lmn} \frac{\bar{\phi}_g^{lmn} - \phi_{gu}^{mn}(u_l)/f_{gu-}^{lmn}}{h_u^l/2} \\ &= -D_g^{l-1,mn} \frac{\phi_{gu}^{mn}(u_l)/f_{gu+}^{l-1,mn} - \bar{\phi}_g^{l-1,mn}}{h_u^{l-1}/2}. \end{aligned} \tag{2.13}$$

When used with the reference values for the currents and fluxes, Eq. (2.13) also serves as the definition of the discontinuity factors.

Although the discontinuity factors are introduced as the correction factors intended to reduce the spatial discretization errors when a large node spacing is used, they also can be used to correct for cross section homogenization errors and diffusion theory approximation errors. These correction factors will be referred to as Coarse Mesh Finite Difference (CMFD) discontinuity factors throughout this thesis to distinguish them from another set of discontinuity factors introduced later in this chapter.

Now, the finite-difference nodal coupling equation, relating surface-averaged currents to node-averaged fluxes, is obtained by eliminating the surface-averaged fluxes in Eq. (2.13) using the continuity condition implied in Eq. (2.12)

$$J_{gu}^{mn}(u_l) = -\left[\frac{h_u^l}{2D_g^{lmn}}\frac{f_{gu-}^{lmn}}{f_{gu+}^{l-1,mn}} + \frac{h_u^{l-1}}{2D_g^{l-1,mn}}\right]^{-1}\left(\frac{f_{gu-}^{lmn}}{f_{gu+}^{l-1,mn}}\bar{\phi}_g^{lmn} - \bar{\phi}_g^{l-1,mn}\right). \tag{2.14}$$

Substituting Eq. (2.14) and its equivalent coupling equation for the node surface u_{l+1} into Eq. (2.5) results in the following finite-difference nodal balance equation

$$\begin{aligned}
&\frac{1}{h_x^i}\left[\frac{h_x^l}{2D_g^{ijk}}\frac{f_{gx-}^{ijk}}{f_{gx+}^{i-1,jk}} + \frac{h_x^{i-1}}{2D_g^{i-1,jk}}\right]^{-1}\left(\frac{f_{gx-}^{ijk}}{f_{gx+}^{i-1,jk}}\bar{\phi}_g^{ijk} - \bar{\phi}_g^{i-1,jk}\right)\\
&+\frac{1}{h_x^i}\left[\frac{h_x^i}{2D_g^{ijk}}\frac{f_{gx+}^{ijk}}{f_{gx-}^{i+1,jk}} + \frac{h_x^{i+1}}{2D_g^{i+1,jk}}\right]^{-1}\left(\frac{f_{gx+}^{ijk}}{f_{gx-}^{i+1,jk}}\bar{\phi}_g^{ijk} - \bar{\phi}_g^{i+1,jk}\right)\\
&+\frac{1}{h_y^j}\left[\frac{h_y^l}{2D_g^{ijk}}\frac{f_{gy-}^{ijk}}{f_{gy+}^{i,j-1,k}} + \frac{h_y^{j-1}}{2D_g^{i,j-1,k}}\right]^{-1}\left(\frac{f_{gy-}^{ijk}}{f_{gy+}^{i,j-1,k}}\bar{\phi}_g^{ijk} - \bar{\phi}_g^{i,j-1,k}\right)\\
&+\frac{1}{h_y^j}\left[\frac{h_y^l}{2D_g^{ijk}}\frac{f_{gy+}^{ijk}}{f_{gy-}^{i,j+1,k}} + \frac{h_y^{i+1}}{2D_g^{i,j+1,k}}\right]^{-1}\left(\frac{f_{gy+}^{ijk}}{f_{gy-}^{i,j+1,k}}\bar{\phi}_g^{ijk} - \bar{\phi}_g^{i,j+1,k}\right)\\
&+\frac{1}{h_z^k}\left[\frac{h_z^k}{2D_g^{ijk}}\frac{f_{gz-}^{ijk}}{f_{gz+}^{ij,k-1}} + \frac{h_z^{k-1}}{2D_g^{ij,k-1}}\right]^{-1}\left(\frac{f_{gz-}^{ijk}}{f_{gz+}^{ij,k-1}}\bar{\phi}_g^{ijk} - \bar{\phi}_g^{ij,k-1}\right)\\
&+\frac{1}{h_z^k}\left[\frac{h_z^k}{2D_g^{ijk}}\frac{f_{gz+}^{ijk}}{f_{gz-}^{ij,k+1}} + \frac{h_z^{k+1}}{2D_g^{ij,k+1}}\right]^{-1}\left(\frac{f_{gz+}^{ijk}}{f_{gz-}^{ij,k+1}}\bar{\phi}_g^{ijk} - \bar{\phi}_g^{ij,k+1}\right)\\
&+\Sigma_{tg}^{ijk}\bar{\phi}_g^{ijk} = \sum_{g'=1}^{G}\left[\frac{1}{\lambda}\chi_g\upsilon\Sigma_{fg'}^{ijk} + \Sigma_{gg'}^{ijk}\right]\bar{\phi}_g^{ijk}.
\end{aligned} \tag{2.15}$$

First, note that only the ratios of the CMFD discontinuity factors appear in the final nodal balance equation. Second, if CMFD discontinuity factors are unity, Eq. (2.15) reduces to the mesh-centered, finite-difference diffusion equation.

Eq. (2.15) is reduced to a more compact form when matrix notation is used to suppress the spatial dependence

$$\underline{\underline{N}}_g \underline{\phi}_g = \frac{1}{\lambda} \sum_{g'=1}^{G} \underline{\underline{F}}_{gg'} \underline{\phi}_{g'} + \sum_{g'=1}^{G} \underline{\underline{\Sigma}}_{gg'} \underline{\phi}_g, \tag{2.16}$$

where

$\underline{\underline{N}}_g$ = N by N seven stripe matrix containing the coupling terms for group g, the total cross section and the in-group scattering terms,

$\underline{\underline{F}}_{gg'}$ = N by N diagonal matrix containing $\left\{\chi_g \upsilon \Sigma_{fg'}^{ijk}\right\}$,

$\underline{\underline{\Sigma}}_{gg'}$ = N by N diagonal matrix containing $\left\{\Sigma_{gg'}^{ijk}\right\}$,

$\underline{\phi}_g$ = column vector of length N containing fluxes for group g,

N = total number of nodes (I x J x K).

An even more compact form results when Eq. (2.16) is written in super-matrix notation with the group dependence suppressed

$$\underline{\underline{L}}\,\underline{\Phi} = \frac{1}{\lambda} \underline{\underline{M}}\,\underline{\Phi}, \tag{2.17}$$

where

$\underline{\underline{L}}$ = NG by NG net loss matrix containing $\left\{\underline{\underline{N}}_g \delta_{gg'} - \underline{\underline{\Sigma}}_{gg'}\right\}$,

$\underline{\underline{M}}$ = NG by NG fission matrix containing $\left\{\underline{\underline{F}}_{gg'}\right\}$,

$\underline{\Phi}$ = column vector of length NG containing $\left\{\underline{\phi}_g\right\}$.

This matrix form is useful because it simplifies the confusing notation caused by many superscripts and subscripts. A variational method will be applied to Eq. (2.17) for the derivation of the steady-state nodal synthesis equation.

2.3.1 Boundary Conditions

The following equation specifies the boundary conditions relating the surface-averaged current and flux [Z-1]

$$\phi_{gu}^{mn}(u_s) = \Gamma_{gu\pm}^{mn} J_{gu}^{mn}(u_s)\, \hat{l} \cdot \hat{n}, \tag{2.18}$$

where

$\phi_{gu}^{mn}(u_s)$ = surface-averaged flux at external boundary,

$J_{gu}^{mn}(u_s)$ = surface-averaged current at external boundary,

u_s = external boundary,

$\hat{l}$ = unit vector in the positive direction of the coordinate axis,

$\hat{n}$ = unit normal vector of external boundary,

$\Gamma_{gu\pm}^{mn}$ = boundary condition factors having the following values:

$\Gamma_{gu\pm}^{mn} = 0$	zero flux
$\Gamma_{gu\pm}^{mn} = 2$	zero incoming current
$\Gamma_{gu\pm}^{mn} = \infty$	zero current
$\Gamma_{gu\pm}^{mn} = \dfrac{\phi_{gu}^{mn}(u_s)}{J_{gu}^{mn}(u_s)\,\hat{l}\cdot\hat{n}}$	albedo condition.

The expression for the current at the external surface needed in Eq. (2.5) results when Eq. (2.18) and (2.13) are combined to eliminate the surface-averaged flux term. The resulting expressions for a lower and an upper external boundary are given by

$$J_{gu}^{mn}(u_s) = -\left[\frac{\Gamma_{gu-}^{mn}}{f_{gu-}^{lmn}} + \frac{h_u^l}{2D_g^{lmn}}\right]^{-1} \bar{\phi}_g^{lmn}, \tag{2.19}$$

and

$$J_{gu}^{mn}(u_s) = \left[\frac{\Gamma_{gu+}^{mn}}{f_{gu+}^{lmn}} + \frac{h_u^l}{2D_g^{lmn}}\right]^{-1} \bar{\phi}_g^{lmn}, \tag{2.20}$$

respectively.

2.3.2 Evaluation of CMFD Discontinuity Factors

Any reference solution (i.e., a transport solution and a fine-mesh finite-difference diffusion solution) along with Eq. (2.13) defines the CMFD discontinuity factors. By rearranging Eq. (2.13), the following expression of the CMFD discontinuity factor ratio is obtained for an interior surface

$$\frac{f_{gu+}^{l-1,mn}}{f_{gu-}^{lmn}} = \frac{\bar{\phi}_g^{lmn} + \dfrac{h_u^l}{2D_g^{lmn}} J_{gu}^{mn}(u_l)}{\bar{\phi}_g^{l-1,mn} - \dfrac{h_u^{l-1}}{2D_g^{l-1,mn}} J_{gu}^{mn}(u_l)}. \tag{2.21}$$

At the lower external boundary, Eq (2.19) can be rearranged to give

$$\frac{\Gamma_{gu-}^{mn}}{f_{gu-}^{lmn}} = -\left(\frac{\bar{\phi}_g^{lmn}}{J_{gu}^{mn}(u_s)} + \frac{h_u^l}{2D_g^{lmn}} \right), \tag{2.22}$$

and at the upper external boundary, Eq. (2.20) can be manipulated to give

$$\frac{\Gamma_{gu+}^{mn}}{f_{gu+}^{lmn}} = \left(\frac{\bar{\phi}_g^{lmn}}{J_{gu}^{mn}(u_s)} - \frac{h_u^l}{2D_g^{lmn}} \right). \tag{2.23}$$

2.4 Discontinuous Synthesis Equation

Synthesis methods assume many different forms depending on the types of expansion functions adopted. The simplest of the flux-synthesis methods is called **point synthesis** and consists of representing the flux as a superposition of known three-dimensional fluxes

$$\phi_g^{ijk} \approx \sum_{p=1}^{P} \psi_g^{ijk,p} T_g^p, \tag{2.24}$$

where the $\psi_g^{ijk,p}$ are predetermined flux expansion functions and the T_g^p are mixing coefficients. This method works well only when the range of reactor conditions for which a given set of expansion functions is to be applied involves homogeneous changes in reactor properties (changes in homogeneous poison concentration, in overall reactor temperature, etc.). However, it is not well suited for heterogeneous changes in reactor conditions It is not possible, for example, to produce an accurate representation of the detailed flux shapes corresponding to a range of control-rod positions using just two or three expansion functions [H-2]. In other words, many different three-dimensional flux expansion functions have to be used in order for the point synthesis to accurately represent the heterogeneous changes in reactor conditions.

This limitation can be circumvented by the use of the **continuous space-dependent synthesis** method. The essential idea is to express the three-dimensional flux shape as a linear combination of predetermined two-dimensional expansion functions $\psi_g^{ij,p}$ multiplied by unknown one-dimensional mixing coefficients $T_g^{k,p}$:

$$\phi_g^{ijk} \approx \sum_{p=1}^{P} \psi_g^{ij,p} T_g^{k,p}. \tag{2.25}$$

The fact that the mixing coefficients depend on axial positions permits the same expansion functions to be used for many control-rod positions [H-2].

There is a fairly obvious way to reduce the number of unknowns without seriously decreasing the accuracy of the continuous space-dependent synthesis scheme. One simply notes that, at a given axial position k, the most important expansion functions will be those characteristic of the radial planes close to k. The coefficients of other expansion functions are expected to be small. At the mid-plane of the reactor, for example, the expansions functions appropriate to the top and bottom reflectors would not be a significant contribution to the actual flux shape. Thus, allowing different sets of expansion functions at different axial locations reduces the computational requirement without seriously compromising the accuracy [H-2]. This type of synthesis is called a **spatially discontinuous synthesis** and is adopted in this thesis. It has the following form in Cartesian geometry

$$\phi_g^{ijk} \approx \sum_{p=f(k)}^{h(k)} \psi_g^{ij,p} T_g^{k,p}, \tag{2.26}$$

where $f(k)$ and $h(k)$ represent the axial dependence of the expansion functions.

There are two central questions that need to be answered in using synthesis methods in general: (1) How should the expansion functions be chosen? and (2) How are the mixing coefficients determined? The answer to the former question is not an easy one because there is no firm theoretical basis for choosing expansion functions. There is no brute-force way (for example, reducing the mesh size in the finite-difference diffusion equation) of ensuring that Eq. (2.26) can adequately represent the true flux shape. The choice of expansion functions depends on the physics of the problem, and adding more expansion functions does not always improve the solution.

The "bracket and blend" approach, where expansion functions corresponding to the reactor conditions which envelope the particular reactor state of interest, is the generally accepted procedure of selecting expansion functions. Although many reactor designers are uncomfortable with synthesis methods because there is no systematic way of estimating and reducing the errors, past experience indicates that an accuracy of a few tenths of a percent in eigenvalue and a maximum error of five percent in the flux shape can be obtained using the "bracket and blend" approach.

The discontinuous synthesis equation having the mixing coefficients as the unknowns can be obtained by two different methods, the **weighted residual** method and the **variational method**. The weighted residual method is easier to understand in that the approximate form assumed in Eq. (2.26) is forced to be the solution of Eq.

(2.15) in a weighted-integral sense. However, the variational method, which is somewhat mysterious at first glance, is much more powerful in that it suggests which weight function be used and provides continuity equations. For these reasons, the variational method will be applied in the derivation of the discontinuous synthesis equation.

The first step in the variational derivation is to find a functional for which the first-order variation is made stationary by the solution of Eq. (2.17). This is accomplished by multiplying Eq. (2.17) by the transpose of an arbitrary weight function $\underline{\Phi}^*$ and solving for $1/\lambda$. The resulting functional is

$$F_s(\underline{\Phi}^*, \underline{\Phi}) = \frac{1}{\lambda} = \frac{\underline{\Phi}^{*T} \underline{\underline{L}}\, \underline{\Phi}}{\underline{\Phi}^{*T} \underline{\underline{M}}\, \underline{\Phi}} , \tag{2.27}$$

where $\underline{\Phi}^*$ is a column vector of length NG. The first-order variation, where second- and higher-order variation are neglected, of Eq (2.27) is then

$$\begin{aligned}
\delta F_s(\underline{\Phi}^*, \underline{\Phi}) &= F_s(\underline{\Phi}^* + \delta\underline{\Phi}^*, \underline{\Phi} + \delta\underline{\Phi}) - F_s(\underline{\Phi}^*, \underline{\Phi}) \\
&= \frac{(\underline{\Phi}^* + \delta\underline{\Phi}^*)^T \underline{\underline{L}}(\underline{\Phi} + \delta\underline{\Phi})}{(\underline{\Phi}^* + \delta\underline{\Phi}^*)^T \underline{\underline{M}}(\underline{\Phi} + \delta\underline{\Phi})} - \frac{\underline{\Phi}^{*T} \underline{\underline{L}} \underline{\Phi}}{\underline{\Phi}^{*T} \underline{\underline{M}} \underline{\Phi}} \\
&= \frac{\underline{\Phi}^{*T} \underline{\underline{L}}\, \underline{\Phi} + \underline{\Phi}^{*T} \underline{\underline{L}}\, \delta\underline{\Phi} + \delta\underline{\Phi}^{*T} \underline{\underline{L}}\, \underline{\Phi} + O(\delta)^2}{\underline{\Phi}^{*T} \underline{\underline{M}}\, \underline{\Phi} + \underline{\Phi}^{*T} \underline{\underline{M}}\, \delta\underline{\Phi} + \delta\underline{\Phi}^{*T} \underline{\underline{M}}\, \underline{\Phi} + O(\delta)^2} - \frac{\underline{\Phi}^{*T} \underline{\underline{L}} \underline{\Phi}}{\underline{\Phi}^{*T} \underline{\underline{M}} \underline{\Phi}} \\
&= \frac{\underline{\Phi}^{*T} \underline{\underline{L}}\, \underline{\Phi} + \underline{\Phi}^{*T} \underline{\underline{L}}\, \delta\underline{\Phi} + \delta\underline{\Phi}^{*T} \underline{\underline{L}}\, \underline{\Phi}}{\underline{\Phi}^{*T} \underline{\underline{M}}\, \underline{\Phi} \left(1 + \dfrac{\underline{\Phi}^{*T} \underline{\underline{M}}\, \delta\underline{\Phi} + \delta\underline{\Phi}^{*T} \underline{\underline{M}}\, \underline{\Phi}}{\underline{\Phi}^{*T} \underline{\underline{M}}\, \underline{\Phi}}\right)} - \frac{\underline{\Phi}^{*T} \underline{\underline{L}} \underline{\Phi}}{\underline{\Phi}^{*T} \underline{\underline{M}} \underline{\Phi}} \\
&= \left(F_s + \frac{\underline{\Phi}^{*T} \underline{\underline{L}}\, \delta\underline{\Phi} + \delta\underline{\Phi}^{*T} \underline{\underline{L}}\, \underline{\Phi}}{\underline{\Phi}^{*T} \underline{\underline{M}}\, \underline{\Phi}}\right)\left(1 - \frac{\underline{\Phi}^{*T} \underline{\underline{M}}\, \delta\underline{\Phi} + \delta\underline{\Phi}^{*T} \underline{\underline{M}}\, \underline{\Phi}}{\underline{\Phi}^{*T} \underline{\underline{M}}\, \underline{\Phi}} + O(\delta)^2\right) - F_s \\
&= \frac{\underline{\Phi}^{*T} \underline{\underline{L}}\, \delta\underline{\Phi} + \delta\underline{\Phi}^{*T} \underline{\underline{L}}\, \underline{\Phi}}{\underline{\Phi}^{*T} \underline{\underline{M}}\, \underline{\Phi}} - \frac{F_s\left(\underline{\Phi}^{*T} \underline{\underline{M}}\, \delta\underline{\Phi} + \delta\underline{\Phi}^{*T} \underline{\underline{M}}\, \underline{\Phi}\right)}{\underline{\Phi}^{*T} \underline{\underline{M}}\, \underline{\Phi}} + O(\delta)^2 \\
&= \frac{\delta\underline{\Phi}^{*T}\left(\underline{\underline{L}}\, \underline{\Phi} - \dfrac{1}{\lambda} \underline{\underline{M}}\, \underline{\Phi}\right) + \delta\underline{\Phi}^{T}\left(\underline{\underline{L}}^T\, \underline{\Phi}^* - \dfrac{1}{\lambda} \underline{\underline{M}}^T\, \underline{\Phi}^*\right)}{\underline{\Phi}^{*T} \underline{\underline{M}}\, \underline{\Phi}} .
\end{aligned} \tag{2.28}$$

From the last line of Eq. (2.28), requiring the first-order variation of the functional F_S to vanish for completely arbitrary $\delta\underline{\Phi}^*$ and $\delta\underline{\Phi}$ produces the following equations

$$\underline{\underline{L}}\,\underline{\Phi} - \frac{1}{\lambda}\underline{\underline{M}}\,\underline{\Phi} = 0\,, \tag{2.29}$$

$$\underline{\underline{L}}^T\,\underline{\Phi}^* - \frac{1}{\lambda}\underline{\underline{M}}^T\,\underline{\Phi}^* = 0\,. \tag{2.30}$$

The fact that Eq. (2.29) is identical to Eq. (2.17) proves that, indeed, the first-order variation of the functional F_S defined by Eq. (2.27) is made stationary by the finite-difference nodal balance equation. Moreover, the variational principle suggests that the weight function should be the solution of Eq. (2.30), the **adjoint** nodal balance equation.

One may question the significance of the variational approach because requiring δF_s to vanish merely leads back to the same finite-difference nodal balance equation. The answer lies in the fact that the space of functions $\underline{\Phi}$ considered in Eq. (2.28) contains the correct solution as one of its elements. If space of expansion functions which does not contain the correct solution, such as Eq. (2.26), is considered, and if the variational principle is applied to such a limited space, the solution that makes the first-order variation vanish will yield a close approximation to $1/\lambda_o$, the fundamental eigenvalue, obtainable from that limited space[1] .

Eq. (2.26) can be expressed more compactly using the following matrix notation

$$\underline{\Phi} \approx \underline{\underline{\Psi}}\,\underline{T}\,, \tag{2.31}$$

where

$\underline{\underline{\Psi}}$ = NG by KP expansion function matrix,

$\underline{T}$ = mixing coefficient column vector of length KP,

P = number of expansion functions.

Similarly, the adjoint weight function can be expressed as the following

---

1 We cannot say that the procedure will yield "the closest approximation" to the fundamental eigenvalue since the functional will not generally assume a minimum value at its stationary point. Instead the stationary point will have more the nature of a point of inflection. That is, if a limited subspace of expansion functions not containing the true flux shape is examined and a vector out of that subspace is found that makes the first-order variation of the functional stationary, it will not in general yield the best value of the fundamental eigenvalue obtainable using expansion functions from the subspace. There will be other vectors in the limited subspace that will yield more accurate value of the fundamental eigenvalue, however no systematic way to find these vectors is known [H-2]. Yet, this is not a great concern since the same equation can be derived using the weighted residual method. Also, practical experience indicates that the approximated eigenvalue is almost always a close approximation to the true, fundamental eigenvalue.

$$\underline{\Phi}^{*} \approx \underline{\underline{\Psi}}^{*}\,\underline{T}^{*}\,. \tag{2.32}$$

Substituting Eq. (2.31) and Eq. (2.32) into Eq. (2.28) and requiring the first-order variation to vanish for arbitrary $\delta\underline{\Phi}^{*}$ yields

$$\delta F_s(\underline{\Phi}^{*},\underline{\Phi}) = \delta\underline{T}^{*T}\underline{\underline{\Psi}}^{*T}\left(\underline{\underline{L}}\,\underline{\underline{\Psi}}\,\underline{T} - \frac{1}{\lambda}\underline{\underline{M}}\,\underline{\underline{\Psi}}\,\underline{T}\right) = 0. \tag{2.33}$$

Finally, the discontinuous synthesis equation containing the mixing coefficients as the unknowns is

$$\left[\underline{\underline{\Psi}}^{*T}\underline{\underline{L}}\,\underline{\underline{\Psi}}\right]\underline{T} = \frac{1}{\lambda}\left[\underline{\underline{\Psi}}^{*T}\underline{\underline{M}}\,\underline{\underline{\Psi}}\right]\underline{T}\,. \tag{2.34}$$

A similar derivation of the adjoint synthesis equation is possible, but it is of no interest because the objective of this thesis is to synthesize the neutron flux shape, not the adjoint shape. The adjoint weight functions and expansion functions will be determined from separate calculations using the CONQUEST code [G-1].

2.5 CMFD Discontinuity Factor Updating Schemes

As defined in Section 2.3.2, the CMFD discontinuity factors can be determined from a reference solution which provides the node-averaged fluxes, the surface-averaged fluxes and the surface-averaged currents. However, this approach is self-defeating in that there is no incentive to solve the finite-difference nodal balance equation if a more accurate reference solution is already available. Solving the finite-difference nodal balance equation merely reproduces the exact reference solution without adding any additional information. Therefore, unless there are other schemes to calculate the CMFD discontinuity factors more efficiently, the nodal theory is a purely academic proposition without much practical significance.

Two different CMFD discontinuity factor updating schemes, which do not require expensive reference calculations, are introduced in this section. One is called a **discontinuity factor synthesis** scheme and the other a **non-linear iteration** scheme.

2.5.1 CMFD Discontinuity Factor Synthesis Scheme

In a fashion analogous to the flux synthesis scheme, the CMFD discontinuity factor can also be synthesized using the following equation [K-1]

$$f_{gu\pm}^{ijk} = \frac{\sum_{p=f(k)}^{h(k)} \zeta_{gu\pm}^{ij,p} \left| T_g^{k,p} \right|}{\sum_{p=f(k)}^{h(k)} \left| T_g^{k,p} \right|}, \qquad u \equiv x, y, z, \tag{2.35}$$

where $\zeta_{gu\pm}^{ij,p}$ are the predetermined CMFD discontinuity factors associated with the expansion functions $\psi_g^{ij,p}$. This scheme is based on the observation that the CMFD discontinuity factors reflect the changes in the flux shape. Thus, if a particular linear combination of known expansion functions closely reproduces the true flux shape, it is physically plausible to expect that the same linear combination of the CMFD discontinuity factors associated with the expansion functions be a good approximation to the true CMFD discontinuity factors. Of course, this justification lacks a firm theoretical basis, but the computational accuracy obtained using this scheme is encouraging [K-1]. Moreover, the computational time, compared with the non-linear iteration scheme introduced in the following section, is minimal.

2.5.2 Non-Linear Iteration Scheme

The application of a non-linear iteration scheme requires an additional nodal coupling equation, which even with an assembly-size node without the introduction of the CMFD discontinuity factors would result in a very accurate evaluation of node-averaged fluxes, surface-averaged fluxes and surface-averaged currents. The polynomial nodal theory, which represents the flux as a quartic polynomial, is adopted for this purpose. The derivation shown in this section closely follows the presentation given in J. Gehin's thesis [G-1].

2.5.2.a Transverse-Integration Procedure

Three coupled, one-dimensional equations are obtained by integrating the neutron diffusion equation in the direction transverse to the direction of interest. This is accomplished by operating on Eq. (2.2a) and Eq. (2.2b) with

$$\frac{1}{h_v^m h_w^n} \int_{v_m}^{v_{m+1}} dv \int_{w_n}^{w_{n+1}} dw \,. \tag{2.36}$$

Thus, a one-dimensional equation in the direction u is obtained by integrating Eq. (2.2a) and Eq. (2.2b) over a node in the direction v and w. The result is

$$\frac{d}{du}J_{gu}^{mn}(u)+\Sigma_{tg}^{lmn}\phi_{gu}^{mn}(u)=\sum_{g'=1}^{G}\left[\frac{1}{\lambda}\chi_g\upsilon\Sigma_{fg'}^{lmn}+\Sigma_{gg'}^{lmn}\right]-S_{gu}^{mn}(u)\,, \tag{2.37a}$$

$$J_{gu}^{mn}(u)=-D_g^{lmn}\frac{d}{du}\phi_{gu}^{mn}(u)\,,\qquad u\equiv x,y,z, \tag{2.37b}$$

where

$$S_{gu}^{mn}(u)=\frac{1}{h_v^m}L_{gv}^{mn}(u)+\frac{1}{h_w^n}L_{gw}^{mn}(u)\,,$$

$$L_{gv}^{mn}(u)=\frac{1}{h_w^n}\int_{w_n}^{w_{n+1}}dw\left[J_{gv}(u,v_{m+1},w)-J_{gv}(u,v_m,w)\right],$$

$$L_{gw}^{mn}(u)=\frac{1}{h_v^m}\int_{v_m}^{v_{m+1}}dv\left[J_{gw}(u,v,w_{n+1})-J_{gw}(u,v,w_n)\right].$$

The transversely-integrated equations (2.37a) and (2.37b) can be combined to obtain a system of ordinary, second-order, inhomogeneous differential equations with constant coefficients. If these equations are solved analytically, the Analytical Nodal Method developed by K. Smith [S-2] results. The resulting solution, however, is rather complicated and for practical application is limited to two energy groups.

An alternate approach is to assume that the transversely-integrated fluxes have a polynomial form and to apply a weighted residual procedure to determine the polynomial coefficients [F-1]. If the transversely-integrated flux can be adequately represented by a low-order polynomial, relatively simply expressions result. Moreover, because the equations for each energy group can be treated separately, generalization to more energy groups is straightforward. For these reasons, the polynomial expansion procedure along with a weighted residual method is adopted.

2.5.2.b Polynomial Expansion

The transversely-integrated flux is approximated by a truncated polynomial

$$\phi_{gu}^{mn}(u)\approx\sum_{p=0}^{P}a_{gup}^{lmn}f_p\left(\frac{u-u_l}{h_u^l}\right)\,,\qquad u\in\left[u_l,u_{l+1}\right]. \tag{2.38}$$

Previous applications of polynomial methods [F-1] have shown that at least a fourth-order polynomial is required to obtain acceptable results for light water reactor applications. Further approximation involving the transverse leakage term, which is to be discussed later, limit the accuracy such that using polynomials higher than fourth-order is not warranted. For the case of a quartic polynomial approximation, the basis functions are defined by [F-1,Z-1]

$$f_0(\xi) = 1\,, \tag{2.39a}$$

$$f_1(\xi) = \xi - \frac{1}{2}\,, \tag{2.39b}$$

$$f_2(\xi) = 3\xi^2 - 3\xi + \frac{1}{2}\,, \tag{2.39c}$$

$$f_3(\xi) = \xi(1-\xi)(\xi - \frac{1}{2})\,, \tag{2.39d}$$

$$f_4(\xi) = \xi(1-\xi)(\xi^2 - \xi + \frac{1}{5})\,. \tag{2.39e}$$

These polynomials are chosen such that

$$\int_0^1 f_p(\xi)d\xi = \begin{cases} 1, & p = 0 \\ 0, & p = 1,2,3,4 \end{cases}. \tag{2.40}$$

In addition, the higher-order basis functions are required to satisfy

$$f_p(0) = f_p(1) = 0, \quad p = 3,4\,. \tag{2.41}$$

This constraint on the higher-order expansion functions is convenient because it leads to expressions which relate the node-averaged and the surface-averaged fluxes only to the first three expansion coefficients.

Several key quantities of interest, namely the node-averaged flux, the surface-averaged flux and the surface-averaged current, are evaluated in terms of the polynomial expansion coefficients by manipulating equations (2.38) through (2.41):

$$\bar{\phi}_g^{lmn} = a_{gu0}^{lmn}\,, \tag{2.42a}$$

$$\phi_{gu}^{mn}(u_{l+1}^-) = a_{gu0}^{lmn} + \frac{1}{2}a_{gu1}^{lmn} + \frac{1}{2}a_{gu2}^{lmn}\,, \tag{2.42b}$$

$$\phi_{gu}^{mn}(u_l^+) = a_{gu0}^{lmn} - \frac{1}{2}a_{gu1}^{lmn} + \frac{1}{2}a_{gu2}^{lmn}\,, \tag{2.42c}$$

$$J_{gu}^{mn}(u_{l+1}) = -\frac{D_g^{lmn}}{h_u^l}\left[a_{gu1}^{lmn} + 3a_{gu2}^{lmn} - \frac{1}{2}a_{gu3}^{lmn} - \frac{1}{5}a_{gu4}^{lmn}\right], \tag{2.42d}$$

$$J_{gu}^{mn}(u_l) = -\frac{D_g^{lmn}}{h_u^l}\left[a_{gu1}^{lmn} - 3a_{gu2}^{lmn} - \frac{1}{2}a_{gu3}^{lmn} + \frac{1}{5}a_{gu4}^{lmn}\right]. \qquad (2.42e)$$

The polynomial expansion coefficients are determined by solving the two-node problem shown in Figure 2.1. The goal in solving this two-node problem is the determination of the surface-averaged current at the interface of the two nodes in terms of the node-averaged fluxes. This will result in a more accurate nodal coupling relation than the finite-difference nodal coupling equation with unity CMFD discontinuity factor ratios.

For this two-node problem, there are five unknown polynomial expansion coefficients for each node and energy group. As Eq. (2.42a) shows, the first polynomial expansion coefficient is the node-averaged flux, leaving four unknown polynomial expansion coefficients for each node and energy group. Thus, eight equations are required for each energy group to completely specify the coefficients. The equations which will be used are:

1. nodal balance equation for each node, (2)
2. continuity of current at the interface, (1)
3. continuity of flux at the interface, (1)
4. two weighted residual equations for each node. (4)

The numbers in parenthesis indicate the number of equations that results from each condition.

2.5.2.c Weighted Residual Procedure

Two equations for each node in the two-node problem are provided by a weighted residual procedure. Because the truncated polynomial cannot match the exact solution of the transversely-integrated diffusion equation, an alternate approach is to require it to satisfy the equation in a weighted-integral sense. The weight functions can be chosen arbitrarily, but two different methods are generally used: Galerkin Weighting, where the polynomials are weighted by themselves; and moments weighting, where polynomials of increasing order are used successively as weight functions. Previous applications of polynomial nodal methods have shown that moments weighting is superior [F-1].

The first step in the weighted residual procedure is to multiply Eq. (2.37a) by a weight function $w_p(u)$ and integrate over the node. The resulting equation is

$$\left\langle w_p(u), \frac{d}{du} J_{gu}^{mn}(u) \right\rangle + \frac{D_g^{lmn}}{\left(h_u^l\right)^2} \sum_{g'=1}^{G} \left(\kappa_u^2\right)_{gg'}^{lmn} \phi_{g'up}^{lmn} + S_{gup}^{lmn} = 0 , \tag{2.43}$$

where the brackets indicate inner products as in the following definitions

$$\phi_{gup}^{lmn} \equiv \left\langle w_p(u), \phi_{gu}^{mn}(u) \right\rangle \equiv \frac{1}{h_u^l} \int_{u_l}^{u_{l+1}} w_p(u) \phi_{gu}^{mn}(u) du , \tag{2.44a}$$

$$S_{gup}^{lmn} \equiv \left\langle w_p(u), S_{gu}^{mn}(u) \right\rangle , \tag{2.44b}$$

and

$$\left(\kappa_u^2\right)_{gg'}^{lmn} \equiv \frac{\left(h_u^l\right)^2}{D_g^{lmn}} \left[\Sigma_{tg}^{lmn} \delta_{gg'} - \Sigma_{gg'}^{lmn} - \frac{1}{\lambda} \Sigma_{fg'}^{lmn} \right] . \tag{2.44c}$$

For moments weighting, the weight functions are given by

$$w_1(u) = f_1\left(\frac{u-u_l}{h_u^l}\right) = \left(\frac{u-u_l}{h_u^l}\right) - \frac{1}{2} , \tag{2.45a}$$

$$w_2(u) = f_2\left(\frac{u-u_l}{h_u^l}\right) = 3\left(\frac{u-u_l}{h_u^l}\right)^2 - 3\left(\frac{u-u_l}{h_u^l}\right) + \frac{1}{2} . \tag{2.45b}$$

Substituting the polynomial approximation into Eq. (2.44a) and performing the necessary integration result in the following first and second flux moments

$$\phi_{gu1}^{lmn} = \frac{1}{12} a_{gu1}^{lmn} + \frac{1}{120} a_{gu3}^{lmn} , \tag{2.46a}$$

$$\phi_{gu2}^{lmn} = \frac{1}{20} a_{gu2}^{lmn} + \frac{1}{700} a_{gu4}^{lmn} . \tag{2.46b}$$

In a similar fashion, the first and second current-derivative moments are obtained by substituting the polynomial approximation into Eq. (2.37b) and evaluating the inner products

$$\left\langle w_1(u), \frac{d}{du} J_{gu}^{mn}(u) \right\rangle = \frac{1}{2} \frac{D_g^{lmn}}{\left(h_u^l\right)^2} a_{gu3}^{lmn} , \tag{2.47a}$$

$$\left\langle w_2(u), \frac{d}{du} J_{gu}^{mn}(u) \right\rangle = \frac{1}{5} \frac{D_g^{lmn}}{\left(h_u^l\right)^2} a_{gu4}^{lmn} . \tag{2.47b}$$

The evaluation of the transverse-leakage moments requires more information because the variation of the transverse leakage within a node in the u-direction is not known. The most common manner of treating this spatial dependence is the quadratic transverse-leakage approximation [B-1]. In this approximation, the u-directed transverse leakage is expressed in a quadratic polynomial which preserves the node-averaged transverse leakages in the node of interest and its two neighbors in the u-direction. The quadratic transverse leakage has the following form for an interior node

$$S_{gu}^{mn}(u) = \overline{S}_{gu}^{lmn} + \left(\overline{S}_{gu}^{l-1,mn} - \overline{S}_{gu}^{lmn}\right)\rho_{u_l}^{l-1}(u) + \left(\overline{S}_{gu}^{l+1,mn} - \overline{S}_{gu}^{lmn}\right)\rho_{u_l}^{l+1}(u)\,, \tag{2.48}$$

where the u-direction node-averaged transverse leakage for node (l,m,n) is given by

$$\overline{S}_{gu}^{lmn} = \frac{1}{h_u^l}\int_{u_l}^{u_{l+1}} S_{gu}^{mn}(u)du\,, \tag{2.49}$$

and the quadratic polynomials are

$$\rho_{u_l}^{l-1}(u) = a_{u_l}^{-} + b_{u_l}^{-}\left(\frac{u-u_l}{h_u^l}\right) + c_{u_l}^{-}\left(\frac{u-u_l}{h_u^l}\right)^2\,, \tag{2.50a}$$

$$\rho_{u_l}^{l+1}(u) = a_{u_l}^{+} + b_{u_l}^{+}\left(\frac{u-u_l}{h_u^l}\right) + c_{u_l}^{+}\left(\frac{u-u_l}{h_u^l}\right)^2\,. \tag{2.50b}$$

The coefficients of these polynomials are determined by requiring that the quadratic form preserve the node-averaged transverse leakages in the three adjacent nodes. The resulting coefficients $a_{u_l}^{\pm}$, $b_{u_l}^{\pm}$, and $c_{u_l}^{\pm}$, depend only on the node widths. The complete specifications of these coefficients, including those in the boundary nodes, and the transverse-leakage moments are given in Appendix A. The resulting evaluation of the transverse-leakage moments for an interior node is

$$S_{gu1}^{lmn} = \frac{1}{12}\left[(b_{u_l}^{-} + c_{u_l}^{-})\overline{S}_{gu}^{l-1,mn} - (b_{u_l}^{-} + b_{u_l}^{+} + c_{u_l}^{-} + c_{u_l}^{+})\overline{S}_{gu}^{lmn} + (b_{u_l}^{+} + c_{u_l}^{+})\overline{S}_{gu}^{l+1,mn}\right], \tag{2.51a}$$

$$S_{gu2}^{lmn} = \frac{1}{60}\left[c_{u_l}^{-}\overline{S}_{gu}^{l-1,mn} - (c_{u_l}^{-} + c_{u_l}^{+})\overline{S}_{gu}^{lmn} + c_{u_l}^{+}\overline{S}_{gu}^{l+1,mn}\right]. \tag{2.51b}$$

Substituting Eqs. (2.46a), (2.46b), (2.47a) and (2.47b) into Eq. (2.43) results in the following two weighted residual equations

$$\frac{1}{2}a_{gu3}^{lmn} + \frac{1}{12}\sum_{g'=1}^{G}\left(\kappa_u^2\right)_{gg'}^{lmn}\left[a_{g'u1}^{lmn} + \frac{1}{10}a_{g'u3}^{lmn}\right] + \frac{\left(h_u^l\right)^2}{D_g^{lmn}}S_{gu1}^{lmn} = 0\,, \tag{2.52a}$$

$$\frac{1}{5}a_{gu4}^{lmn}+\frac{1}{20}\sum_{g'=1}^{G}\left(\kappa_u^2\right)_{gg'}^{lmn}\left[a_{g'u2}^{lmn}+\frac{1}{35}a_{g'u4}^{lmn}\right]+\frac{\left(h_u^l\right)^2}{D_g^{lmn}}S_{gu2}^{lmn}=0\,. \tag{2.52b}$$

Before continuing, a discussion of the errors introduced by the quadratic leakage approximation, Eq. (2.48), and the choice of the fourth-order polynomial is pertinent. The error introduced by the quadratic leakage approximation is expected to be of the same order as a third-order polynomial approximation for the transversely-integrated flux because the leakages are related to the currents which are in turn related to the spatial derivative of the flux. Hence, the leakages for a third-order polynomial approximation have a quadratic form. Because the magnitude of the leakage terms are typically smaller than that of the currents, errors in the leakages should be smaller than and less significant than the errors in the currents. Therefore, the use of a quartic polynomial approximation seems to be a reasonable choice with the quadratic transverse-leakage approximation [G-1].

Empirical evidence also supports this choice. A convergence analysis of a two-dimensional, homogenous, bare-core problem performed by M. Zerkle [Z-1] shows that the spatial discretization errors in k_{eff} (λ) is $O(h^4)$ for both the cubic and quartic polynomial methods. A subsequent one-dimensional analysis, however, indicates that in the absence of the transverse-leakage approximation the quartic approximation has a truncation error of $O(h^6)$ while the cubic error remains $O(h^4)$. The comparison of the one-dimensional to the two-dimensional result suggests that the quadratic transverse-leakage approximation introduces an error of $O(h^4)$ and this error is more significant than the quartic polynomial approximation error.

2.5.2.d Expansion Coefficient Solution

The expansion for the two-node problem has eight unknown expansion coefficients per energy group. The complete set of equations for a given interface is:

1. nodal balance equation for node *l-1*:

$$6a_{gu2}^{l-1,mn}-\frac{2}{5}a_{gu4}^{l-1,mn}=\sum_{g'=1}^{G}\left(\kappa_u^2\right)_{gg'}^{l-1,mn}\bar{\phi}_{g'}^{l-1,mn}+\frac{\left(h_u^{l-1}\right)^2}{D_g^{l-1,mn}}\bar{S}_{gu}^{l-1,mn}\,. \tag{2.53}$$

   This is an alternate form of the nodal balance represented by Eq. (2.5) and is obtained by using the weight function $w_o = 1$ in Eq. (2.43).

2. first moment equation for node *l-1*:

$$\frac{1}{2}a_{gu3}^{l-1,mn}+\frac{1}{12}\sum_{g'=1}^{G}\left(\kappa_u^2\right)_{gg'}^{l-1,mn}\left[a_{g'u1}^{l-1,mn}+\frac{1}{10}a_{g'u3}^{l-1,mn}\right]=-\frac{\left(h_u^{l-1}\right)^2}{D_g^{l-1,mn}}S_{gu1}^{l-1,mn}\,. \tag{2.54}$$

3. second moment equation for node *l-1*:

$$\frac{1}{5}a_{gu4}^{l-1,mn}+\frac{1}{20}\sum_{g'=1}^{G}\left(\kappa_u^2\right)_{gg'}^{l-1,mn}\left[a_{g'u2}^{l-1,mn}+\frac{1}{35}a_{g'u4}^{l-1,mn}\right]=-\frac{\left(h_u^{l-1}\right)^2}{D_g^{l-1,mn}}S_{gu2}^{l-1,mn}\,. \tag{2.55}$$

4. nodal balance equation for node *l*:

$$6a_{gu2}^{lmn}-\frac{2}{5}a_{gu4}^{lmn}=\sum_{g'=1}^{G}\left(\kappa_u^2\right)_{gg'}^{lmn}\bar{\phi}_{g'}^{lmn}+\frac{\left(h_u^{l}\right)^2}{D_g^{lmn}}\bar{S}_{gu}^{lmn}\,. \tag{2.56}$$

5. first moment equation for node *l*:

$$\frac{1}{2}a_{gu3}^{lmn}+\frac{1}{12}\sum_{g'=1}^{G}\left(\kappa_u^2\right)_{gg'}^{lmn}\left[a_{g'u1}^{lmn}+\frac{1}{10}a_{g'u3}^{lmn}\right]=-\frac{\left(h_u^{l}\right)^2}{D_g^{lmn}}S_{gu1}^{lmn}\,. \tag{2.57}$$

6. second moment equation for node *l*:

$$\frac{1}{5}a_{gu4}^{lmn}+\frac{1}{20}\sum_{g'=1}^{G}\left(\kappa_u^2\right)_{gg'}^{lmn}\left[a_{g'u2}^{lmn}+\frac{1}{35}a_{g'u4}^{lmn}\right]=-\frac{\left(h_u^{l}\right)^2}{D_g^{lmn}}S_{gu2}^{lmn}\,. \tag{2.58}$$

7. continuity of flux at the node interface:

$$\left(\bar{\phi}_g^{l-1,mn}+\frac{1}{2}a_{gu1}^{l-1,mn}+\frac{1}{2}a_{gu2}^{l-1,mn}\right)\mathbf{f}_{gu+}^{l-1,mn}=\left(\bar{\phi}_g^{lmn}-\frac{1}{2}a_{gu1}^{lmn}+\frac{1}{2}a_{gu2}^{lmn}\right)\mathbf{f}_{gu-}^{lmn}\,. \tag{2.59}$$

Note that the discontinuity factors introduced in this equation, $\mathbf{f}_{gu+}^{l-1,mn}$ and $\mathbf{f}_{gu-}^{lmn}$, are different from the CMFD discontinuity factors. As for the finite-difference equation, these discontinuity factors can be used to correct for spatial, homogenization and diffusion theory errors. Because the quartic polynomial approximation leads to small spatial errors, their primary purpose is to provide homogenization correction. Generally, these discontinuity factors will be constant throughout the entire calculation.

8. continuity of the current at the node interface:

$$-\frac{D_g^{l-1,mn}}{h_u^{l-1}}\left[a_{gu1}^{l-1,mn}+3a_{gu2}^{l-1,mn}-\frac{1}{2}a_{gu3}^{l-1,mn}-\frac{1}{5}a_{gu4}^{l-1,mn}\right]= \\ -\frac{D_g^{lmn}}{h_u^{l}}\left[a_{gu1}^{lmn}-3a_{gu2}^{lmn}-\frac{1}{2}a_{gu3}^{lmn}+\frac{1}{5}a_{gu4}^{lmn}\right]. \tag{2.60}$$

These equations represents a $8G$ by $8G$ coupled system of equations which would be very time-consuming to solve, especially for a large number of energy groups. With further manipulation, however, the solution procedure can be simplified [G-1]. Note that the nodal balance equation and the second moment equation for each node consist of only the even expansion coefficients and are not coupled to the other node. Thus, by solving the nodal balance equation, Eq. (2.56), for a_{gu2}^{lmn} and substituting it into the second moment equation, Eq. (2.58), a_{gu2}^{lmn} and a_{gu4}^{lmn} are obtained with one G by G solution. Next, the continuity conditions, Eqs. (2.59) and (2.60), can be used to obtain $a_{gu1}^{l-1,mn}$ and a_{gu1}^{lmn} in terms of $a_{gu3}^{l-1,mn}$ and a_{gu3}^{lmn}. These expressions can then be substituted into the first moment equations, Eqs. (2.54) and (2.57), to obtain a $2G$ by $2G$ equations for $a_{gu3}^{l-1,mn}$ and a_{gu3}^{lmn}. Thus, the $8G$ by $8G$ problem can be reduced to one G by G and one $2G$ by $2G$ problem per interface.

The coupling relations for the polynomial nodal method are simply the surface averaged current expressions given in Eqs. (2.42d) and (2.42e). Because of their complicated nature, they cannot be easily combined with the nodal balance equation to form a single nodal equation as in the finite-difference method.

2.5.2.e Boundary Conditions

The boundary conditions applied to the polynomial equations are a generalization of those applied to the finite-difference equation, Eq. (2.18), and are given by

$$\phi_{gu}^{mn}(u_s)=\hat{l}\cdot\hat{n}\sum_{g'=1}^{G}\Gamma_{gg'u\pm}^{mn}J_{g'u}^{mn}(u_s). \tag{2.61}$$

Note that if the off-diagonal elements of $\Gamma_{gg'u\pm}^{mn}$ are zero, Eq. (2.61) reverts back to the same form as in Eq. (2.18). Substituting the polynomial expansion approximations of the surface-averaged flux and current results in the following equation at the lower boundary surface

$$\left[\bar{\phi}_g^{lmn} - \frac{1}{2}a_{gu1}^{lmn} + \frac{1}{2}a_{gu2}^{lmn}\right]\mathbf{f}_{gu-}^{lmn} = \sum_{g'=1}^{G}\Gamma_{gg'u-}^{mn}\frac{D_{g'}^{lmn}}{h_u^l}\left[a_{g'u1}^{lmn} - 3a_{g'u2}^{lmn} - \frac{1}{2}a_{g'u3}^{lmn} + \frac{1}{5}a_{g'u4}^{lmn}\right], \quad (2.62)$$

and at the upper boundary surface

$$\left[\bar{\phi}_g^{lmn} + \frac{1}{2}a_{gu1}^{lmn} + \frac{1}{2}a_{gu2}^{lmn}\right]\mathbf{f}_{gu+}^{lmn} = -\sum_{g'=1}^{G}\Gamma_{gg'u+}^{mn}\frac{D_{g'}^{lmn}}{h_u^l}\left[a_{g'u1}^{lmn} + 3a_{g'u2}^{lmn} - \frac{1}{2}a_{g'u3}^{lmn} - \frac{1}{5}a_{g'u4}^{lmn}\right]. \quad (2.63)$$

These equations are combined with the other expansion coefficient equations given in Section 2.5.2.d to form the complete set of equations for nodes at the boundaries.

2.5.2.f Non-Linear Iteration Procedure

Eqs. (2.53) through (2.60), including the node-averaged flux as an unknown, can be solved as a complete set. The system of equations having the polynomial expansion coefficients as the unknowns, however, is quite large and complex because of both spatial and energy coupling terms. The non-linear iteration scheme was first introduced by K. Smith [S-3] as an efficient way of solving the polynomial nodal equations. The scheme takes advantage of the property of the finite-difference nodal method in which any reference solution can be exactly replicated if appropriate CMFD discontinuity factors are provided. By solving the finite-difference nodal equation and the polynomial nodal equations in a iterative manner, a significant reduction in storage and computing time can be realized.

The crux of the non-linear iteration procedure is that the CMFD discontinuity factor ratios, defined in Section 2.3.2, are updated using the node-averaged fluxes obtained by solving the finite-difference nodal equation and the surface-averaged currents obtained by solving the polynomial nodal equations. The uniqueness of the solution of the nodal equations guarantees that if this scheme converges, if will converge to the solution of the polynomial nodal equations. The non-linear scheme adopted in this thesis utilizes exactly the same procedure except that the node-averaged fluxes are found by solving the discontinuous synthesis equation rather than the finite-difference equation.

A flow diagram of the non-linear iteration scheme is shown in Figure 2.2. Beginning with an initial guess for the CMFD discontinuity factor ratios, the discontinuous synthesis equation can be solved to compute the node-averaged fluxes. These fluxes are then used in the polynomial equations to calculate the expansion coefficients and, hence the currents at the interface. From these polynomial currents and

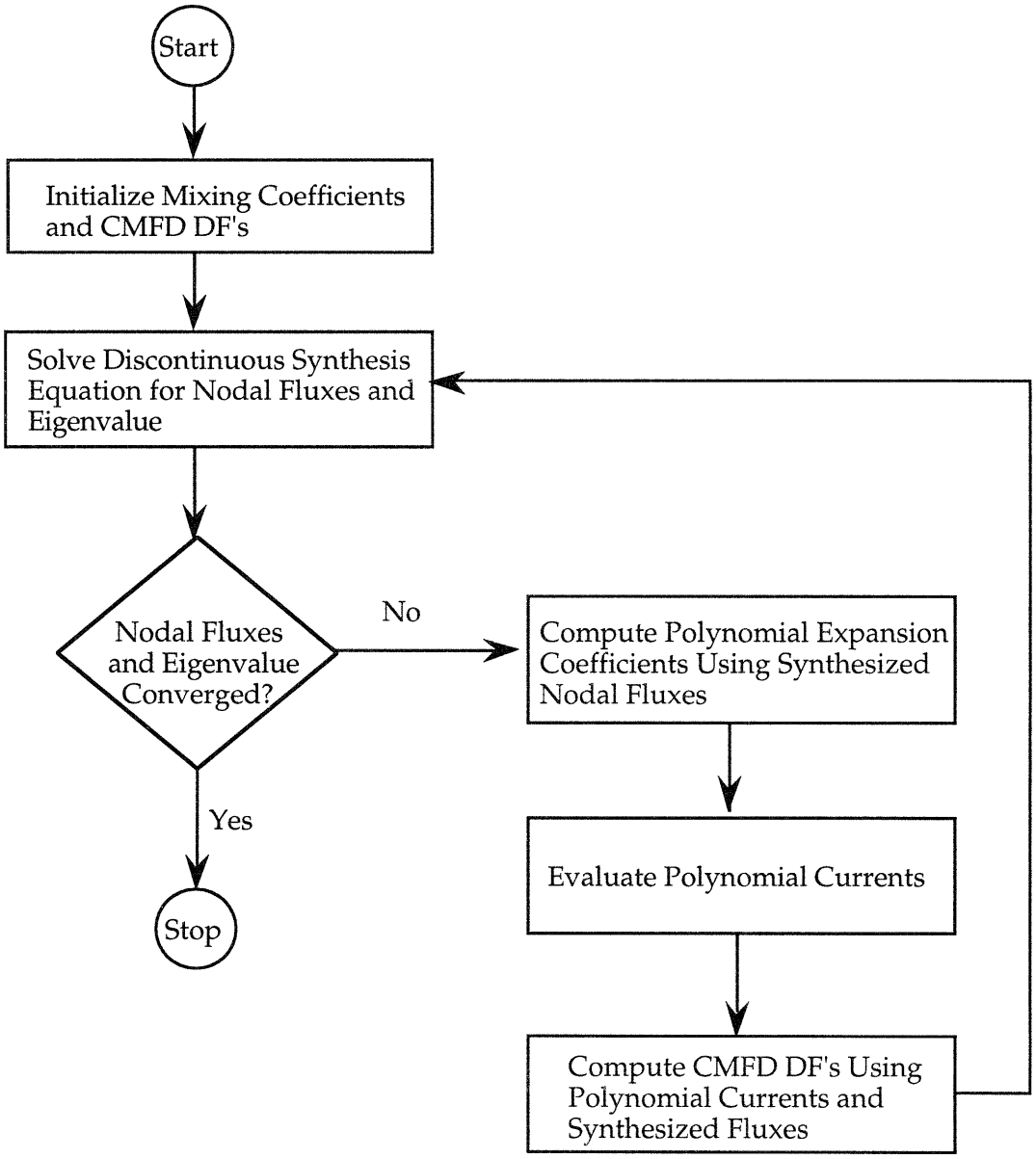

Figure 2.2: Non-linear iteration flow diagram.

the synthesized node-averaged fluxes, discontinuity factor ratios may be computed. These discontinuity factor ratios are in turn used in the discontinuous synthesis equation and the process is repeated until the node-averaged fluxes converge.

2.6 Summary

The derivation of the discontinuous nodal synthesis method is presented in this chapter. A variational principle is applied to the finite-difference nodal equation to achieve the derivation. In addition to providing the discontinuous synthesis equation, the variational principle suggests that the solution of the adjoint nodal equation be used as the weight function. Two different CMFD discontinuity factor (the equivalence parameter which corrects for the errors in spatial, homogenization and diffusion theory errors) updating schemes are also presented in this chapter. The CMFD discontinuity factor synthesis scheme, based on physical intuition, is simple and efficient, but lacks a firm theory. On the other hand, the non-linear iteration scheme, in which the discontinuous synthesis solution is forced to match a more accurate quartic polynomial solution, has a concrete theoretical basis, but even with the simplified solution procedure described in Section 2.5.2.d, it is much more complex and time-consuming than the CMFD discontinuity factor synthesis scheme.

CHAPTER 3

TRANSIENT NODAL SYNTHESIS METHOD

3.1 Introduction

The transient nodal synthesis method is presented in this chapter. As in the steady-state case, the derivation starts from the time-dependent, finite-difference nodal equation. A functional, for which the first-order variation is made stationary by the time-dependent, finite-difference nodal equation, is then introduced, and the same variational procedure is applied for the derivation of the transient nodal synthesis method. Although, not implemented in this thesis, the implications of using different number of expansion functions at different time steps and of allowing flux and adjoint expansion functions change at the same time are discussed in light of the variational principle. Next, the same CMFD discontinuity factor updating schemes used in the steady-state case are reiterated. The same non-linear iteration procedure described in Chapter 2 is used with the introduction of dynamic frequencies and modified cross sections while the CMFD discontinuity factor synthesis scheme is applied without any modification. Finally, the WIGL thermal hydraulic and a linear cross section feedback model as well as a cusping correction model are presented.

3.2 Time-Dependent, Finite-Difference Nodal Equation

The derivation of the time-dependent, finite-difference nodal equation starts from the time-dependent, few-group diffusion equations [H-2]

$$\frac{1}{v_g}\frac{\partial}{\partial t}\phi_g(\boldsymbol{r},t) = -\nabla\cdot J_g(\boldsymbol{r},t) - \Sigma_{tg}(\boldsymbol{r},t)\phi_g(\boldsymbol{r},t)$$
$$+\sum_{g'=1}^{G}\left[(1-\beta)\chi_{pg}\upsilon\Sigma_{fg'}(\boldsymbol{r},t) + \Sigma_{gg'}(\boldsymbol{r},t)\right]\phi_{g'}(\boldsymbol{r},t) \qquad (3.1a)$$
$$+\sum_{d=1}^{D}\chi_{dg}\lambda_d c_d(\boldsymbol{r},t)\,,$$

$$J_g(\boldsymbol{r},t) = -D_g(\boldsymbol{r},t)\nabla\phi_g(\boldsymbol{r},t)\,, \qquad g=1,2,...,G \qquad (3.1b)$$

$$\frac{\partial}{\partial t}c_d(\boldsymbol{r},t) = \beta_d\sum_{g'=1}^{G}\upsilon\Sigma_{fg'}(\boldsymbol{r},t)\phi_{g'}(\boldsymbol{r},t) - \lambda_d c_d(\boldsymbol{r},t)\,, \quad d=1,2,...,D, \qquad (3.1c)$$

where in addition to the quantities defined in Section 2.2

D	=	total number of delayed neutron precursor families,
v_g	=	neutron speed for group g,
χ_{pg}	=	prompt fission spectrum for group g,
χ_{dg}	=	delayed neutron spectrum for precursor family d, group g,
λ_d	=	decay constant for precursor family d,
c_d	=	density of delayed neutron precursor family d,
β_d	=	fractional yield of delayed neutron family d,
β	=	total fractional yield of delayed neutrons, $\beta = \sum_{d=1}^{D}\beta_d$.

As in the steady-state case, the time-dependent nodal balance equation is obtained by integrating Eqs. (3.1a) and (3.1c) over the volume of node (i,j,k) and then dividing by the nodal volume

$$\frac{1}{v_g}\frac{d}{dt}\bar{\phi}_g^{ijk}(t) = -\frac{1}{h_x^i}\left[J_{gx}^{jk}(x_{i+1},t) - J_{gx}^{jk}(x_i,t)\right] - \frac{1}{h_y^j}\left[J_{gy}^{ik}(y_{j+1},t) - J_{gy}^{ik}(y_j,t)\right]$$
$$-\frac{1}{h_z^k}\left[J_{gz}^{ij}(z_{k+1},t) - J_{gz}^{ij}(z_k,t)\right] - \Sigma_{tg}^{ijk}(t)\bar{\phi}_g^{ijk}(t) \qquad (3.2a)$$
$$+\sum_{g'=1}^{G}\left[(1-\beta)\chi_{pg}\Sigma_{fg'}^{ijk}(t) + \Sigma_{gg'}^{ijk}(t)\right]\bar{\phi}_{g'}^{ijk}(t) + \sum_{d=1}^{D}\chi_{dg}\lambda_d\bar{c}_d^{ijk}(t),$$

$$\frac{d}{dt}\bar{c}_d^{ijk}(t) = \beta_d \sum_{g'=1}^{G} \upsilon\Sigma_{fg'}^{ijk}(t)\bar{\phi}_{g'}^{ijk}(t) - \lambda_d \bar{c}_d^{ijk}(t). \tag{3.2b}$$

The same definitions given in Section 2.2 apply to the node-averaged flux and the surface-averaged current, and the cross sections represent averages over the node. In addition, the node-averaged precursor density is defined by

$$\bar{c}_d^{ijk}(t) \equiv \frac{1}{V^{ijk}} \int_{x_i}^{x_{i+1}} dx \int_{y_j}^{y_{j+1}} dy \int_{z_k}^{z_{k+1}} dz\, c_d(x,y,z). \tag{3.3}$$

The time-dependent, finite-difference nodal coupling equation, relating surface-averaged currents to node-averaged fluxes, is exactly same as the steady-state case because the time derivative in Eq. (3.1b) is neglected. Thus, the coupling equation for node interface u_l is

$$J_{gu}^{mn}(u_l,t) = -\left[\frac{h_u^l}{2D_g^{lmn}(t)}\frac{f_{gu-}^{lmn}(t)}{f_{gu+}^{l-1,mn}(t)} + \frac{h_u^{l-1}}{2D_g^{l-1,mn}(t)}\right]^{-1}\left(\frac{f_{gu-}^{lmn}(t)}{f_{gu+}^{l-1,mn}(t)}\bar{\phi}_g^{lmn}(t) - \bar{\phi}_g^{l-1,mn}(t)\right). \tag{3.4}$$

Except that the CMFD discontinuity factor and cross sections are time-dependent, Eq. (3.4) is exactly same as Eq. (2.14). Substituting Eq. (3.4) and the similar coupling equation for the node interface u_{l+1} into Eq.(3.2a) leads to the following time-dependent, finite-difference nodal balance equation in matrix form.

$$\begin{aligned}\frac{1}{\underline{\underline{V}}_g^{-1}}\frac{d}{dt}\underline{\phi}_g(t) = &-\underline{\underline{N}}_g(t)\underline{\phi}_g(t) + \sum_{g'=1}^{G}(1-\beta)\underline{\underline{F}}_{p,gg'}(t)\underline{\phi}_{g'}(t) \\ &+ \sum_{\substack{g'=1 \\ g'\neq g}}^{G}\underline{\underline{\Sigma}}_{gg'}(t)\underline{\phi}_{g'}(t) + \sum_{d=1}^{D}\lambda_d \underline{c}_{dg}(t),\end{aligned} \tag{3.5a}$$

$$\frac{d}{dt}\underline{c}_{dg}(t) = \beta_d \sum_{g'=1}^{G}\underline{\underline{F}}_{d,gg'}(t)\underline{\phi}_{g'}(t) - \lambda_d \underline{c}_{dg}(t), \qquad d = 1,2,\ldots,D, \tag{3.5b}$$

where in addition to the terms defined in Section 2.3

$\underline{\underline{V}}_g$ = N by N diagonal matrix containing neutron group speed $\{v_g\}$,

$\underline{\underline{F}}_{p,gg'}$ = N by N diagonal matrix containing $\{\chi_{pg}\upsilon\Sigma_{fg'}^{ijk}\}$,

$\underline{\underline{F}}_{d,gg'}$ = N by N diagonal matrix containing $\{\chi_{dg}\upsilon\Sigma_{fg'}^{ijk}\}$,

$\underline{c}_{dg}$ = column vector of length N containing $\left\{\chi_{dg}\bar{c}_d^{ijk}\right\}$.

Eqs. (3.5a) and (3.5b) can be simplified further by suppressing the group dependence using super-matrix notations

$$\underline{\underline{V}}^{-1}\frac{d}{dt}\underline{\Phi}(t)=\left[\underline{\underline{M}}_p(t)-\underline{\underline{L}}(t)\right]\underline{\Phi}(t)+\sum_{d=1}^{D}\lambda_d\underline{c}_d(t), \tag{3.6a}$$

$$\frac{d}{dt}\underline{c}_d(t)=\underline{\underline{M}}_d(t)\underline{\Phi}(t)-\lambda_d\underline{c}_d(t), \quad d=1,2,\ldots,D, \tag{3.6b}$$

where in addition to the terms defined for the steady-state case

$\underline{\underline{V}}$ = NG by NG diagonal matrix containing $\left\{\underline{\underline{V}}_g\right\}$,

$\underline{\underline{M}}_p$ = NG by NG prompt fission matrix containing $\left\{\underline{\underline{F}}_{p,gg'}\right\}$,

$\underline{\underline{M}}_d$ = NG by NG delayed fission matrix containing $\left\{\underline{\underline{F}}_{d,gg'}\right\}$,

$\underline{c}_d$ = column vector of length NG containing $\left\{\underline{c}_{dg}\right\}$.

3.3 Discontinuous, Time-Dependent Synthesis Equation

The extension of the spatially discontinuous synthesis concept into time domain leads to the **discontinuous space-time dependent synthesis** method. As spatially discontinuous expansion functions are allowed in the steady-state case, temporally discontinuous expansion functions reduce the computational requirement without seriously compromising accuracy. Adopting discontinuous synthesis in time domain allows the flexibility to drop or add the expansion functions during transients. A set of expansion functions used in the beginning of a transient may be replaced by another set at a later stage to reflect the changes in reactor conditions. The discontinuous space-time dependent synthesis adopted in this thesis has the following form

$$\phi_g^{ijk}(t)\approx\sum_{p=f(k,t)}^{h(k,t)}\psi_g^{ij,p}T_g^{k,p}(t)\,, \tag{3.7}$$

where $f(k,t)$ and $h(k,t)$ represent the axial and temporal dependence of the expansion functions. Although different expansion functions may be permitted at different time steps, **their total number will be kept constant**. Eq. (3.7) can be expressed compactly using matrix notation

$$\underline{\Phi}(t) \approx \underline{\underline{\Psi}}^{n}\underline{T}(t)\,, \tag{3.8}$$

where superscript n represents the temporal dependence of the expansion functions.

The functional used for the discontinuous, time-dependent synthesis derivation has the following form

$$F_t(\underline{\Phi}^{*}(t),\underline{c}_1^{*}(t),\cdots,\underline{c}_D^{*}(t),\underline{\Phi}(t),\underline{c}_1(t),\cdots,\underline{c}_D(t)) \;=$$

$$\int_{t_o}^{t_f} dt \begin{pmatrix} \underline{\Phi}^{*T}(t) \\ \underline{c}_1^{*T}(t) \\ \vdots \\ \underline{c}_D^{*T}(t) \end{pmatrix}^T \begin{pmatrix} \underline{\underline{M}}_p(t) - \underline{\underline{L}}(t) - \underline{\underline{V}}^{-1}\dfrac{d}{dt} & \lambda_1 & \cdots & \lambda_D \\ \underline{\underline{M}}_1(t) & -\lambda_1 - \dfrac{d}{dt} & \cdots & 0 \\ \vdots & \vdots & \ddots & \vdots \\ \underline{\underline{M}}_D(t) & 0 & \cdots & -\lambda_D - \dfrac{d}{dt} \end{pmatrix} \begin{pmatrix} \underline{\Phi}(t) \\ \underline{c}_1(t) \\ \vdots \\ \underline{c}_D(t) \end{pmatrix}$$

$$- \begin{pmatrix} \underline{\Phi}^{*T}(t_o) \\ \underline{c}_1^{*T}(t_o) \\ \vdots \\ \underline{c}_D^{*T}(t_o) \end{pmatrix}^T \begin{pmatrix} \underline{\underline{V}}^{-1}\{\underline{\Phi}(t_o) - \underline{\Phi}_o\} \\ \underline{c}_1(t_o) - \underline{c}_{1o} \\ \vdots \\ \underline{c}_D(t_o) - \underline{c}_{Do} \end{pmatrix} + \begin{pmatrix} \underline{\Phi}_f^{*T} \\ \underline{c}_{1f}^{*T} \\ \vdots \\ \underline{c}_{Df}^{*T} \end{pmatrix}^T \begin{pmatrix} \underline{\underline{V}}^{-1}\underline{\Phi}(t_f) \\ \underline{c}_1(t_f) \\ \vdots \\ \underline{c}_D(t_f) \end{pmatrix} \tag{3.9}$$

$$-\frac{1}{2}\left\{\underline{\Phi}^{*T}(t_n^+) + \underline{\Phi}^{*T}(t_n^-)\right\}\underline{\underline{V}}^{-1}\left\{\underline{\Phi}(t_n^+) - \underline{\Phi}(t_n^-)\right\} - \sum_{d=1}^{D}\frac{1}{2}\left\{\underline{c}_d^{*T}(t_n^+) + \underline{c}_d^{*T}(t_n^-)\right\}\left\{\underline{c}_d(t_n^+) - \underline{c}_d(t_n^-)\right\}.$$

The t_o and tf represent the initial and final time, respectively, and t_n represents the times when the space of functions considered are discontinuous. Also, The superscript + and - represent the positive and negative side of time discontinuity t_n. In addition, the subscript o and f in the second and third term of Eq. (3.9) symbolize the initial and final condition, specified by users, respectively. The first-order variation of the functional is then

$$\delta F_t = \int_{t_o}^{t_f} dt \begin{pmatrix} \delta\underline{\Phi}^{*T}(t) \\ \delta\underline{c}_1^{*T}(t) \\ \vdots \\ \delta\underline{c}_D^{*T}(t) \end{pmatrix}^T \begin{pmatrix} \underline{\underline{M}}_p(t) - \underline{\underline{L}}(t) - \underline{\underline{V}}^{-1}\dfrac{d}{dt} & \lambda_1 & \cdots & \lambda_D \\ \underline{\underline{M}}_1(t) & -\lambda_1 - \dfrac{d}{dt} & \cdots & 0 \\ \vdots & \vdots & \ddots & \vdots \\ \underline{\underline{M}}_D(t) & 0 & \cdots & -\lambda_D - \dfrac{d}{dt} \end{pmatrix} \begin{pmatrix} \underline{\Phi}(t) \\ \underline{c}_1(t) \\ \vdots \\ \underline{c}_D(t) \end{pmatrix}$$

$$+\int_{t_o}^{t_f} dt \begin{pmatrix} \underline{\Phi}^{*T}(t) \\ \underline{c}_1^{*T}(t) \\ \vdots \\ \underline{c}_D^{*T}(t) \end{pmatrix}^T \begin{pmatrix} \underline{\underline{M}}_p(t) - \underline{\underline{L}}(t) - \underline{\underline{V}}^{-1}\frac{d}{dt} & \lambda_1 & \cdots & \lambda_D \\ \underline{\underline{M}}_1(t) & -\lambda_1 - \frac{d}{dt} & \cdots & 0 \\ \vdots & \vdots & \ddots & \vdots \\ \underline{\underline{M}}_D(t) & 0 & \cdots & -\lambda_D - \frac{d}{dt} \end{pmatrix} \begin{pmatrix} \delta\underline{\Phi}(t) \\ \delta\underline{c}_1(t) \\ \vdots \\ \delta\underline{c}_D(t) \end{pmatrix}$$

$$-\begin{pmatrix} \delta\underline{\Phi}^{*T}(t_o) \\ \delta\underline{c}_1^{*T}(t_o) \\ \vdots \\ \delta\underline{c}_D^{*T}(t_o) \end{pmatrix}^T \begin{pmatrix} \underline{\underline{V}}^{-1}\{\underline{\Phi}(t_o) - \underline{\Phi}_o\} \\ \underline{c}_1(t_o) - \underline{c}_{1o} \\ \vdots \\ \underline{c}_D(t_o) - \underline{c}_{Do} \end{pmatrix} - \begin{pmatrix} \underline{\Phi}^{*T}(t_o) \\ \underline{c}_1^{*T}(t_o) \\ \vdots \\ \underline{c}_D^{*T}(t_o) \end{pmatrix}^T \begin{pmatrix} \underline{\underline{V}}^{-1}\delta\underline{\Phi}(t_o) \\ \delta\underline{c}_1(t_o) \\ \vdots \\ \delta\underline{c}_D(t_o) \end{pmatrix} + \begin{pmatrix} \underline{\Phi}_f^{*T} \\ \underline{c}_{1f}^{*T} \\ \vdots \\ \underline{c}_{Df}^{*T} \end{pmatrix}^T \begin{pmatrix} \underline{\underline{V}}^{-1}\delta\underline{\Phi}(t_f) \\ \delta\underline{c}_1(t_f) \\ \vdots \\ \delta\underline{c}_D(t_f) \end{pmatrix}$$

$$-\frac{1}{2}\left\{\delta\underline{\Phi}^{*T}(t_n^+) + \delta\underline{\Phi}^{*T}(t_n^-)\right\}\underline{\underline{V}}^{-1}\left\{\underline{\Phi}(t_n^+) - \underline{\Phi}(t_n^-)\right\}$$
$$-\frac{1}{2}\left\{\underline{\Phi}^{*T}(t_n^+) + \underline{\Phi}^{*T}(t_n^-)\right\}\underline{\underline{V}}^{-1}\left\{\delta\underline{\Phi}(t_n^+) - \delta\underline{\Phi}(t_n^-)\right\} \tag{3.10}$$

$$-\sum_{d=1}^{D}\frac{1}{2}\left\{\delta\underline{c}_d^{*T}(t_n^+) + \delta\underline{c}_d^{*T}(t_n^-)\right\}\left\{\underline{c}_d(t_n^+) - \underline{c}_d(t_n^-)\right\}$$
$$-\sum_{d=1}^{D}\frac{1}{2}\left\{\underline{c}_d^{*T}(t_n^+) + \underline{c}_d^{*T}(t_n^-)\right\}\left\{\delta\underline{c}_d(t_n^+) - \delta\underline{c}_d(t_n^-)\right\} + O(\delta)^2.$$

The time derivative term, $\int_{t_o}^{t_f}\underline{\Phi}^{*T}(t)\underline{\underline{V}}^{-1}\frac{d}{dt}\delta\underline{\Phi}(t)$, in Eq. (3.10) becomes

$$\int_{t_o}^{t_f}\underline{\Phi}^{*T}(t)\underline{\underline{V}}^{-1}\frac{d}{dt}\delta\underline{\Phi}(t) = \int_{t_o}^{t_f}\frac{d}{dt}\left\{\underline{\Phi}^{*T}(t)\underline{\underline{V}}^{-1}\delta\underline{\Phi}(t)\right\} - \int_{t_o}^{t_f}\delta\underline{\Phi}^{T}(t)\underline{\underline{V}}^{-1}\frac{d}{dt}\underline{\Phi}^{*}(t)$$

$$= \underline{\Phi}^{*T}(t_f)\underline{\underline{V}}^{-1}\delta\underline{\Phi}(t_f) - \underline{\Phi}^{*T}(t_n^+)\underline{\underline{V}}^{-1}\delta\underline{\Phi}(t_n^+) + \underline{\Phi}^{*T}(t_n^-)\underline{\underline{V}}^{-1}\delta\underline{\Phi}(t_n^-)$$
$$-\underline{\Phi}^{*T}(t_o)\underline{\underline{V}}^{-1}\delta\underline{\Phi}(t_o) - \int_{t_o}^{t_f}\delta\underline{\Phi}^{T}(t)\underline{\underline{V}}^{-1}\frac{d}{dt}\underline{\Phi}^{*}(t). \tag{3.11}$$

Similarly, the time derivatives involving weighted precursor densities become

$$\int_{t_o}^{t_f}\underline{c}_d^{*T}(t)\frac{d}{dt}\delta\underline{c}_d(t) = \underline{c}_d^{*T}(t_f)\delta\underline{c}_d(t_f) - \underline{c}_d^{*T}(t_n^+)\delta\underline{c}_d(t_n^+) + \underline{c}_d^{*T}(t_n^-)\delta\underline{c}_d(t_n^-)$$
$$-\underline{c}_d^{*T}(t_o)\delta\underline{c}_d(t_o) - \int_{t_o}^{t_f}\delta\underline{c}_d^{T}(t)\frac{d}{dt}\underline{c}_d^{*}(t). \tag{3.12}$$

With the substitution of Eqs. (3.11) and (3.12) into Eq. (3.10), the first-order variation of the functional leads to the following expression after some algebraic manipulations

$$\delta F_t = \int_{t_o}^{t_f} dt \begin{pmatrix} \delta\underline{\Phi}^{*T}(t) \\ \delta\underline{c}_1^{*T}(t) \\ \vdots \\ \delta\underline{c}_D^{*T}(t) \end{pmatrix}^T \begin{pmatrix} \underline{\underline{M}}_p(t) - \underline{\underline{L}}(t) - \underline{\underline{V}}^{-1}\frac{d}{dt} & \lambda_1 & \cdots & \lambda_D \\ \underline{\underline{M}}_1(t) & -\lambda_1 - \frac{d}{dt} & \cdots & 0 \\ \vdots & \vdots & \ddots & \vdots \\ \underline{\underline{M}}_D(t) & 0 & \cdots & -\lambda_D - \frac{d}{dt} \end{pmatrix} \begin{pmatrix} \underline{\Phi}(t) \\ \underline{c}_1(t) \\ \vdots \\ \underline{c}_D(t) \end{pmatrix}$$

$$+ \int_{t_o}^{t_f} dt \begin{pmatrix} \delta\underline{\Phi}^{T}(t) \\ \delta\underline{c}_1^{T}(t) \\ \vdots \\ \delta\underline{c}_D^{T}(t) \end{pmatrix}^T \begin{pmatrix} \underline{\underline{M}}_p^T(t) - \underline{\underline{L}}^T(t) + \underline{\underline{V}}^{-1}\frac{d}{dt} & \underline{\underline{M}}_1^T(t) & \cdots & \underline{\underline{M}}_D^T(t) \\ \lambda_1 & -\lambda_1 + \frac{d}{dt} & \cdots & 0 \\ \vdots & \vdots & \ddots & \vdots \\ \lambda_D & 0 & \cdots & -\lambda_D + \frac{d}{dt} \end{pmatrix} \begin{pmatrix} \underline{\Phi}^*(t) \\ \underline{c}_1^*(t) \\ \vdots \\ \underline{c}_D^*(t) \end{pmatrix}$$

$$+\delta\underline{\Phi}^{*T}(t_o)\underline{\underline{V}}^{-1}\left\{\underline{\Phi}_o - \underline{\Phi}(t_o)\right\} + \sum_{d=1}^{D} \delta\underline{c}_d^{*T}(t_o)\left\{\underline{c}_{do} - \underline{c}_d(t_o)\right\}$$
$$+\delta\underline{\Phi}^{T}(t_f)\underline{\underline{V}}^{-1}\left\{\underline{\Phi}^*_f - \underline{\Phi}^*(t_f)\right\} + \sum_{d=1}^{D} \delta\underline{c}_d^{T}(t_f)\left\{\underline{c}^*_{df} - \underline{c}^*_d(t_f)\right\} \tag{3.13}$$

$$-\frac{1}{2}\left\{\delta\underline{\Phi}^{*T}(t_n^+) + \delta\underline{\Phi}^{*T}(t_n^-)\right\}\underline{\underline{V}}^{-1}\left\{\underline{\Phi}(t_n^+) - \underline{\Phi}(t_n^-)\right\}$$
$$-\frac{1}{2}\sum_{d=1}^{D}\left\{\delta\underline{c}_d^{*T}(t_n^+) + \delta\underline{c}_d^{*T}(t_n^-)\right\}\left\{\underline{c}_d(t_n^+) - \underline{c}_d(t_n^-)\right\}$$
$$+\frac{1}{2}\left\{\delta\underline{\Phi}^{T}(t_n^+) + \delta\underline{\Phi}^{T}(t_n^-)\right\}\underline{\underline{V}}^{-1}\left\{\underline{\Phi}^*(t_n^+) - \underline{\Phi}^*(t_n^-)\right\}$$
$$+\frac{1}{2}\sum_{d=1}^{D}\left\{\delta\underline{c}_d^{T}(t_n^+) + \delta\underline{c}_d^{T}(t_n^-)\right\}\left\{\underline{c}^*_d(t_n^+) - \underline{c}^*_d(t_n^-)\right\}.$$

Now, requiring Eq. (3.13) to vanish for arbitrary $\delta\underline{\Phi}^*$ and $\delta\underline{c}_d^*$ should reproduce the time-dependent, finite-difference nodal equation, Eqs. (3.6a) and (3.6b). Indeed, this is true from the first term of Eq. (3.13). Furthermore, Eq. (3.13) reveals other relations that the space of functions must obey. From the third and fourth term, the following initial conditions are apparent

$$\underline{\Phi}(t_o) = \underline{\Phi}_o, \tag{3.14a}$$

$$\underline{c}_d(t_o) = \underline{c}_{do}. \tag{3.14b}$$

These relations specify the initial conditions. The seventh and eighth term of Eq. (3.13) lead to the time continuity conditions, and they are

$$\underline{\Phi}(t_n^+) = \underline{\Phi}(t_n^-), \tag{3.15a}$$

$$\underline{c}_d(t_n^+) = \underline{c}_d(t_n^-). \tag{3.15b}$$

In fact, Eq. (3.15a) are obtained twice if the variations $\delta\underline{\Phi}^*(t_n^+)$ and $\delta\underline{\Phi}^*(t_n^-)$ are treated as independent. Also, a similar statement can be made about Eq. (3.15b). This redundancy does not cause any trouble at this point. The variational procedure selects only continuous functions among a generally discontinuous space of functions. As long as the continuity conditions are satisfied, one can be indifferent as to whether $\delta\underline{\Phi}^*(t_n^+)$ and $\delta\underline{\Phi}^*(t_n^-)$ are independent variations or not. The redundancy, however, foreshadows over-determination difficulties in the synthesis approximation for which the space of functions considered do not include continuous functions [S-4].

In addition to the time-dependent, finite-difference nodal equation and its initial and continuity conditions, Eq. (3.13) reveals what the weigh function should be. Namely, requiring Eq. (3.13) to vanish for arbitrary $\delta\underline{\Phi}$ and $\delta\underline{c}_d$ leads to the time-dependent, finite-difference, adjoint nodal equation and its final and continuity conditions. However, the time-dependent adjoint equation is of no interest in this thesis of which the goal is to synthesize the flux shape, not the adjoint shape. From a precise theoretical standpoint, the solution of the time-dependent adjoint equation should be used as the weight function because that is what the variational procedure suggests. However, this is very undesirable from a practical standpoint. It is expensive to solve the time-dependent adjoint equation, requiring as much computational time as solving the time-dependent nodal equation. For this reason, this thesis resort to the **steady-state adjoint solution** as the weight function even in the time-dependent synthesis scheme.

Similar to Eq. (3.8), the adjoint weight function can be expressed as the following

$$\underline{\Phi}^*(t) \approx \underline{\underline{\Psi}}^{*n}\underline{T}^*(t)\,, \tag{3.16}$$

where, again, the superscript n represents the temporal dependence of the weight function. Substituting Eqs. (3.8) and (3.16) into Eq. (3.13) and requiring the first-order variation to vanish for arbitrary variations $\delta\underline{\Phi}^*$ and $\delta\underline{c}_d^*$ result in the discontinuous synthesis equation. The first term in Eq. (3.13) becomes

$$\begin{pmatrix} \delta\underline{T}^{*T}(t)\underline{\underline{\Psi}}^{*nT} \\ \delta\underline{c}_1^{*T}(t) \\ \vdots \\ \delta\underline{c}_D^{*T}(t) \end{pmatrix}^T \begin{pmatrix} \underline{\underline{M}}_p(t) - \underline{\underline{L}}(t) - \underline{\underline{V}}^{-1}\frac{d}{dt} & \lambda_1 & \cdots & \lambda_D \\ \underline{\underline{M}}_1(t) & -\lambda_1 - \frac{d}{dt} & \cdots & 0 \\ \vdots & \vdots & \ddots & \vdots \\ \underline{\underline{M}}_D(t) & 0 & \cdots & -\lambda_D - \frac{d}{dt} \end{pmatrix} \begin{pmatrix} \underline{\underline{\Psi}}^n\underline{T}(t) \\ \underline{c}_1(t) \\ \vdots \\ \underline{c}_D(t) \end{pmatrix}, \quad (3.17)$$

and it has to vanish. Therefore, within the continuous time domain where both expansion and weight functions do not change, the synthesis equation is

$$\underline{\underline{\Psi}}^{*nT}\underline{\underline{V}}^{-1}\underline{\underline{\Psi}}^n\frac{d}{dt}\underline{T}(t) = \underline{\underline{\Psi}}^{*nT}\left[\underline{\underline{M}}_p(t) - \underline{\underline{L}}(t)\right]\underline{\underline{\Psi}}^n\underline{T}(t) + \underline{\underline{\Psi}}^{*nT}\sum_{d=1}^{D}\lambda_d\underline{c}_d(t), \quad (3.18a)$$

$$\frac{d}{dt}\underline{c}_d(t) = \underline{\underline{M}}_d(t)\underline{\underline{\Psi}}^n\underline{T}(t) - \lambda_d\underline{c}_d(t), \quad d = 1,2,...,D. \quad (3.18b)$$

Similarly, the seventh term leads to

$$\underline{\underline{\Psi}}^{*n+1T}\underline{\underline{V}}^{-1}\left\{\underline{\underline{\Psi}}^{n+1}\underline{T}(t_n^+) - \underline{\underline{\Psi}}^n\underline{T}(t_n^-)\right\} = 0, \quad (3.19a)$$

and

$$\underline{\underline{\Psi}}^{*nT}\underline{\underline{V}}^{-1}\left\{\underline{\underline{\Psi}}^{n+1}\underline{T}(t_n^+) - \underline{\underline{\Psi}}^n\underline{T}(t_n^-)\right\} = 0. \quad (3.19b)$$

Now, the over-determination difficulty is apparent. While the number of unknowns is *KP*, there are *2KP* equations to satisfy. This difficulty can be overcome by requiring that the expansion and adjoint weight functions not be discontinuous at the same time. The adjoint weight function does not have to be continuous throughout the entire time domain, but it has to be when the flux expansion function is discontinuous. Thus, in this case, if $\underline{\underline{\Psi}}^{*n+1} = \underline{\underline{\Psi}}^{*n}$ at time t_n, the over-determination problem vanishes and the continuity condition is given by

$$\underline{\underline{\Psi}}^{*nT}\underline{\underline{V}}^{-1}\underline{\underline{\Psi}}^{n+1}\underline{T}(t_n^+) = \underline{\underline{\Psi}}^{*nT}\underline{\underline{V}}^{-1}\underline{\underline{\Psi}}^n\underline{T}(t_n^-). \quad (3.20)$$

Another possible way to bypass this over-determination problem is to solve Eqs. (3.19a) and (3.19b) in a least-square sense. Although the physical meaning of the least-square solution is not clear in this case, there exist, nonetheless, a well established mathematical procedure. This thesis adopts the former approach to overcome the over-determination difficulty. Furthermore, the adjoint weight function is **kept constant throughout a transient**. Unlike the point kinetics approach which assumes that the initial flux shape

persists throughout a transient, the discontinuous synthesis allows different flux shapes at different time steps, and therefore, the error associated with a particular choice of weight function is expected to be small.

The third term of Eq. (3.13) leads to the following initial condition

$$\underline{\underline{\Psi}}^{*T}\underline{\underline{V}}^{-1}\underline{\underline{\Psi}}^{n_0}\underline{T}(t_o)=\underline{\underline{\Psi}}^{*T}\underline{\underline{V}}^{-1}\underline{\Phi}_o, \tag{3.21}$$

where the temporal dependence of the adjoint weight function is suppressed in light of the assumption mentioned in the previous paragraph. A closer examination of Eq. (3.21) shows that this initial condition is a specialized case of the continuity condition given by Eq. (3.20). For example, if one wants to use a set of expansion functions, $\underline{\underline{\Psi}}^{s}$, for the steady-state synthesis solution and another set for the transient synthesis solution, Eq. (3.21) becomes

$$\underline{\underline{\Psi}}^{*T}\underline{\underline{V}}^{-1}\underline{\underline{\Psi}}^{n_0}\underline{T}(t_o)=\underline{\underline{\Psi}}^{*T}\underline{\underline{V}}^{-1}\underline{\underline{\Psi}}^{s}\underline{T}_s,$$

very similar to the continuity equation given by Eq. (3.20).

The initial and continuity conditions on the weighted precursor density are the same as given by Eqs. (3.14b) and (3.15b). Unlike the nodal flux, the space of functions considered for the weighted precursor density is not limited by the synthesis approximation, and therefore, the same initial and continuity conditions are applicable for all variations of $\underline{c}_d^*$ values.

Before finalizing the time-dependent synthesis equation, let us consider what happens if the number of expansion functions are changed in light of the variation procedure. First of all, Eq. (3.18a), in its time-discretized form, becomes either over- or under-determined system of equations and, so does Eq. (3.20). These equations could be solved in a least-square sense, but the computational complexity and expense are enormous. If the adjoint weight functions and the flux expansion functions are allowed to be discontinuous at the same time and their numbers are kept same, the over- and under-determination difficulty in Eq. (3.18a) disappears. The time-continuity relation, however, still retains the over-determination problem as shown in Eqs. (3.19a) and (3.19b). Therefore, one cannot avoid solving either an under- or over-determined system of equations if the number of expansion functions are allowed to change from one time step to the next. For this reason, the number of expansion functions is kept constant in the development of the time-dependent synthesis method in this thesis.

The complete set of the time-dependent synthesis equations derived with the assumptions of (1) continuous, initial adjoint weight functions throughout a transient and (2) a constant number of flux expansion functions is then:

1. within the continuous time domain where the flux expansion function do not change:

$$\underline{\underline{\Psi}}^{*T}\underline{\underline{V}}^{-1}\underline{\underline{\Psi}}\frac{d}{dt}\underline{T}(t)=\underline{\underline{\Psi}}^{*T}\left[\underline{\underline{M}}_p(t)-\underline{\underline{L}}(t)\right]\underline{\underline{\Psi}}\underline{T}(t)+\underline{\underline{\Psi}}^{*T}\sum_{d=1}^{D}\lambda_d\underline{c}_d(t), \tag{3.22a}$$

$$\frac{d}{dt}\underline{c}_d(t)=\underline{\underline{M}}_d(t)\underline{\underline{\Psi}}\underline{T}(t)-\lambda_d\underline{c}_d(t), \quad d=1,2,...,D. \tag{3.22b}$$

2. initial conditions on the mixing coefficients and the weighted precursor densities:

$$\underline{\underline{\Psi}}^{*T}\underline{\underline{V}}^{-1}\underline{\underline{\Psi}}^{n_o}\underline{T}(t_o)=\underline{\underline{\Psi}}^{*T}\underline{\underline{V}}^{-1}\underline{\Phi}_o, \tag{3.23a}$$

$$\underline{c}_d(t_o)=\underline{c}_{do}. \tag{3.23b}$$

3. continuity conditions on the mixing coefficients and the weighted precursor densities when the flux expansion functions are discontinuous:

$$\underline{\underline{\Psi}}^{*T}\underline{\underline{V}}^{-1}\underline{\underline{\Psi}}^{n+1}\underline{T}(t_n^+)=\underline{\underline{\Psi}}^{*T}\underline{\underline{V}}^{-1}\underline{\underline{\Psi}}^{n}\underline{T}(t_n^-), \tag{3.24a}$$

$$\underline{c}_d(t_n^+)=\underline{c}_d(t_n^-). \tag{3.24b}$$

3.4 CMFD Discontinuity Factor Updating Schemes

The same CMFD discontinuity factor updating schemes, introduced in Chapter 2, are reiterated in this section. The discontinuity factor synthesis scheme assumes the exact same form as in the steady-state case. The non-linear iteration scheme, however, is applied with modified cross sections as a result of the introduction of dynamic frequencies. This approach is necessary if one wants to avoid solving time-dependent, polynomial nodal equations.

3.4.1 CMFD Discontinuity Factor Synthesis Scheme

The time-dependent CMFD discontinuity factor synthesis scheme has the exact same form as given in Eq. (2.35). A linear combination of the predetermined CMFD discontinuity factors associated with the expansion functions selected for a particular transient is assumed to represent closely the true CMFD discontinuity factors. Eq. (2.35) can be rewritten with the time dependence explicitly shown

$$f_{gu\pm}^{ijk}(t) = \frac{\sum_{p=f(k,t)}^{h(k,t)} \zeta_{gu\pm}^{ij,p} \left| T_g^{k,p}(t) \right|}{\sum_{p=f(k,t)}^{h(k,t)} \left| T_g^{k,p}(t) \right|}, \quad u \equiv x,y,z. \tag{3.25}$$

3.4.2 Non-Linear Iteration Scheme

The same transverse integration procedure introduced in Chapter 2 is applied to Eq. (3.1a) to obtain one-dimensional equations. Integrating Eq. (3.1a) in the direction v and w for node (l,m,n) leads to

$$\begin{aligned} \frac{1}{v_g}\frac{\partial}{\partial t}\phi_{gu}^{mn}(u,t) = &-\frac{\partial}{\partial u}J_{gu}^{mn}(u,t) - \Sigma_{tg}^{lmn}(t)\phi_{gu}^{mn}(u,t) \\ &+\sum_{g'=1}^{G}\left[(1-\beta)\chi_{pg}\upsilon\Sigma_{fg'}^{lmn}(t) + \Sigma_{gg'}^{lmn}(t)\right]\phi_{g'u}^{mn}(u,t) \\ &+\sum_{d=1}^{D}\chi_{dg}\lambda_d c_{du}^{mn}(u,t) - S_{gu}^{mn}(u,t), \qquad g = 1,2,\ldots,G, \end{aligned} \tag{3.26a}$$

$$\frac{\partial}{\partial t}c_{du}^{mn}(u,t) = \beta_d\sum_{g'=1}^{G}\upsilon\Sigma_{fg'}^{lmn}(t)\phi_{g'u}^{mn}(u,t) - \lambda_d c_{du}^{mn}(u,t), \qquad d = 1,2,\ldots,D. \tag{3.26b}$$

The time derivatives in these equations present a difficulty. They require the equations to be differenced in time and past values of the expansion coefficients to be saved from one time step to the next [G-1]. Also, the transverse integration procedure has led to the directionally-dependent precursor densities, $c_{du}^{mn}(u,t)$. Eqs. (3.26a) and (3.26b) can be simplified with the introduction of dynamic frequencies defined by the following expressions [G-1]

$$w_g^{lmn}(t) \equiv \frac{1}{\phi_{gu}^{mn}(u,t)} \frac{\partial}{\partial t} \phi_{gu}^{mn}(u,t), \tag{3.27}$$

and

$$w_d^{lmn}(t) \equiv \frac{1}{c_{du}^{mn}(u,t)} \frac{\partial}{\partial t} c_{du}^{mn}(u,t). \tag{3.28}$$

Note that these frequencies vary neither spatially nor directionally within a given node. A method of estimating these frequencies is presented in Chapter 4. Substituting Eq. (3.28) into Eq. (3.26b) results in the following equation relating the transversely-integrated precursor densities in terms or the transversely-integrated fluxes

$$c_{du}^{mn}(u,t) = \frac{\beta_d}{\left(w_d^{lmn}(t) + \lambda_d\right)} \sum_{g'=1}^{G} \upsilon \Sigma_{fg'}^{lmn}(t) \phi_{g'u}^{mn}(u,t), \qquad u \in \left[u_l, u_{l+1}\right]. \tag{3.29}$$

Eq. (3.29) and Eq. (3.27) can then be substituted into Eq. (3.26a) to obtain

$$\begin{aligned} \frac{\partial}{\partial u} J_{gu}^{mn}(u,t) + \tilde{\Sigma}_{tg}^{lmn}(t) \phi_{gu}^{mn}(u,t) = & \sum_{g'=1}^{G} \left[\tilde{\chi}_g^{lmn}(t) \upsilon \Sigma_{fg'}^{lmn}(t) + \Sigma_{gg'}^{lmn}(t) \right] \phi_{gu}^{mn}(u,t) \\ & - S_{gu}^{mn}(u,t), \quad g = 1,2,\ldots,G, \end{aligned} \tag{3.30}$$

where an effective total cross section, $\tilde{\Sigma}_{tg}^{lmn}(t)$, and an effective fission spectrum, $\tilde{\chi}_g^{lmn}(t)$, are defined by

$$\tilde{\Sigma}_{tg}^{lmn}(t) \equiv \Sigma_{tg}^{lmn}(t) + \frac{w_g^{lmn}(t)}{v_g},$$

$$\tilde{\chi}_g^{lmn}(t) \equiv (1-\beta)\chi_{pg} + \sum_{d=1}^{D} \frac{\lambda_d \beta_d \chi_{dg}}{w_d^{lmn}(t) + \lambda_d}.$$

Now, Eq. (3.30) closely resembles the transversely-integrated equation for the steady-state case, Eq. (2.37a). Thus, the steady-state equations for the polynomial expansion coefficients may be applied with the modified cross sections. Once the polynomial expansion coefficients are determined, the polynomial current expressions, Eqs. (2.42d) and (2.42e), are applied and the CMFD discontinuity factors are computed. Hence, the non-linear iteration procedure described in Section 2.5.2.f remains unchanged.

3.5 Time-Integration of the Synthesis Equation

The derivation in Section 3.3 has resulted in spatially discretized, time-dependent, ordinary differential equations in terms or mixing coefficients and weighted precursor densities. The methods applied for the solution of the synthesis equation is a direct integration of the precursor equation and a theta-differencing scheme for the mixing coefficient equation.

The time domain is represented by discrete points at which the desired solution is to be computed

$$t = t_0, t_1, t_2, \ldots$$

and the time intervals are defined as

$$\Delta t_n \equiv t_{n+1} - t_n.$$

First, consider the precursor equation, Eq. (3.22b). A direct integration of this equation from t_n to t_{n+1} leads to

$$\underline{c}_d^{(n+1)} = e^{-\lambda_d \Delta t_n} \underline{c}_d^{(n)} + e^{-\lambda_d \Delta t_n} \int_{t_n}^{t_{n+1}} e^{-\lambda_d (t-t_n)} \underline{\underline{M}}_d(t) \underline{\underline{\Psi}} \underline{T}(t) dt, \quad d = 1, 2, \ldots, D. \tag{3.31}$$

The superscript represents the time at which the quantities are evaluated, for example

$$\underline{c}_d^{(n+1)} = \underline{c}_d(t_{n+1}).$$

Now, if $\underline{\underline{M}}_d(t) \underline{\underline{\Psi}} \underline{T}(t)$ is assumed to vary linearly across the time step, the integral in Eq. (3.31) can be evaluated to give

$$\underline{c}_d^{(n+1)} = k_{1,d} \underline{c}_d^{(n)} + k_{2,d} \frac{1}{\lambda_d} \underline{\underline{M}}_d^{(n+1)} \underline{\underline{\Psi}} \underline{T}^{(n+1)} - k_{3,d} \frac{1}{\lambda_d} \underline{\underline{M}}_d^{(n)} \underline{\underline{\Psi}} \underline{T}^{(n)}, \tag{3.32}$$

where

$$k_{1,d} \equiv e^{-\lambda_d \Delta t_n}, \quad k_{2,d} \equiv 1 - \frac{1 - e^{-\lambda_d \Delta t_n}}{\lambda_d \Delta t_n}, \quad k_{3,d} \equiv e^{-\lambda_d \Delta t_n} - \frac{1 - e^{-\lambda_d \Delta t_n}}{\lambda_d \Delta t_n}.$$

Note that in computer applications $k_{1,d}$, $k_{2,d}$ and $k_{3,d}$ should be evaluated using Taylor series expansions to avoid round-off errors for small Δt_n.

Now, the theta method [V-1] applied to the mixing coefficient equation, Eq. (3.22a), results in

$$\underline{\underline{\Psi}}^{*T}\underline{\underline{V}}^{-1}\underline{\underline{\Psi}}\frac{\underline{T}^{(n+1)}-\underline{T}^{(n)}}{\Delta t_n}=\theta\left\{\underline{\underline{\Psi}}^{*T}\left[\underline{\underline{M}}_p^{(n+1)}-\underline{\underline{L}}^{(n+1)}\right]\underline{\underline{\Psi}}\underline{T}^{(n+1)}+\underline{\underline{\Psi}}^{*T}\sum_{d=1}^{D}\lambda_d\underline{c}_d^{(n+1)}\right\}$$
$$+(1-\theta)\left\{\underline{\underline{\Psi}}^{*T}\left[\underline{\underline{M}}_p^{(n)}-\underline{\underline{L}}^{(n)}\right]\underline{\underline{\Psi}}\underline{T}^{(n)}+\underline{\underline{\Psi}}^{*T}\sum_{d=1}^{D}\lambda_d\underline{c}_d^{(n)}\right\}. \tag{3.33}$$

The choices of θ and their numerical implications are given in Chapter 4.

Substituting Eq. (3.32) into Eq. (3.33) eliminates the precursor densities at the new time step t_{n+1}, and subsequent rearranging leads to

$$\underline{\underline{\Psi}}^{*T}\left\{\underline{\underline{V}}^{-1}\frac{1}{\Delta t_n}-\theta\left[\underline{\underline{M}}_p^{(n+1)}-\underline{\underline{L}}^{(n+1)}+\sum_{d=1}^{D}k_{2,d}\underline{\underline{M}}_d^{(n+1)}\right]\right\}\underline{\underline{\Psi}}\underline{T}^{(n+1)}=$$
$$\underline{\underline{\Psi}}^{*T}\left\{\underline{\underline{V}}^{-1}\frac{1}{\Delta t_n}+(1-\theta)\left[\underline{\underline{M}}_p^{(n)}-\underline{\underline{L}}^{(n)}\right]-\theta\sum_{d=1}^{D}k_{3,d}\underline{\underline{M}}_d^{(n)}\right\}\underline{\underline{\Psi}}\underline{T}^{(n)} \tag{3.34}$$
$$+\underline{\underline{\Psi}}^{*T}\sum_{d=1}^{D}\lambda_d\underline{c}_d^{(n)}\left[1-\theta(1-k_{1,d})\right].$$

Eq. (3.34) is applicable only within the continuous time domain where the expansion functions do not change. As soon as the expansion functions are changed, Eq. (3.24a) has to be solved before the solution procedure can be advanced again using Eq. (3.34).

The subdivision of the time steps in the synthesis method is shown in Figure 3.1. The largest time step, Δt_l, is allotted for the expansion function changes, while the CMFD discontinuity factors are updated with a smaller time step, Δt_m. The smallest time step, Δt_n, is used to obtain the mixing coefficients. For the slowly developing transients in which the changes in the CMFD discontinuity factors are also very gradual, skipping several mixing coefficient time steps before updating the next CMFD discontinuity factors reduces computing time without noticeable effect on accuracy. For this reason, Δt_m is chosen to be larger than Δt_n.

3.6 Thermal Hydraulic and Cross Section Feedback Models

A realistic investigation of space-time neutron behaviors must consider thermal hydraulic effects. In fact, the neutron flux shape is a strong function of fuel and coolant temperatures and many transients are initiated by changes in thermal characteristics of a reactor core. A simple thermal hydraulic model, called the WIGL model, and a linear cross section feedback model are described in this section.

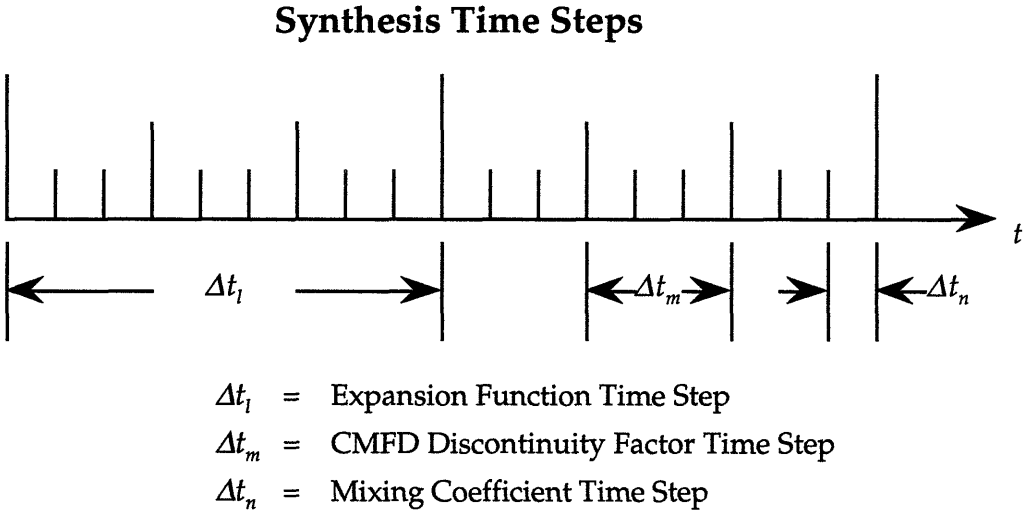

Figure 3.1: Diagram showing the subdivision of time steps in synthesis method.

3.6.1 WIGL Thermal Hydraulic Model

The WIGL model [V-1] uses a simple, one-dimensional, lumped heat capacity representation of the reactor core. Also, boiling effects are neglected in the model, making it inapplicable for Boiling Water Reactors (BWR). Despite these limitations, the WIGL model provides a reasonable representation of the PWR core thermal hydraulic behaviors. As a result, many reactor problems have been analyzed based on the WIGL model [G-1]. The WIGL model is incorporated in this thesis for its simplicity and for comparison purposes.

The appropriate heat transfer equations for a given thermal hydraulic region are

$$\rho_f V_f^{ijk} C_f \frac{d\overline{T}_f^{ijk}}{dt} = (1-r)\left(q'''\right)^{ijk} V_f^{ijk} - V_c^{ijk}\left[\frac{1}{A_H U} + \frac{1}{A_H h_o}\left(\frac{W}{W_o}\right)^{0.8}\right]^{-1}\left(\overline{T}_f^{ijk} - \overline{T}_c^{ijk}\right), \quad (3.35a)$$

$$V_c^{ijk}\left(\frac{\partial \rho_c H}{\partial \overline{T}_c}\right)\frac{d\overline{T}_c^{ijk}}{dt} = V_c^{ijk}\left[\frac{1}{A_H U} + \frac{1}{A_H h_o}\left(\frac{W}{W_o}\right)^{0.8}\right]^{-1}\left(\overline{T}_f^{ijk} - \overline{T}_c^{ijk}\right) + 2W_r^{ijk} C_c\left(T_b^{ijk} - \overline{T}_c^{ijk}\right) + r\left(q'''\right)^{ijk} V_f^{ijk}, \quad (3.35b)$$

$$T_b^{ijk} = 2\overline{T}_c^{ij,k-1} - T_b^{ij,k-1}, \quad (3.35c)$$

where

r = fraction of fission power deposited in coolant,
$\overline{T}_f^{ijk}$ = average fuel temperature in node (i,j,k),
$\overline{T}_c^{ijk}$ = average coolant temperature in node (i,j,k),
T_b^{ijk} = inlet coolant temperature of node (i,j,k),
ρ_f = fuel density,
ρ_c = coolant density,
C_f = specific heat of fuel,
C_c = specific heat of coolant,
$\left(q'''\right)^{ijk}$ = volumetric heat generation rate in node (i,j,k),
V_f^{ijk} = volume of fuel in node (i,j,k),
V_c^{ijk} = volume of coolant in node (i,j,k),
A_H = ratio of total heat transfer area to coolant volume within node (i,j,k),
U = ratio of conductivity to conduction length of cladding,
h_o = convective heat transfer coefficient at initial flow rate,
W_o = initial total core mass flow rate,
W = total core mass flow rate,
W_r^{ijk} = mass flow rate in node (i,j,k),
$\left(\frac{\partial \rho_c H}{\partial \overline{T}_c}\right)$ = energy needed to raise temp. of a unit volume of coolant one temp. unit.

For steady-state calculations, the time derivatives in Eqs. (3.35a) and (3.35b) are set to zero. Time-dependent applications employ a fully-implicit time integration method with the same time step used as for mixing coefficient calculations. The numerical properties of a fully-implicit WIGL model are compared with those of a fully-implicit donor cell model and results are presented in Appendix B. For all practical purposes, there are little differences between the WIGL model and the donor cell model.

3.6.2 Cross Section Feedback

This thesis uses a linear cross section feedback model, where all macroscopic cross sections (and inverse of diffusion coefficients) are assumed to be linear functions of the node-averaged fuel temperature, coolant temperature and coolant density

$$\Sigma_{\alpha}^{ijk}\left(\overline{T}_f^{ijk},\overline{T}_c^{ijk},\rho_c^{ijk}\right)=\Sigma_{\alpha}^{ijk}\left(\overline{T}_{fo},\overline{T}_{co},\rho_{co}\right)+\left(\frac{\partial\Sigma_{\alpha}^{ijk}}{\partial\overline{T}_f^{ijk}}\right)\left(\overline{T}_f^{ijk}-\overline{T}_{fo}\right)$$
$$+\left(\frac{\partial\Sigma_{\alpha}^{ijk}}{\partial\overline{T}_c^{ijk}}\right)\left(\overline{T}_c^{ijk}-\overline{T}_{co}\right)+\left(\frac{\partial\Sigma_{\alpha}^{ijk}}{\partial\rho_c^{ijk}}\right)\left(\rho_c^{ijk}-\rho_{co}\right), \tag{3.36}$$

where $\overline{T}_{fo}$, $\overline{T}_{co}$ and ρ_{co} represent the reference values and the partial derivatives with respect to temperature are at constant density. In general, the linear functional dependence can accurately represent the actual cross sections over only limited ranges of the temperatures and densities. Actual design calculations may warrant more elaborate schemes (table look-up or polynomial fitting) to represent cross section changes more accurately [G-1]. But, for the purposes of this thesis, the linear assumption is sufficient.

3.7 Control Rod Cusping Correction

Transients are initiated by perturbations in reactor conditions. The perturbations can be cause by many different mechanisms including control rod motion and thermal hydraulic changes. The control rod motion, in particular, raises a question in nodal theory concerning cross sections of a partially rodded node.

The nodal method treats control rod motions as spatially uniform changes in macroscopic cross sections. The simplest scheme of obtaining the cross sections for a partially rodded node is to use a volume-weighted average of the rodded and unrodded nodal cross sections. This procedure, however, introduces a modeling error because the neutron flux within the node in not spatially uniform. In fact, the rodded flux shape is very much different from the unrodded flux shape. As a result, the volume-weighted scheme causes a cusp-like time behavior of the flux as the control rod moves through a node. An elaborate correction scheme was developed by H. Joo [J-2] and incorporated in the QUANDRY code to reduce the error caused by the cusping effect. However, a simple correction scheme developed by J. Gehin [G-1] is used in this thesis.

If the average fluxes in the rodded and unrodded portions of a node are known, a new homogenized cross section can be obtained by a flux-weighted scheme

$$\overline{\Sigma}_{\alpha g}^{ijk}=\frac{h_k^{nr}\phi_g^{nr}\Sigma_{\alpha g}^{nr}+h_k^{r}\phi_g^{r}\Sigma_{\alpha g}^{r}}{h_k^{nr}\phi_g^{nr}+h_k^{r}\phi_g^{r}}, \tag{3.37}$$

where superscript *r* and *nr* represent the rodded and unrodded portions of the node, respectively. The nodal method, however, computes just the average flux of the entire

node, not of the two regions of interest. In the case of a strongly absorbing rod, the neutron flux makes a sharp change at the rod tip, and varies more slowly away from the tip. Based on this observation, one can approximate the flux in the unrodded portion of the node as the average of the node-averaged flux of the partially rodded node and its lower neighbor. (Note that this statement implicitly assumes that control rods are inserted from the top of a core, but an analogous statement can be made about control rods inserted from the bottom of a core.) Likewise, the flux in the rodded portion can be approximated as the average of the flux in the partially rodded node and its upper neighbor. These approximations lead to

$$\phi_g^{nr} = \frac{h_k^{nr}\phi_g^{ijk} + h_{k-1}\phi_g^{ij,k-1}}{h_k^{nr} + h_{k-1}}, \tag{3.38a}$$

and

$$\phi_g^{r} = \frac{h_k^{r}\phi_g^{ijk} + h_{k+1}\phi_g^{ij,k+1}}{h_k^{r} + h_{k+1}}. \tag{3.38b}$$

Eqs. (3.38a) and (3.38b) are substituted into Eq. (3.37) to obtain flux-weighted nodal cross sections. In spite of its simplicity, this method has been found to perform as well as more elaborate models [G-1].

Other perturbations initiated by thermal hydraulic changes in reactor conditions, including coolant inlet temperature and core flow rate changes, in general, affect an entire node homogeneously and do not cause a cusp-like behavior in the neutron flux.

3.8 Summary

The time-dependent synthesis method, which allows discontinuous expansion functions is presented in this chapter. The functional for which the first-order variation is made stationary by the time-dependent, finite-difference nodal equation assumes a more complex form and the synthesis derivation requires a bit more algebraic manipulation than the steady-state case because of discontinuous expansion functions. As a result, the variational procedure reveals some interesting numerical implications. An over-determination difficulty arises if both flux expansion functions and the adjoint weight functions are allowed to be discontinuous at the same time. Although the resulting over-determined system of equations could be solved in a least-square sense, the variational procedure suggests that the adjoint weight function be continuous if the over-determination problem is to be avoided. Further, the variational procedure discloses that either an over- or under-determination problem cannot be avoided if

different numbers of expansion functions are employed at different time steps. For these reasons, it is assumed that the adjoint weight functions are continuous throughout a transient, and that the number of expansion functions is constant.

The same CMFD discontinuity factor updating schemes used in the steady-state case are applicable for the time-dependent application. The CMFD discontinuity factor synthesis scheme is a straightforward, but the non-linear iteration scheme requires the introduction of dynamic frequencies if solving the time-dependent polynomial nodal equations is to be avoided. With modified cross sections, the non-linear iteration procedure describe in Section 2.5.2.f can be applied for the time-dependent case as well.

The direct integration of the precursor density equation and the theta scheme for the mixing coefficient equation are the methods selected for the solution of the time-dependent synthesis equation. The overall time advancing strategy uses three different time steps. The largest time step is reserved for possible expansion function changes and the smallest time step for mixing coefficient calculations. The CMFD discontinuity factor updating time step is allowed to be larger than the mixing coefficient time step to reduce the computational expense for transients which do not require frequent discontinuity factor updates. Finally, the WIGL thermal hydraulic model as well as the linear cross section feedback model is introduced for their simplicity and for comparison purposes. A simple control rod cusping correction model to determine the macroscopic cross sections of a partially rodded node is also described.

CHAPTER 4

NUMERICAL SOLUTION METHODS

4.1 Introduction

This chapter presents the numerical methods for solving the steady-state and transient synthesis equations. The introduction of predetermined, two-dimensional expansion functions yields several significant numerical implications in solving the synthesis equation. First, the resulting matrix in the synthesis equation lacks the structure that guarantees that iterative matrix inversion techniques will converge. As a result, there is no choice but to resort to a direct inversion technique. Second, the synthesis eigenvalue problem loses the property that guarantees the existence of a largest, positive eigenvalue and its corresponding unique positive eigenvector. This has potentially serious consequences because the resulting eigenvalue and the synthesized flux can assume physically unacceptable values. There is no theoretical resolution of this problem, but the past experience with synthesis methods indicates that negative eigenvalues and fluxes are rarely encountered [Y-1,Y-2,Y-3]. Third, the implementation of Wielandt's eigenvalue acceleration scheme necessitates a simultaneous group solution procedure. The group-wise solution procedure developed by T. Sutton [S-5] has a convergence problem and is, therefore, not applicable to synthesis methods.

4.2 Steady-State Solution Methods

The complete set of steady-state equations for which a solution is sought is Eq. (2.34) along with either the polynomial nodal equations (2.53) through (2.60) or the CMFD discontinuity factor synthesis equation (2.35). The CMFD discontinuity factor updating schemes, both the non-linear iteration scheme and the CMFD discontinuity factor synthesis scheme, discussed in Chapter 2 require the determination of the mixing coefficients for their implementation. This section presents the numerical methods for solving Eq. (2.34) for the eigenvalue and the mixing coefficients.

4.2.1 Numerical Properties

The finite-difference nodal balance equation from which the synthesis equation is derived has the following form in matrix notation

$$\underline{\underline{L}}(\underline{\Phi},\lambda)\underline{\Phi} = \frac{1}{\lambda}\underline{\underline{M}}\underline{\Phi}, \tag{2.17}$$

where the dependence of the loss matrix $\underline{\underline{L}}$ on the node-averaged fluxes and the eigenvalue is explicitly indicated. The diagonal dominance of the matrix $\underline{\underline{L}}$ is no longer guaranteed because of the introduction of the CMFD discontinuity factors. However, if the CMFD discontinuity factors are assume to be unity, Eq. (2.17) reduces to the finite-difference diffusion equation and the matrix $\underline{\underline{L}}$ has the following properties [V-2]:

1. $\underline{\underline{L}}$ is real,
2. the diagonal elements of $\underline{\underline{L}}$ are positive,
3. the off-diagonal elements of $\underline{\underline{L}}$ are non-positive,
4. $\underline{\underline{L}}$ is diagonally dominant,
5. $\underline{\underline{L}}$ is irreducible.

A matrix which has these properties is called an S-matrix and its inverse, $\underline{\underline{L}}^{-1}$, exists and has all positive elements [N-1]. These properties render a significant numerical importance in solving the finite-difference nodal balance equation. First, the diagonal-dominance guarantees the convergence of iterative inversion methods. Second, the positivity and the irreducibility of $\underline{\underline{L}}^{-1}$ guarantee the existence and uniqueness of a largest positive eigenvalue and its corresponding positive eigenvector [N-1] (physically acceptable effective multiplication factor and node-averaged fluxes).

Now, let us consider the numerical properties of the resulting matrix for the synthesis equation. Recall that the synthesis equation in matrix form is

$$\underline{\underline{L}}'\underline{T} = \frac{1}{\lambda}\underline{\underline{M}}'\underline{T}, \tag{2.34}$$

where

$$\underline{\underline{L}}' = \left[\underline{\underline{\Psi}}^{*T}\underline{\underline{L}}\underline{\underline{\Psi}}\right] \text{ and } \underline{\underline{M}}' = \left[\underline{\underline{\Psi}}^{*T}\underline{\underline{M}}\underline{\underline{\Psi}}\right].$$

Because of the introduction of arbitrary expansion functions and weight functions (which, although not selected arbitrarily, can be considered arbitrary for the purpose of this discussion), the resulting matrix $\underline{\underline{L}}'$ is no longer guaranteed to be diagonally-dominant; hence iterative inversion techniques cannot be applied. Also, the existence and uniqueness of a largest positive eigenvalue and its corresponding eigenvector is not assured any more. This has a rather significant consequence in that the convergence of the power method is not guaranteed. Furthermore, even if the power method has a converged solution, it may contain physically unacceptable values (i.e., a negative eigenvalue or negative node-averaged fluxes).

A theoretically trivial but a numerically significant concern is that the matrix $\underline{\underline{L}}'$ is, in general, ill-conditioned. Theoretically, the use of linearly independent weight and expansion functions ensures a non-singular matrix. However, because the expansion functions and the weight functions are, in general, all nearly the same size, the resulting matrix $\underline{\underline{L}}'$ becomes nearly singular. Under these circumstances it is possible to run into significant rounding-off errors in solving Eq. (2.34). This difficulty can be overcome by using linear combinations of original expansion and weight functions. For example, use of $[\Psi_1]$, $[\Psi_1 - \Psi_2]$,...,$[\Psi_1 - \Psi_P]$, and $[\Psi_1^*]$, $[\Psi_1^* - \Psi_2^*]$,...,$[\Psi_1^* - \Psi_P^*]$ in place of the original $[\Psi_p]$ and $[\Psi_p^*]$ is usually sufficient to avoid rounding-off errors. If not, an actual orthogonalization can be carried out. Such a transformation does not affect the answer mathematically; hence, from that viewpoint, the procedure is unnecessary. It can, however, affect the numerical answer considerably [H-2].

4.2.2 CMFD Discontinuity Factor Iterations

The top iteration level in the steady-state solution procedure is the CMFD discontinuity factor updating. In this iteration, the synthesis equation is solved for the mixing coefficients. Then, using these mixing coefficients, the CMFD discontinuity factors are computed either from the non-linear iteration scheme or the CMFD

discontinuity factor synthesis scheme. This process is repeated until a desired convergence is achieved.

By having the top iteration level be the CMFD discontinuity factor updating, all CMFD discontinuity factors are kept constant throughout the solution of the synthesis equation. In addition, cross section updating required by thermal hydraulic changes is performed with the CMFD discontinuity factor updates. As a result, the non-linearity is eliminated from the synthesis equation.

4.2.3 Outer Iterations

Eq. (2.34) can be rewritten in the following form

$$\underline{T} = \frac{1}{\lambda}\underline{\underline{R}}\underline{T}, \tag{4.1}$$

where

$$\underline{\underline{R}} \equiv \underline{\underline{L}}'^{-1}\underline{\underline{M}}'.$$

The largest (magnitude) eigenvalue and its corresponding eigenvector can be found using the power method [N-1], which can be written as

$$\underline{T}^{(l+1)} = \frac{1}{\lambda^{(l)}}\underline{\underline{R}}\underline{T}^{(l)}, \tag{4.2a}$$

$$\lambda^{(l+1)} = \lambda^{(l)}\frac{\left\langle \underline{w}, \underline{T}^{(l+1)} \right\rangle}{\left\langle \underline{w}, \underline{T}^{(l)} \right\rangle}, \quad l = 1,2,\ldots,\infty \tag{4.2b}$$

where l is the iteration number and $\underline{w}$ is a weighting vector. According to the Perron-Frobenius theorem, an irreducible matrix having non-negative elements has a unique, positive eigenvalue greater in magnitude than the modulus of any other eigenvalue of the matrix. Further, its corresponding eigenvector has all positive elements.

Unfortunately, the matrix in Eq. (4.1) lacks these properties and the eigenvalue and the eigenvector found using the power method may well be physically unacceptable. Moreover, if the largest eigenvalue of Eq. (4.1) is complex, the power method does not converge at all. In fact, both the convergence problem and physically unacceptable eigenvalues have been observed in past studies [A-1,L-1,L-2,Y-4]. The anomalies observed in these studies, however, all stem from the poor choice of expansion functions. V Luco observed negative eigenvalues when expansion functions of highly-oscillatory modes are considered [L-1,L-2]. C. Adams found anomalies in the

collapsed-group synthesis approximation resulting from inaccurate fast-to-thermal flux ratios [A-1].

On the contrary, past experience with the group-dependent synthesis employing fundamental mode expansion and weight functions has been encouraging in that no convergence problem or negative fluxes were observed [Y-1,Y-2,Y-3]. Thus, although there is no firm theoretical basis, past experience provides some confidence that, with a proper choice of expansion functions, the solution obtained from the power method will be a close approximation to the physically acceptable one.

The selection of the weighting vector in Eq. (4.2b) is arbitrary, but does affect the rate of convergence. One common choice is to set the elements of $\underline{w}$ to unity. Another choice for the weighting vector is the product of nodal fission cross sections and the expansion functions, $\underline{\underline{M}}\underline{\Psi}$, summed over axial planes such that the inner products perform summations over the fission source. This represents a more physical approach of determining the eigenvalue by taking the ratio of the neutron production in the current "generation" to the previous "generation", where a "generation" now represents an iteration. This weighting vector choice also has the benefit of using only information in the fueled regions which leads to a more stable iteration procedure and possibly faster convergence [G-1]. An alternate choice of the weighting vector is the fission source vector summed over axial planes from the previous iteration. The eigenvalue calculated with this method can be shown to converge faster than the power method with unity weighting [N-1].

While the choice of a particular weighting vector does impact the rate of convergence of the power method, the asymptotic convergence rate is primarily dependent on the ratio of the moduli of the two largest eigenvalues

$$d \equiv \frac{|\lambda_1|}{|\lambda_0|}, \tag{4.3}$$

where λ_0 and λ_1 are the eigenvalues with the largest and the second largest moduli, respectively. This ratio is called the dominance ratio and for most of the problem of interest, is so close to unity that the power method converges very slowly [G-1]. One acceleration scheme which can be applied to synthesis methods is Wielandt's fractional iteration or eigenvalue shifting [W-1]. In Wielandt's scheme, a portion of the right-hand side of Eq. (2.34) is moved to the left-hand side as follows

$$\left[\underline{\underline{L}}' - \frac{1}{\lambda'}\underline{\underline{M}}'\right]\underline{T} = \frac{1}{\Lambda}\underline{\underline{M}}'\underline{T}, \tag{4.4}$$

where

$$\frac{1}{\Lambda}=\frac{1}{\lambda}-\frac{1}{\lambda'}.$$

Whatever eigenvalue shift, λ', is chosen, the Wielandt's scheme will converge to the eigenvalue closest to it. Since the eigenvalue of interest in synthesis methods is the largest positive one, certain restrictions, which will be discussed later, are imposed on the choice of the eigenvalue shift.

Applying the power method to Eq. (4.4) results in the following equations

$$\underline{T}^{(l+1)}=\frac{1}{\Lambda^{(l)}}\left[\underline{\underline{L}}'-\frac{1}{\lambda'}\underline{\underline{M}}'\right]^{-1}\underline{\underline{M}}'\underline{T}^{(l)}, \tag{4.5a}$$

$$\Lambda^{(l+1)}=\Lambda^{(l)}\frac{\left\langle \underline{w},\underline{T}^{(l+1)}\right\rangle}{\left\langle \underline{w},\underline{T}^{(l)}\right\rangle}, \tag{4.5b}$$

$$\lambda^{(l+1)}=\frac{\Lambda^{(l+1)}\lambda'}{\Lambda^{(l+1)}+\lambda'}. \tag{4.5c}$$

The eigenvector, which is associated with the largest eigenvalue, Λ, is identical to the eigenvector associated with the eigenvalue closest to the eigenvalue shift value of the unshifted equations [W-1]. Thus, if the eigenvalue shift is chosen such that its modulus exceeds, λ_o, the new dominance ratio is given by

$$d'=\frac{\frac{1}{\lambda_o}-\frac{1}{\lambda'}}{\frac{1}{\lambda_1}-\frac{1}{\lambda'}}, \tag{4.6}$$

and is less than the unshifted dominance ratio, d. Choosing the eigenvalue shift to be infinite results in the unaccelerated power method of Eqs. (4.2a) and (4.2b). Choosing λ' very close to λ_o gives a very small dominance ratio; hence accelerates the convergence rate of the power method.

Since λ_o is not known *a priori*, the eigenvalue shift may be changed during the solution procedure to ensure optimum performance. A common procedure is to let the eigenvalue shift value be the current estimate of the eigenvalue plus an arbitrary positive constant

$$\lambda'=\lambda^{(l)}+\delta\lambda. \tag{4.7}$$

This eigenvalue shift factor, $\delta\lambda$, guarantees that the power method converges to the correct eigenvalue and eigenvector. However, changing the eigenvalue shift value requires that the matrix inversion shown in Eq. (4.5a) be performed in every outer iteration. This requirement is not a serious one if the matrix inversion is carried out using a iterative solution technique. But, for the reason stated in Section 4.2.1, a direct inversion method, called LU factorization method [G-2], will be adopted. It is desirable to have a constant eigenvalue shift value since, than, the time-consuming LU factorization needs to be performed only once per CMFD discontinuity factor iteration. These two competing factors can be reconciled as follows: A few iterations using a reasonable eigenvalue shift value {1.2~1.5} are carried out to obtain a reasonable guess for λ_o. Then, the eigenvalue shift value, which is kept constant for the rest of the problem, is calculated using Eq. (4.7) with the current estimate of λ_o and the eigenvalue shift factor, $\delta\lambda$ {0.001-0.05}.

One of the advantages of using LU factorization is that the computing time of the matrix inversion procedure is independent of a particular choice of the eigenvalue shift factor. Thus, an aggressive shifting (very small eigenvalue shift factor) can be employed. This is not the case for the iterative inversion techniques, for which the convergence rate decreases as the eigenvalue shift factor is reduced. However, one must be cautious about a very small shift factor. Recall that λ' must exceed λ_o for proper convergence to the right eigenvalue. If the a low estimate of λ_o is obtained (this is possible especially because the CMFD discontinuity factors are changing) during the solution procedure and the eigenvalue shift factor is small, λ_o may exceed λ' and the Wielandt's scheme may converge to an incorrect eigenvalue.

As shown in Eq. (4.4), the eigenvalue shifting scheme results in a coefficient matrix that resembles a problem with strong up-scattering since $\underline{\underline{M}}'$ is generally a full matrix. Thus, the implementation of Wielandt's method generally requires that all energy groups be solved simultaneously [G-1]. T. Sutton's group-wise solution procedure [S-5], successfully implemented in the CONQUEST code [G-1], was attempted for the solution of the synthesis equation given by Eq. (4.4), but failed to give a converged solution. The success of the group-wise solution procedure in the solution of the finite-difference nodal equation is attributed to the quick convergence of the "spectrum ratios" [S-5]. However, the generalization of the "spectrum ratios" to the synthesis equation ("mixing coefficient ratios" would be more appropriate in this case) failed to converge because of the presence of expansion functions which contribute minimally to the overall flux shape. For this reason, a simultaneous group solution has to used in conjunction with the Wielandt's eigenvalue acceleration scheme.

4.2.4 LU Factorization

At each outer iteration, the matrix $\left[\underline{\underline{L}}'-1/\lambda'\underline{\underline{M}}'\right]$ must be inverted. Because the diagonal-dominance of this matrix is not assured, the matrix inversion cannot be carried out using iterative techniques. Therefore, a direct inversion method has to be used. The method used in this thesis is called LU factorization. The size of the matrix appearing in the synthesis formulation is on the order of tens to hundreds, and thus, makes the direct inversion technique practical. Furthermore, the sparse, banded structure of the matrix can be exploited to reduce the computational requirement.

During the outer iterations the equations of the form $\underline{\underline{A}}\underline{x}=\underline{b}$ must be solved, where

$$\underline{\underline{A}} \equiv \underline{\underline{L}}' - \frac{1}{\lambda'}\underline{\underline{M}}', \tag{4.8a}$$

$$\underline{b} \equiv \frac{1}{\Lambda^{(l)}}\underline{\underline{M}}'\underline{T}^{(l)}, \tag{4.8b}$$

$$\underline{x} \equiv \underline{T}^{(l+1)}. \tag{4.8c}$$

In LU factorization, the matrix $\underline{\underline{A}}$ is written as a product of two triangular matrices $\underline{\underline{L}}$ and $\underline{\underline{U}}$ (non-singular matrix $\underline{\underline{A}}$ ensures the existence and uniqueness of the LU factorization [G-2])

$$\underline{\underline{A}} = \underline{\underline{L}}\,\underline{\underline{U}}, \tag{4.9}$$

where $\underline{\underline{L}}$ is a unit lower triangular matrix and $\underline{\underline{U}}$ is an upper triangular matrix. Once the LU factorization is obtained, the solution of the original $\underline{\underline{A}}\underline{x}=\underline{b}$ problem is found by a two step triangular solve process

$$\underline{\underline{L}}\underline{y} = \underline{b}, \tag{4.10a}$$

$$\underline{\underline{U}}\underline{x} = \underline{y}. \tag{4.10b}$$

where Eqs. (4.10a) and (4.10b) are solved using simple algorithms known as forward substitution and back substitution, respectively [G-2}. The LU factorization is the most time-consuming part requiring $(2/3)n^3$ flops while both the forward and back substitutions require n^2 flops, where n is the matrix size [G-2}. Now, the advantage of keeping the eigenvalue shift value constant is apparent. Whenever the eigenvalue shift

value changes, the time-consuming LU factorization must be performed. By maintaining a constant eigenvalue shift value, both forward and back substitutions can be carried out repeatedly for different values of $\underline{b}$ with the same LU factorization.

Another way to reduce the computational requirement of the LU factorization is to take advantage of the banded structure of the matrix $\underline{\underline{A}}$. $\underline{\underline{A}}$ is a block 5-stripe matrix, where the size of each block is P by P (recall P is the number of expansion functions used at each axial position). For example, the matrix $\underline{\underline{A}}$ for two energy group, four axial node, one expansion function problem has the following structure

$$\begin{pmatrix} x & x & & & x & & & \\ x & x & x & & & x & & \\ & x & x & x & & & x & \\ & & x & x & x & & & x \\ x & & & x & x & x & & \\ & x & & & x & x & x & \\ & & x & & & x & x & x \\ & & & x & & & x & x \end{pmatrix}, \tag{4.11}$$

where x represents non-zero elements. If the matrix $\underline{\underline{A}}$ has lower bandwidth p and upper bandwidth q, and if $n >> p$ and $n >> q$ then the LU factorization involves about $2npq$ flops, substantially less than $(2/3)n^3$ flops of a dense matrix of the size n [G-2].

The bandwidths can be further reduced by a simple reordering of the mixing coefficients. By listing all group mixing coefficients at each axial position as a block rather then listing all axial mixing coefficients in a group as a block, the band widths of the matrix shown in (4.11) can be decreased as follows

$$\begin{pmatrix} x & x & x & & & & & \\ x & x & & x & & & & \\ x & & x & x & x & & & \\ & x & x & x & & x & & \\ & & x & & x & x & x & \\ & & & x & x & x & & x \\ & & & & x & & x & x \\ & & & & & x & x & x \end{pmatrix}. \tag{4.12}$$

For a problem with more energy groups and/or more axial nodes, the reduction in bandwidths from this simple reordering of mixing coefficients can be substantial.

The rounding-off error associated with the LU factorization is a serious concern since it can ultimately affect the global convergence of the synthesis solution procedure. The rounding-off error is proportional to the machine precision, the matrix size, the condition number of the matrix and the growth factor of the matrix [G-2]. There is no way to remedy the errors stemming from the machine precision, the matrix size and the condition number of the matrix[2], but a method called partial pivoting can substantially reduce the error due to a large growth factor. In practice, the growth factor is usually of order 10 but it can be as large as 2^{n-1}. Despite this, most numerical analysts regard the serious element growth in the LU factorization with partial pivoting as highly unlikely in practice [G-2]. The implementation of partial pivoting, however, does expand the bandwidths; hence the computational time is increased compared to the LU factorization without pivoting.

4.2.5 Steady-State Iteration Strategy

As mentioned in the previous sections, there are two levels of iterations, namely the CMFD discontinuity factor iteration and the outer iteration. The Wielandt eigenvalue shifting scheme accelerates only the convergence rate of the outer iteration. The convergence rate of the CMFD discontinuity factor iteration is not well known because of its non-linear nature, but experience indicates that LWR problems with assembly-size nodes typically requires about 5 to 15 iterations [G-1].

The following is the general iteration procedure for the solution of the steady-state synthesis equation:

1. Make initial guesses of the mixing coefficients, the eigenvalue and the CMFD discontinuity factors.
2. Perform outer iterations with a constant eigenvalue shift value known to be larger than the eigenvalue (For most problems, the eigenvalue is near unity so that the eigenvalue shift value in the range of 1.2 to 1.5 can be used.) until a coarse convergence is achieved (~ 10^{-2})

$$\left|\lambda^{(l+1)} - \lambda^{(l)}\right| < \varepsilon_1,$$

[2] The rounding-off error resulting from a large condition number (ill-conditioned matrix) can be reduced by employing the Singular Value Decomposition (SVD) method [G-2]. But, the SVD scheme was not implemented because it is extremely time-consuming, especially for the matrix size considered in the space-dependent synthesis methods.

where ε_1 is a user-specified coarse eigenvalue convergence value.

3. Next, the eigenvalue shift value, to be used throughout the subsequent iterations, is computed from the latest estimate of the eigenvalue and a user-specified positive eigenvalue shift factor

$$\lambda' = \lambda^{(l)} + \delta\lambda,$$

where $\delta\lambda$ value is typically 0.001 to 0.05.

4. Now, the fully accelerated iterations proceed until the specified convergence in the eigenvalue and the nodal power is achieved

$$\left|\lambda^{(l+1)} - \lambda^{(l)}\right| < \varepsilon_2,$$

$$\text{Max. over all nodes}\left\{\frac{\left|P_i^{(l+1)} - P_i^{(l)}\right|}{P_i^{(l)}}\right\} < \varepsilon_3,$$

where P_i represents the power in node i and ε_2 and ε_3 are the user-specified, global eigenvalue and fission source convergence values, respectively. An eigenvalue convergence of 10^{-5} and a fission source convergence of 10^{-4} are generally sufficient. Also, the iteration procedure can be terminated if some user-specified maximum number of iterations is exceeded.

This procedure has been successfully implemented in the steady-state synthesis solution routine. Some of the steady-state synthesis calculation results are given in Chapter 5.

4.3 Transient Solution Methods

The equations to be solved in transient synthesis analyses are Eqs. (3.22a) through (3.24b). The initial and the continuity equations (3.23a) and (3.24a) can be solved easily by applying the LU factorization discussed in Section 4.2.4, and the solution of Eqs. (3.23b) and (3.24b) is trivial. Thus, the following discussion may be concentrated on the numerical methods to solve Eqs. (3.22a) and (3.22b), or their time-differenced equations (3.32) and (3.34). While the numerical schemes to solve Eq. (3.34) requires a further discussion, obtaining the solution of Eq. (3.32) is simple in that it only requires matrix multiplication. The following sections describe the general transient solution procedure starting from the numerical properties of Eq. (3.34).

4.3.1 Numerical Properties

Recall that the time-dependent synthesis equation is

$$\underline{\underline{\Psi}}^{*T}\left\{\underline{\underline{V}}^{-1}\frac{1}{\Delta t_n}-\theta\left[\underline{\underline{M}}_p^{(n+1)}-\underline{\underline{L}}^{(n+1)}+\sum_{d=1}^{D}k_{2,d}\underline{\underline{M}}_d^{(n+1)}\right]\right\}\underline{\underline{\Psi}}\underline{T}^{(n+1)}=$$

$$\underline{\underline{\Psi}}^{*T}\left\{\underline{\underline{V}}^{-1}\frac{1}{\Delta t_n}+(1-\theta)\left[\underline{\underline{M}}_p^{(n)}-\underline{\underline{L}}^{(n)}\right]-\theta\sum_{d=1}^{D}k_{3,d}\underline{\underline{M}}_d^{(n)}\right\}\underline{\underline{\Psi}}\underline{T}^{(n)} \qquad (3.34)$$

$$+\underline{\underline{\Psi}}^{*T}\sum_{d=1}^{D}\lambda_d\underline{c}_d^{(n)}\left[1-\theta(1-k_{1,d})\right].$$

The value of θ can be chosen to give the standard time-differencing scheme:

θ	= 0	Forward Difference (or Fully Explicit),
θ	= 1/2	Trapezoidal Rule (or Crank-Nicholson),
θ	= 1	Backward Difference (or Fully Implicit).

In order for a space-time finite-difference solution scheme to be reliable, it must be stable. The issue of stability is the major determining factor in choosing the value of θ. It can be shown that the theta method is unconditionally stable when $\theta \geq 1/2$ [L-3].

When the values of θ less than 1/2 are chosen, restrictions on the time step size are required to ensure stability. Typically, the upper limit of the time step size is on the same time scale as the fastest varying quantities in the system of equations. The system of equations in reactor analysis, however, has quantities with vastly different time constants [G-1]. The behavior of the neutron flux can have time constants on the order of $1/(v\Sigma)$ (neutron mean free path divided by neutron speed) which may be smaller than 10^{-8} seconds for fast neutrons [S-1]. The delayed neutron precursors, on the other hand, have decay constants ranging from hundredths of seconds to several seconds. Such systems of differential equations with widely varying time scales are said to be **stiff**. With the conditionally stable methods, the time step size must be extremely small to follow all short-lived transient modes of the neutron behavior, even if they are of no interest. And this, in turn, translates to a large computational time.

Consequently, the values of θ to be considered in solution of the time-differenced synthesis equation are greater than or equal to 1/2. Without other consideration, θ = 1/2 (Crank-Nicholson) is the best choice because it is the most accurate. The Crank-Nicholson method, however, exhibits a slowly decaying oscillatory

behavior for stiff systems if moderately large time steps are used [G-1]. Therefore, the most appropriate value of θ is 1, the fully implicit method.

With appropriate definitions, the fully implicit version of Eq. (3.34) can be written as

$$\underline{\underline{A}}^{(n+1)}\underline{T}^{(n+1)} = \underline{s}^{(n)}. \tag{4.13}$$

This equation has the same exact form considered in Section 4.2.4, and therefore, can be solved using the same matrix inversion technique. However, the LU factorization must be performed at each time step because of the changes in cross sections which alter the matrix $\underline{\underline{A}}$ at every time step. In other words, the computational saving realized in the steady-state solution procedure is not present in transient analyses.

4.3.2 Dynamic Frequency Estimation

In Section 3.4.2, dynamic frequencies were introduced to eliminate the time derivatives in the polynomial nodal equations. The frequencies at time step n are approximated by the following expressions

$$\left(w_g^{ijk}\right)^{(n)} = \frac{1}{\Delta t_{n-1}} ln\left(\frac{\left(\bar{\phi}_g^{ijk}\right)^{(n)}}{\left(\bar{\phi}_g^{ijk}\right)^{(n-1)}}\right), \tag{4.14a}$$

$$\left(w_d^{ijk}\right)^{(n)} = \frac{1}{\Delta t_{n-1}} ln\left(\frac{\left(\bar{C}_d^{ijk}\right)^{(n)}}{\left(\bar{C}_d^{ijk}\right)^{(n-1)}}\right). \tag{4.14b}$$

4.3.3 Transient Solution Procedure

Before a transient is initiated by perturbations in reactor conditions (i.e., control rod motions and thermal hydraulic changes), the initial flux shape and the eigenvalue[3] are obtained by applying the solution methods described in Section 4.2.5. If a set of expansion functions, different from the one used in the steady-state analysis, is to be

[3] The nodal fission cross sections are divided by the eigenvalue for the subsequent transient analysis. This does not mean that the fission cross sections in the transient analysis are physically different from those in the steady-state case. Rather, the division by the eigenvalue is required for a numerically consistent solution.

used in the beginning of the transient, Eq. (3.23a) must be solved first. Otherwise, the fully implicit solution of Eq. (3.34) may proceed.

First, the CMFD discontinuity factors are computed using a large time step, Δt_m, with the thermal hydraulic conditions at the beginning of the time step (the CMFD discontinuity factors are relatively insensitive to the changes in thermal hydraulic conditions). The mixing coefficients are then determined using a smaller time step, Δt_n. The CMFD discontinuity factors used in this calculation are obtained by a linear interpolation of the values at t_m and t_{m+1}.

These steps are repeated until a different set of expansion functions are adopted to reflect changes in reactor conditions. At time t_l of the expansion function change, Eq. (3.24a) must be solved before proceeding with the steps mentioned in the previous paragraph. Although discontinuous expansion functions are allowed, one must be reasonably sure, from physical intuition, that the expansion functions replaced do not contribute significantly to the actual flux shape. If not, distinct discontinuities may be apparent at those time steps when the expansion function changes occur.

4.4 Summary

The complete description of the numerical methods and the solution procedures for the steady-state and transient synthesis equations were presented in this chapter. The steady-state synthesis equation lacks certain properties which ensure the convergence of iterative matrix inversion techniques and the existence and uniqueness of the positive, largest eigenvalue and its associated positive eigenvector. The resolution of the convergence problem is not difficult in that a direct matrix inversion scheme called LU factorization can be applied. However, there is no theoretical resolution of the latter; hence past experience with synthesis methods is the only assurance that the power method will converge to a physically acceptable solution. Though the use of fundamental mode expansion functions has been shown to produce reasonable results, one should not be surprised even if physically unacceptable negative fluxes or eigenvalues are observed in some cases.

The power method, accelerated by the Wielandt's eigenvalue shifting scheme, is used for outer iterations. Adoption of the Wielandt's eigenvalue shifting scheme necessitates the use of simultaneous group solution. T. Sutton's group-wise solution procedure [S-5] used in synthesis methods was found to have convergence problems; hence not implemented in this study. The bandwidth of the matrix, resulting from the simultaneous group solution scheme, is minimized by a simple reordering of the mixing

coefficients, and the banded structure is exploited to reduce the computational requirement associated with the LU factorization. Also, partial pivoting is introduced to minimize the rounding-off errors in the LU factorization routine.

The stability consideration forces the use of a fully implicit time differencing scheme for the solution of the transient synthesis equation, and the LU factorization is again applied in the transient solution procedure. The introduction of discontinuous expansion functions requires the solution of a time continuity equation in addition to the transient synthesis equation. When replacing a set of expansion functions by another set, one must be careful with the choice in order not to introduce apparent discontinuities in core power.

CHAPTER 5

APPLICATION OF SYNTHESIS METHOD

5.1 Introduction

The steady-state and transient synthesis methods presented in Chapter 2 and Chapter 3 along with their numerical solution methods discussed in Chapter 4 are applied to a few benchmark problems in this chapter to investigate their accuracy and efficiency. Two CMFD discontinuity factor updating approaches, the CMFD discontinuity factor synthesis scheme and the non-linear iteration scheme, are applied to every problem presented. The comparison of these two CMFD discontinuity factor updating approaches, with respect to their computational speed and accuracy, is the main result presented in this chapter.

Transients involving control rod motion are investigated extensively since they present a significant challenge in synthesis methods with substantial changes in flux shapes. A coolant inlet temperature transient based on a realistic reactor configuration is also tested and presented in this chapter. These problems are analyzed using all the options incorporated in the synthesis method to ensure their functionality. The potential convergence problems discussed in Chapter 4 were not observed, especially with the orthogonalization of expansion and adjoint weight functions.

5.2 Prelude to Synthesis Results

The description of the computer code, execution time and error estimation is given in this section before the presentation of computational results.

5.2.1 Computer Code

The steady-state and transient synthesis methods presented in Chapter 2 and Chapter 3 along with their numerical solution schemes discussed in Chapter 4 are incorporated into a computer code which has been named DISCOVER (**DI**scontinuous **S**ynthesis **CO**de for **VER**ification). This computer code solves three-dimensional, few-group, steady-state and transient problems without extraneous neutron sources. It requires as inputs, two-dimensional expansion and weight functions and, if the CMFD discontinuity factor synthesis scheme is to be applied, the CMFD discontinuity factors associated with the expansion functions. Either a series of two-dimensional calculations or a full three-dimensional calculation produce the necessary expansion and adjoint weight functions. However, a three-dimensional calculation is mandated to provide the axial CMFD discontinuity factors if the CMFD discontinuity factor synthesis scheme is to be applied. For this study, three-dimensional calculations are performed using a computer code called CONQUEST (**CO**de for **N**odal **QU**asi-Static Theory) to generate expansion functions, adjoint weight functions and the CMFD discontinuity factors associated with the expansion functions.

DISCOVER is written in standard FORTRAN 77, except for a few system dependent routines which return the system time and date. DISCOVER has been compiled and executed without problem on a SUN SPARCclassic machine. All computations are performed in single precision to minimize execution times and storage requirements. Some of the salient features of DISCOVER are reiterated as follows

1. Adoption of both continuous and discontinuous expansion functions,
2. Orthogonalization of expansion and weight functions,
3. Direct inversion of matrices using LU factorization,
4. Simultaneous group solution procedure for outer iterations,
5. Wielandt's fractional iteration to accelerate eigenvalue convergence,
6. Fully Implicit time-differencing,
7. Two CMFD discontinuity factor updating approaches, the non-linear iteration scheme and the CMFD discontinuity factor synthesis scheme.

A diagonal symmetry option is allowed; however users have to be careful not to input asymmetric expansion functions nor asymmetric weight functions and CMFD discontinuity factors when this option is utilized. Non-uniform node spacings are also allowed, but irregular geometry (jagged boundaries) are not allowed in DISCOVER. There is no limit on the number of energy groups, and up-scattering is also permitted. The implementation of the transient synthesis method lets users specify when the CMFD discontinuity factors are to be updated allowing additional execution time savings for the transients involving little flux shape changes.

5.2.2 Transverse Leakage Approximations

In Chapter 2, the quadratic transverse leakage approximation was introduced in describing the non-linear iteration scheme. In this approximation, the transverse leakage is expanded as a quadratic polynomial which preserves the node-averaged transverse leakage in the three adjacent nodes. This does not present a problem for nodes in the reactor interior or at boundaries of symmetry. Nodes at the reactor surface, however, do not have the third adjacent node required to perform the quadratic leakage expansion. Therefore, the transverse leakage expansion for nodes on the reactor surface is performed using the three nodes closest to the surface [G-1].

For problems with large reflectors, a quadratic transverse leakage approximation in the core and a flat transverse leakage in the reflector has been found to give good results. The reason for this is that the leakages deep within the reflector tend to be small and only have small effect on the core power distribution. In fact, approximating the transverse leakage in large reflectors as a quadratic polynomial has resulted in stability problems which are not present when the flat approximation is used [G-1].

5.2.3 Power Distribution Errors

The synthesis solutions presented in this chapter are compared to the reference solutions obtained from the CONQUEST calculations. For the purpose of summarizing the errors in the power densities, the maximum node error is defined to be

$$\varepsilon_{max} \equiv \text{Max. over all nodes } \left\{ \frac{\left| P_i - P_i^{ref} \right|}{P_i^{ref}} \right\},$$

where P_i represents the power density in node i and P_i^{ref} represents the reference power density in node i. Also, the average node error is defined to be

$$\bar{\varepsilon} \equiv \frac{1}{V_{core}} \sum_i \frac{\left|P_i - P_i^{ref}\right|}{P_i^{ref}} V_i,$$

where V_i is the volume of node i and V_{core} is the total volume of the reactor core. The convergence criterion on the maximum nodal power changes of 10^{-4} has been used in steady-state calculations and 10^{-1} to 10^{-3} for transient calculations.

5.2.4 Execution Times

The execution times of computer codes are commonly used to compare their relative efficiency. Direct comparison of execution times, however, are often difficult and misleading because the calculation speeds of computer systems vary widely. In order to establish a meaningful comparison, both DISCOVER and CONQUEST calculations have been perform on a SUN SPARCclassic machine. Furthermore, both computer codes are compiled using the same optimizing feature available.

Another factor that significantly affects the execution time is the various convergence criteria adopted. For example, setting the convergence criterion of 10^{-5} on the maximum nodal power error requires a longer execution time than setting one of 10^{-4}. Thus, the same convergence criteria are adopted consistently in both DISCOVER and CONQUEST calculations whenever possible, and in transient analyses the same time steps are used. Only with such consistent choices of convergence criteria and transient time steps is the execution time comparison meaningful in that many peripheral factors contributing to the execution times are eliminated and only the inherent differences in theoretical formulations and numerical solution methods are present.

However, this is not always possible since different codes use different convergence criteria. For instance, CONQUEST uses the average power error as the convergence criterion in transient calculations while DISCOVER uses the maximum power error. For this case, a range of execution times corresponding to different convergence criteria is presented for comparison purposes. Table 5.1 shows the convergence criteria used throughout this chapter. The average power error of 10^{-3} is normally equivalent to a maximum power error somewhere between 10^{-1} to 10^{-3}.

Table 5.1: Convergence criteria used in DISCOVER and CONQUEST.

	DISCOVER	CONQUEST
Steady-State Calculations	Eigenvalue: 10^{-5} Max. Power Error: 10^{-4}	Eigenvalue: 10^{-5} Max. Power Error: 10^{-4}
Transient Calculations	Max. Power Error: 10^{-1} to 10^{-3}	Avg. Power Error: 10^{-3}

5.3 The Three-Dimensional LMW Reactor

The three-dimensional LMW (Langenbuch-Maurer-Werner) reactor [L-4] is a highly simplified LWR as described in Appendix C. The reactor is modeled with two neutron energy groups and six precursor groups. In the steady-state condition, control rod group 2 (a bank of five control rods) is completely withdrawn while control rod group 1 (a bank of four control rods) is inserted half way into the core. The transient involves the withdrawal of the control rod group 1 and the subsequent insertion of the control rod group 2. This complicated control rod motion leads to significant flux shape changes and large cusping effects, and thus, presents a good test for the synthesis method. This problem has been solved with and without thermal hydraulic feedback.

5.3.1 The Three-Dimensional LMW Problem Without Feedback

The steady-state calculation is performed with the 20 x 20 x 20 cm node spacing and eighth-core symmetry. The reference solutions are the CONQUEST calculations with the same node spacing. The expansion functions as well as the adjoint weight functions and the CMFD discontinuity factors needed for synthesis calculations are generated from three-dimensional CONQUEST fluxes for three different reactor conditions. They are: (1) all control rods withdrawn (CR Out), (2) control rod group 1 fully-inserted (Bank 1 In) with control rod group 2 fully withdrawn, and (3) control rod group 2 fully-inserted (Bank 2 In) with control rod group 1 fully withdrawn. The expansion functions used for the LMW steady-state problem without feedback are shown in Table 5.2. Numbers in parenthesis indicate the axial plane from which the two-dimensional expansion functions were taken. Expansion functions from axial plane $k = 5$ are repeatedly used for planes from $k = 3$ to $k = 8$ because the flux shape well

within the core is not expected to vary significantly. On the contrary, the flux shape in the reflector and reflector/core boundary planes can not be represented well with the flux shape at the mid-plane, and therefore, the expansion functions from corresponding planes are selected for boundary and reflector/core boundary planes.

The steady-state results using the three expansion functions given in Table 5.2 are summarized in Table 5.3. The errors in eigenvalue and power densities are small for both the CMFD discontinuity factor synthesis and the non-linear iteration schemes. The maximum errors in nodal power densities occur at a low power density node on the reflector/core interface. The execution time of the CMFD discontinuity synthesis scheme is about a factor of eight less than that of the reference CONQUEST solution confirming its computational efficiency over the non-linear iteration scheme.

The execution time of the non-linear iteration scheme, however, is comparable to that of the reference solution. This is a expected result considering that the solution of quartic polynomial equations is the most time consuming routine in CONQUEST. Since the same exact non-linear iteration scheme is incorporated in DISCOVER, any saving in execution time comes from the decrease in the number of unknowns and the direction matrix inversion solution technique. This saving is offset by the additional CPU time spent in performing matrix multiplication and the reduced convergence rate. It took 12 CMFD discontinuity factor iterations for the synthesis solution while only 8 iterations were needed for the reference CONQUEST solution. The exact cause of this degradation in convergence rate is not known, but the approximate nature of the synthesis equation in conjunction with the formally exact polynomial equations may be a contributing factor.

The transient calculations were performed using the same expansion functions. Fully implicit calculations were carried out with both the mixing coefficient and the CMFD discontinuity factor updating time steps of 1 second. The results of these calculations are presented numerically in Table 5.4 and graphically in Figure 5.1. It is evident from Table 5.4 and Figure 5.1 that the non-linear iteration scheme produces a better result. The maximum errors in nodal power densities occur in either reflector/core boundary nodes or nodes in which control rods are moving.

The transient execution times are listed given in Table 5.5. The real-time calculation is realized in the reference CONQUEST solution as well as in the DISCOVER solution with the CMFD discontinuity factor synthesis scheme. There is about factor of three to four reduction in execution time, much less than that shown in the steady-state result. This is attributed to the time-consuming matrix multiplication which have to be performed whenever cross sections are updated. The cross section updating in turn

Table 5.2: Expansion functions for the LMW steady-state problem without feedback. (3 Expansion functions)

Axial Plane (k)	Description of Expansion Functions (Axial Plane, k)		
	Expansion Function 1	Expansion Function 2	Expansion Function 3
1	CR Out (1)	Bank 1 In (1)	Bank 2 In (1)
2	CR Out (2)	Bank 1 In (2)	Bank 2 In (2)
3	CR Out (5)	Bank 1 In (5)	Bank 2 In (5)
4	CR Out (5)	Bank 1 In (5)	Bank 2 In (5)
5	CR Out (5)	Bank 1 In (5)	Bank 2 In (5)
6	CR Out (5)	Bank 1 In (5)	Bank 2 In (5)
7	CR Out (5)	Bank 1 In (5)	Bank 2 In (5)
8	CR Out (5)	Bank 1 In (5)	Bank 2 In (5)
9	CR Out (9)	Bank 1 In (9)	Bank 2 In (9)
10	CR Out (10)	Bank 1 In (10)	Bank 2 In (10)

Table 5.3: A summary of the results for the LMW steady-state problem without feedback (3 Expansion Functions).

	CONQUEST (Ref.)	DISCOVER (DF Syn.)	DISCOVER (Non-Lin.)
Eigenvalue	0.999643	0.999853	0.999665
Number of DF Iterations	8	4	12
Number of Outer Iterations	27	18	34
CPU Time (s)	4.4	0.56	4.5
Avg. Nodal Power Error (%)	--	0.70	0.20
Max. Nodal Power Error (%), Node (i,j,k), Ref. Normalized Power Density	--	4.54 (1,4,9) 0.47	1.46 (1,4,6) 0.18
Error In Max. Power Node (%), Node (i,j,k), Ref. Normalized Power Density	--	0.27 (1,1,5) 2.45	-0.16 (1,1,5) 2.45

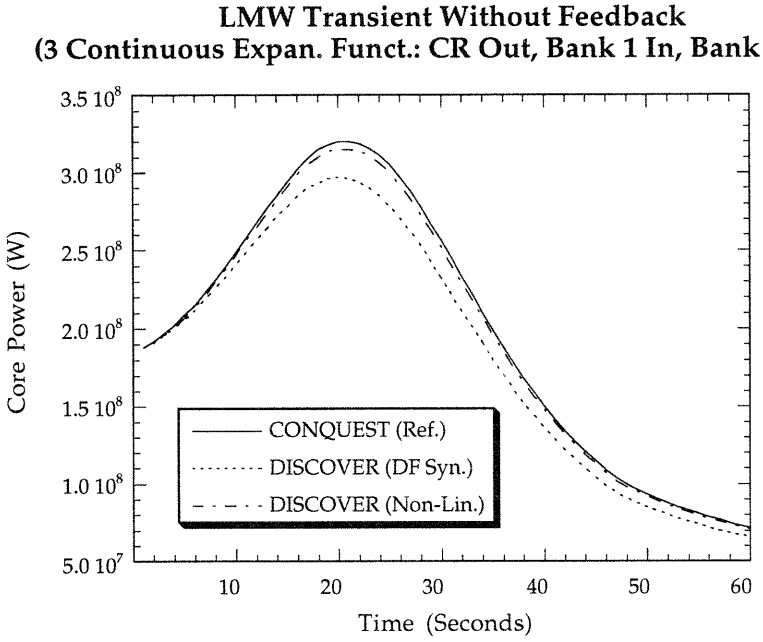

Figure 5.1: Core power vs. time for the LMW transient without feedback. (3 Cont. Expan. Functions: CR Out, Bank 1 In, Bank 2 In)

Table 5.4: A comparison of errors for the LMW transient without feedback.

	DF Synthesis Scheme			Non-Linear Iteration Scheme		
Time (s)	Avg. Nodal Power Error (%)	Max. Nodal Power Error (%), Node (*i,j,k*), Ref. Normalized Power Density	Error In Max. Power Node (%), Node (*i,j,k*), Ref. Normalized Power Density	Avg. Nodal Power Error (%)	Max. Nodal Power Error (%), Node (*i,j,k*), Ref. Normalized Power Density	Error In Max. Power Node (%), Node (*i,j,k*), Ref. Normalized Power Density
0	0.70	4.54, (1,4,9), 0.47	0.27, (1,1,5), 2.45	0.20	1.46, (1,1,10), 0.18	0.16, (1,1,5), 2.45
5	1.40	5.73, (1,4,9), 0.47	-0.96, (1,1,5), 2.44	0.55	1.20, (1,4,6), 0.57	-0.72, (1,1,5), 2.44
10	3.30	7.61, (1,4,9), 0.48	-2.92, (1,1,5), 2.43	0.79	1.69, (1,5,8), 0.63	-0.94, (1,1,5), 2.43
20	7.16	11.6, (1,1,9), 0.72	-6.75, (1,1,5), 2.43	1.44	2.64, (1,1,10), 0.17	-1.49, (1,1,5), 2.43
30	9.14	14.1, (1,1,9), 0.69	-8.79, (1,1,5), 2.43	1.61	2.06, (4,5,5), 0.62	-1.60, (1,1,5), 2.43
40	9.25	13.9, (1,1,9), 0.70	-9.77, (1,2,5), 2.29	1.66	2.40, (4,5,4), 0.55	-1.85, (1,2,5), 2.29
50	8.74	13.3, (1,1,9), 0.72	-9.38, (1,2,5), 2.26	1.45	2.42, (4,5,3), 0.40	-1.70, (1,2,5), 2.26
60	8.70	13.3, (1,1,9), 0.72	-9.31, (1,2,5), 2.26	1.40	2.38, (4,5,3), 0.40	-1.62, (1,2,5), 2.26

Table 5.5: A summary of execution times for the LMW transient without feedback.

	CPU Time (s)	CPU Time (s)	CPU Time (s)
CONQUEST (Ref.)	36.7 [a]	36.7 [a]	36.7 [a]
DISCOVER (DF Syn.)	13.2 [b]	12.9 [c]	8.3 [d]
DISCOVER (Non-Lin.)	74.2 [b]	53.8 [c]	27.5 [d]

[a] Avg. nodal power error convergence criterion = 10^{-3}.
[b] Max. nodal power error convergence criterion = 10^{-3}.
[c] Max. nodal power error convergence criterion = 10^{-2}.
[d] Max. nodal power error convergence criterion = 10^{-1}.

necessitates the need for the time-consuming LU factorization routine, and thereby, increases the computational requirement further. The non-linear iteration scheme, which has a slower convergence rate as well as the aforementioned requirements, gives execution times that are, at best, comparable to the reference result.

Figure 5.2 shows the transient results obtained from the CMFD discontinuity factor synthesis scheme with several different discontinuity factor time steps. The mixing coefficient time step of 1 second is used for all calculations. The result obtained with the CMFD discontinuity factor update time step of 2 seconds shows excellent agreement with that obtained with the CMFD discontinuity factor time step of 1 second. However, the 4 second calculation (in 4 seconds, a control rod traverses more than half of a node in this problem) shows a bit of fluctuation. Figure 5.3 shows similar results obtained from the non-linear iteration scheme.

The core power versus time for calculations with and without the cusping correction are given in Figure 5.4. The volume-averaging of the cross sections leads to an over-prediction of the control rod's "worth" as the rod traverses the node. As a result, the core power is under-predicted. The calculation employing the cusping correction, however, displays no discernible cusping effects [G-1].

All previous calculations were performed with temporally continuous expansion functions, that is at a given axial plane the same expansion functions were used throughout the transient. To test the accuracy of temporally discontinuous synthesis method, the same transient calculations have been performed again using two expansion functions. The initial steady-state condition is calculated before the initiation of the transient. Table 5.6 and Table 5.7 provide the description of the expansion functions employed and the steady-state results, respectively. Comparison of Table 5.7 with

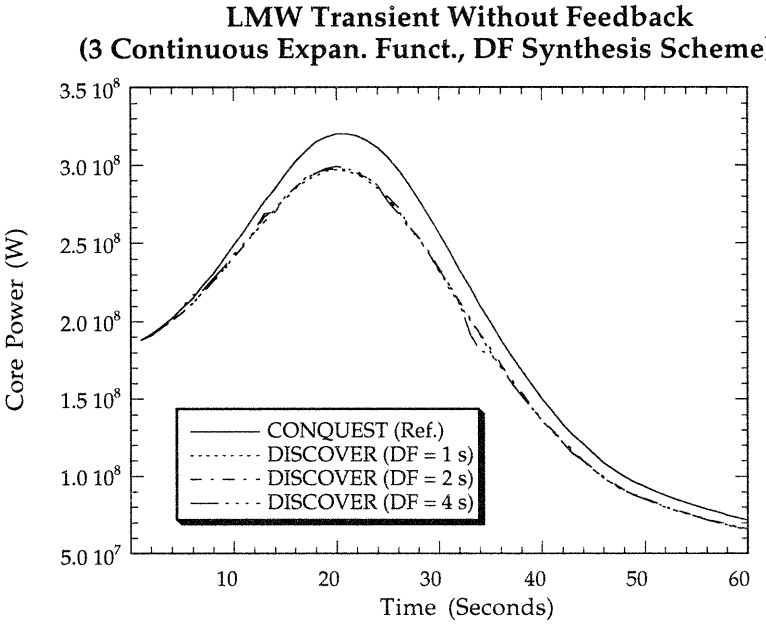

Figure 5.2: Core power vs. time for the LMW transient without feedback. (DF Synthesis Scheme with different time steps)

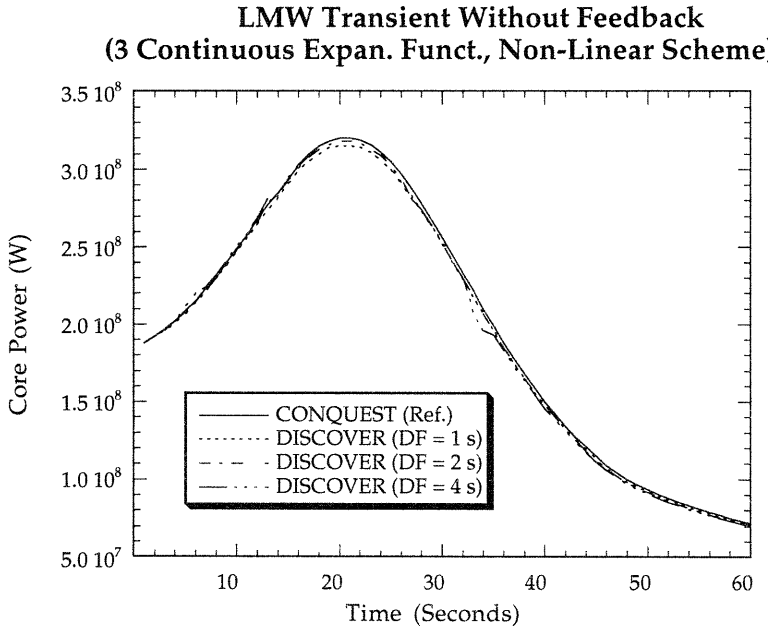

Figure 5.3: Core Power vs. time for the LMW transient without feedback. (Non-Linear Iteration Scheme with different time steps)

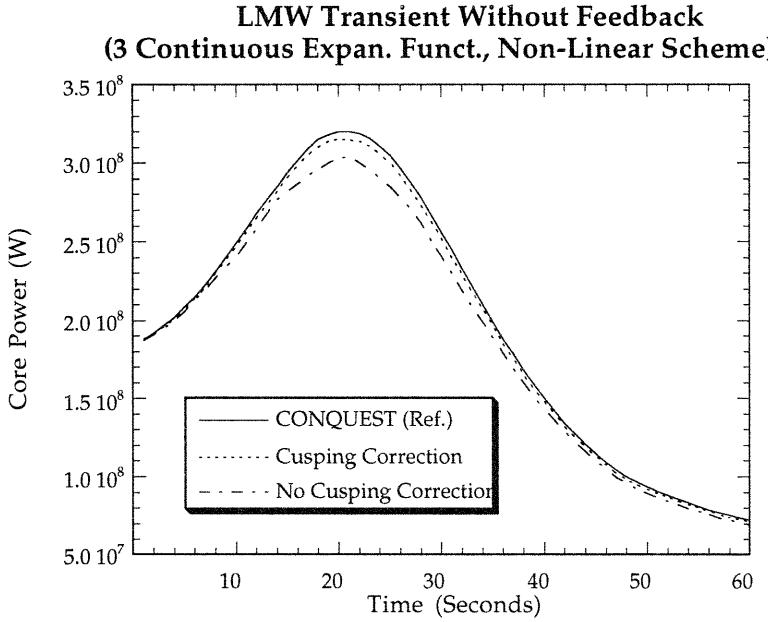

Figure 5.4: Core power vs. time for the LMW transient without feedback demonstrating the cusping correction.

Table 5.6: Expansion functions for the LMW steady-state problem without feedback. (2 Expansion Functions)

Axial Plane (k)	Description of Expansion Functions (Axial Plane, k)	
	Expansion Function 1	Expansion Function 2
1	CR Out (1)	Bank 1 In (1)
2	CR Out (2)	Bank 1 In (2)
3	CR Out (5)	Bank 1 In (5)
4	CR Out (5)	Bank 1 In (5)
5	CR Out (5)	Bank 1 In (5)
6	CR Out (5)	Bank 1 In (5)
7	CR Out (5)	Bank 1 In (5)
8	Bank 1 In (5)	CR Out (5)
9	Bank 1 In (9)	CR Out (9)
10	Bank 1 In (10)	CR Out (10)

Table 5.7: A summary of the results for the LMW steady-state problem without feedback (2 Expansion Functions).

	CONQUEST (Ref.)	DISCOVER (DF Syn.)	DISCOVER (Non-Lin.)
Eigenvalue	0.999643	0.999732	0.999668
Number of DF Iterations	8	4	12
Number of Outer Iterations	27	18	35
CPU Time (s)	4.4	0.40	4.2
Avg. Nodal Power Error (%)	--	0.65	0.18
Max. Nodal Power Error (%),		3.35	1.34
Node (*i,j,k*),	--	(1,4,9)	(1.4,6)
Ref. Normalized Power Density		0.47	0.180
Error In Max. Power Node (%),		0.28	-0.29
Node (*i,j,k*),	--	(1,1,5)	(1,1,5)
Ref. Normalized Power Density		2.45	2.45

Table 5.3 reveals little difference because the control rod group 2 expansion function is not needed for the steady-state calculation.

Temporally discontinuous expansion functions, different from those used in the steady-state calculation, are given in Table 5.8 and the graph of core power versus time is shown in Figure 5.5. Bank 2 In expansion function replaced one of the expansion functions as the control rod group 2 is being inserted into the core. An attempt has been made to ensure, by intuition, that the expansion being replaced contributed minimally to the actual flux shape. However, with the complicated control rod motion and limited number of expansion functions, it was not always possible to achieve the right combination. Figure 5.5 shows the distinct discontinuities caused by a sudden removal of a expansion function which still has a significant contribution to the synthesized flux shape.

Consequently, the temporally discontinuous application of the synthesis method has been attempted once more, but this time with three expansion functions instead of two. The same expansion functions given in Table 5.2 were employed initially and any change in expansion functions are given in Table 5.9. A little after the control rod group 1 is completely withdrawn from a plane, the Bank 1 In expansion function is replaced with another CR Out expansion function (recall that the expansion functions have to be linearly independent not to cause a singular matrix). Intuitively, this should have a

Table 5.8: Changes in expansion functions for the LMW transient problem without feedback (2 Expansion Functions).

Time (s)	Axial Plane (k)	Description of Expansion Functions (Axial Plane, k)	
t=0 to t=6	None	None	
t=6 to t=12	9	Bank 1 In (9)	Bank 2 In (9)
t=12 to t=18	8	Bank 1 In (5)	Bank 2 In (5)
t=18 to t=24	7	CR Out (5)	Bank 2 In (5)
t=24 to t=32	6	CR Out (5)	Bank 2 In (5)
t=32 to t=38	5	CR Out (5)	Bank 2 In (5)
t=38 to t=60	4	CR Out (5)	Bank 2 In (5)

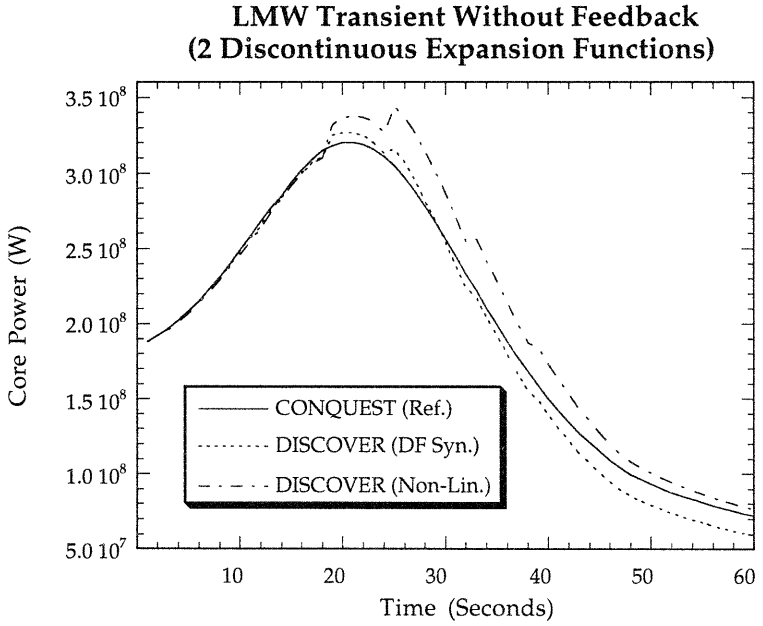

Figure 5.5: Core power vs. time for the LMW transient without feedback. (2 Discontinuous Expansion Functions)

Table 5.9: Changes in expansion function for the LMW transient problem without feedback (3 Expansion Functions).

Time (s)	Axial Plane (k)	Description of Expansion Functions (Axial Plane, k)		
t=0 to t=8	None	None		
t=8 to t=15	6	CR Out (5)	CR Out (2)	Bank 2 In (5)
t=15 to t=22	7	CR Out (5)	CR Out (2)	Bank 2 In (5)
t=22 to t=28	8	CR Out (5)	CR Out (2)	Bank 2 In (5)
t=28 to t=60	9	CR Out (9)	CR Out (2)	Bank 2 In (9)

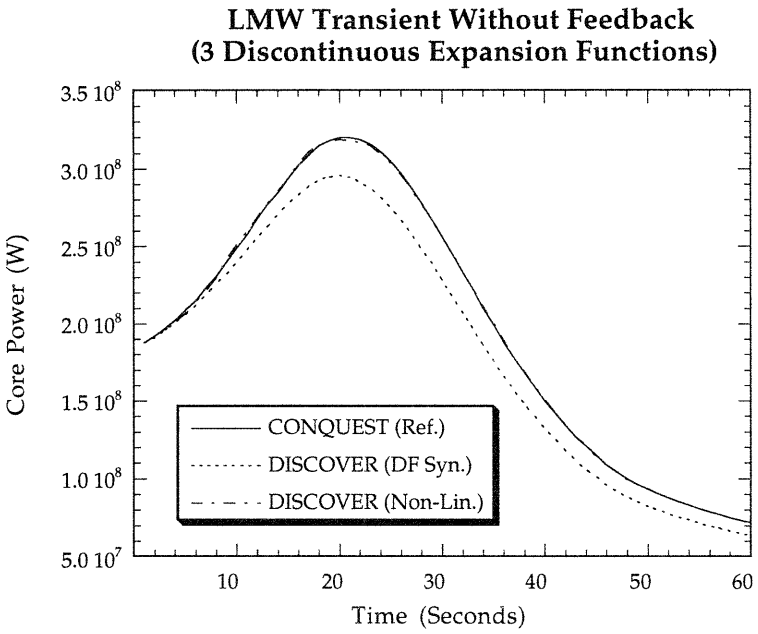

Figure 5.6: Core power vs. time for the LMW transient without feedback. (3 Discontinuous Expansion Functions)

negligible effect because once the control rod group 1 is out of an axial plane, the CR Out shape should be the dominant one. In fact, Figure 5.6 shows that the discontinuities apparent in Figure 5.5 disappear even with temporally discontinuous expansion functions. Furthermore, the result improved, at least for the non-linear iteration scheme, as a result of the replacement of out-dated expansion functions with ones that better approximate the true flux shape.

5.3.2 The Three-Dimensional LMW Problem With Feedback

The three-dimensional LMW problem has been combined with the WIGL thermal hydraulic parameters which are representative of an operating PWR [S-2]. The WIGL parameters are given in Appendix C. The same node spacing of 20 x 20 x 20 cm and eighth-core symmetry is maintained. Again, the reference solutions are obtained from the CONQUEST calculations. The expansion functions, the adjoint weight functions and the CMFD discontinuity factors needed for synthesis application are generated, from steady-state CONQUEST calculations, for the same reactor conditions considered in Section 5.3.1: (1) all control rods withdrawn (CR Out), (2) control rod group 1 fully-inserted (Bank 1 In) and (3) control rod group 2 fully-inserted (Bank 2 In). All steady-state CONQUEST calculations were performed at the power level of 184.8 MW_{th}.

The expansion functions employed for the steady-state calculations are given in Table 5.10 and the synthesis results are summarized in Table 5.11. The CMFD discontinuity factor synthesis scheme still shows about five-fold reduction in execution time while the non-linear iteration scheme requires the same execution time as the reference calculation. The average nodal power errors are greater than those observed in the problem without feedback. This in turn explains the relatively large errors in eigenvalues. However, both the CMFD discontinuity factor synthesis scheme and the non-linear iteration scheme show comparable nodal power errors.

The transient calculations were performed using the same expansion functions shown in Table 5.10. The mixing coefficient and the CMFD discontinuity factor updating time step of 1 second is used. Figure 5.7 and Table 5.12 show the graphical and numerical results, respectively. Again, the nodal power errors in both schemes are comparable. The superior accuracy of the non-linear iteration scheme, observed in the LMW transient problem without feedback, is not present because of the thermal hydraulic feedback effects. The transient calculation times are given in Table 5.13.

Figure 5.8 shows the transient results obtained from the CMFD discontinuity factor synthesis scheme with several different discontinuity factor time steps. The mixing coefficient time step of 1 second is used for all calculations. The discontinuity factor time step of 4 seconds results in a large oscillation when a new set of discontinuity factors are updated. This fluctuation was also observed in the LMW transient without feedback, but the thermal hydraulic feedback amplifies the fluctuation (recall that the CMFD discontinuity factors are updated without taking the thermal hydraulic changes into consideration). Figure 5.9 shows the similar results obtained for

Table 5.10: Expansion functions for the LMW steady-state problem with feedback. (All expansion functions generated at 184.8 MW_{th})

Axial Plane (k)	Description of Expansion Functions (Axial Plane, k)		
	Expansion Function 1	Expansion Function 2	Expansion Function 3
1	CR Out (1)	Bank 1 In (1)	Bank 2 In (1)
2	CR Out (2)	Bank 1 In (2)	Bank 2 In (2)
3	CR Out (5)	Bank 1 In (5)	Bank 2 In (5)
4	CR Out (5)	Bank 1 In (5)	Bank 2 In (5)
5	CR Out (5)	Bank 1 In (5)	Bank 2 In (5)
6	CR Out (5)	Bank 1 In (5)	Bank 2 In (5)
7	CR Out (5)	Bank 1 In (5)	Bank 2 In (5)
8	CR Out (5)	Bank 1 In (5)	Bank 2 In (5)
9	CR Out (9)	Bank 1 In (9)	Bank 2 In (9)
10	CR Out (10)	Bank 1 In (10)	Bank 2 In (10)

Table 5.11: A summary of the results for the LMW steady-state problem with feedback.

	CONQUEST (Ref.)	DISCOVER (DF Syn.)	DISCOVER (Non-Lin.)
Eigenvalue	0.983160	0.986085	0.985846
Number of DF Iterations	8	8	12
Number of Outer Iterations	34	27	35
CPU Time (s)	5.47	1.24	5.0
Avg. Nodal Power Error (%)	--	3.01	3.24
Max. Nodal Power Error (%)	--	7.34	6.96
Node (i,j,k),		(1,1,9)	(1,1,9)
Ref. Normalized Power Density		0.65	0.65
Error In Max. Power Node (%),	--	-0.15	-0.31
Node (i,j,k),		(1,1,5)	(1,1,5)
Ref. Normalized Power Density		2.45	2.45

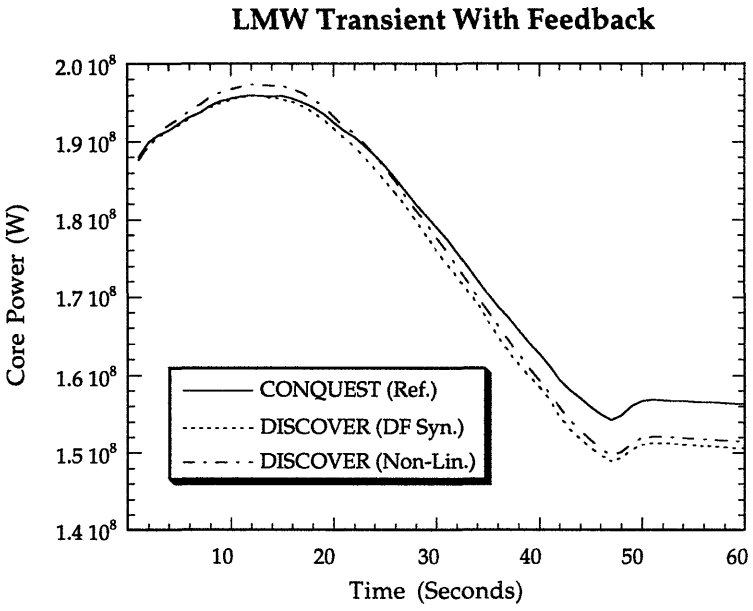

Figure 5.7: Core power vs. time for the LMW transient with feedback.

Table 5.12: A comparison of errors for the LMW transient with feedback.

	DF Synthesis Scheme			Non-Linear Iteration Scheme		
Time (s)	Avg. Nodal Power Error (%)	Max. Nodal Power Error (%), Node (*i,j,k*), Ref. Normalized Power Density	Error In Max. Power Node (%), Node (*i,j,k*), Ref. Normalized Power Density	Avg. Nodal Power Error (%)	Max. Nodal Power Error (%), Node (*i,j,k*), Ref. Normalized Power Density	Error In Max. Power Node (%), Node (*i,j,k*), Ref. Normalized Power Density
0	3.0	7.34, (1,1,9), 0.65	-0.15, (1,1,5), 2.26	3.2	6.96, (1,1,9), 0.65	-0.31, (1,1,5), 2.26
5	3.0	7.50, (1,1,9), 0.65	-0.13, (1,1,5), 2.24	3.3	7.61, (1,1,9), 0.65	0.15, (1,1,5), 2.24
10	2.9	7.30, (1,1,9), 0.64	-0.03, (1,1,5), 2.23	3.4	8.43, (1,1,9), 0.64	0.56, (1,1,5), 2.23
20	2.9	8.18, (4,5,9), 0.19	0.36, (1,1,5), 2.23	3.3	7.33, (1,1,8), 1.16	0.44, (1,1,5), 2.23
30	3.0	7.03, (4,5,2), 0.25	-1.69, (1,1,5), 2.23	3.3	5.92, (3,3,2), 0.68	-0.82, (1,1,5), 2.23
40	3.3	7.96, (3,3,2), 0.68	-4.18, (1,2,5), 2.14	3.3	7.12, (3,3,2), 0.68	-2.98, (1,2,5), 2.14
50	3.8	10.0, (1,1,4), 1.96	-5.58, (1,2,5), 2.13	3.5	8.02, (3,3,2), 0.66	-4.41, (1,2,5), 2.13
60	3.8	10.0, (1,1,4), 1.96	-5.60, (1,2,5), 2.13	3.5	8.08, (3,3,2), 0.66	-4.42, (1,2,5), 2.13

Table 5.13: A summary of execution times for the LMW transient with feedback.

	CPU Time (s)	CPU Time (s)	CPU Time (s)
CONQUEST (Ref.)	46.2 [a]	46.2 [a]	46.2 [a]
DISCOVER (DF Syn.)	16.1 [b]	14.9 [c]	11.3 [d]
DISCOVER (Non-Lin.)	77.0 [b]	51.7 [c]	30.7 [d]

[a] Avg. nodal power error convergence criterion = 10^{-3}.
[b] Max. nodal power error convergence criterion = 10^{-3}.
[c] Max. nodal power error convergence criterion = 10^{-2}.
[d] Max. nodal power error convergence criterion = 10^{-1}.

the non-linear iteration scheme.

A comparison of the calculations with and without the cusping correction are presented in Figure 5.10. The cusping correction introduces no distortion when a control rod leaves one node and enters another while the result with no correction shows more prominent distortion. Figure 5.10 shows that the cusping effects are much more significant than those in the non-feedback calculations.

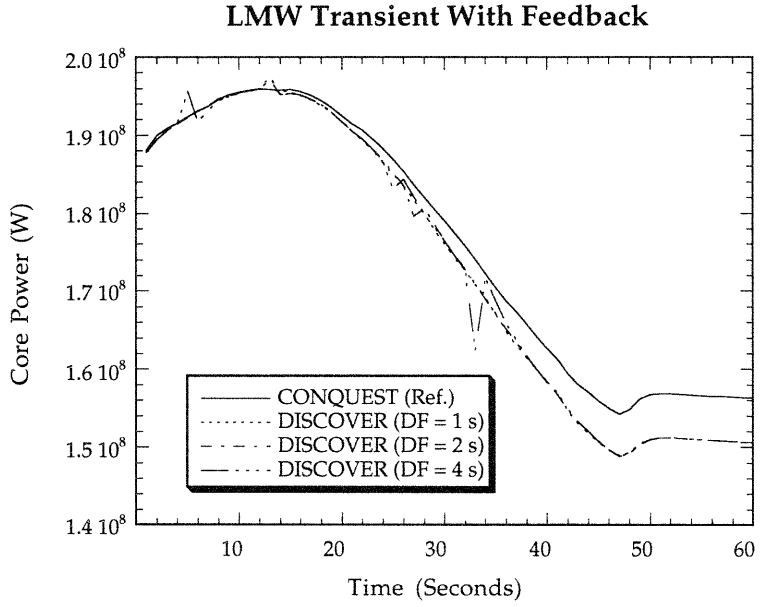

Figure 5.8: Core power vs. time for the LMW transient with feedback. (DF Synthesis Scheme with several different time steps)

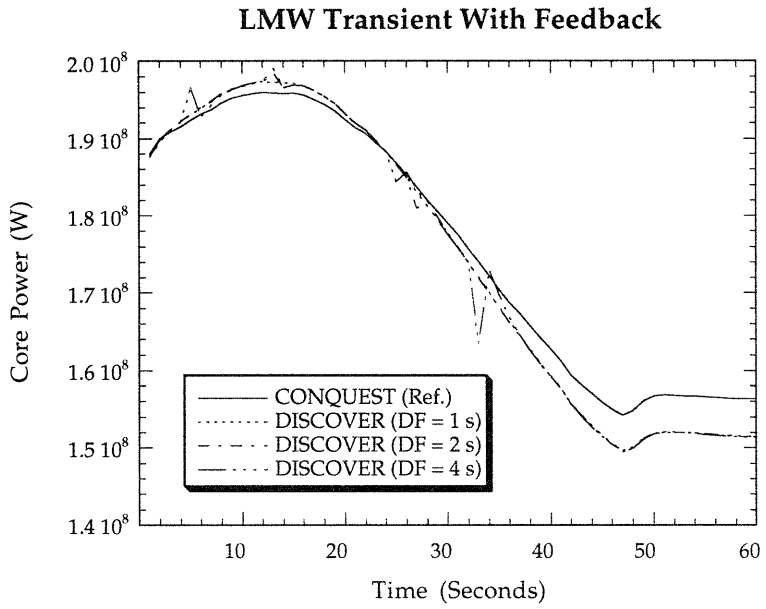

Figure 5.9: Core power vs. time for the LMW transient with feedback. (Non-Linear Iteration Scheme with several different time steps)

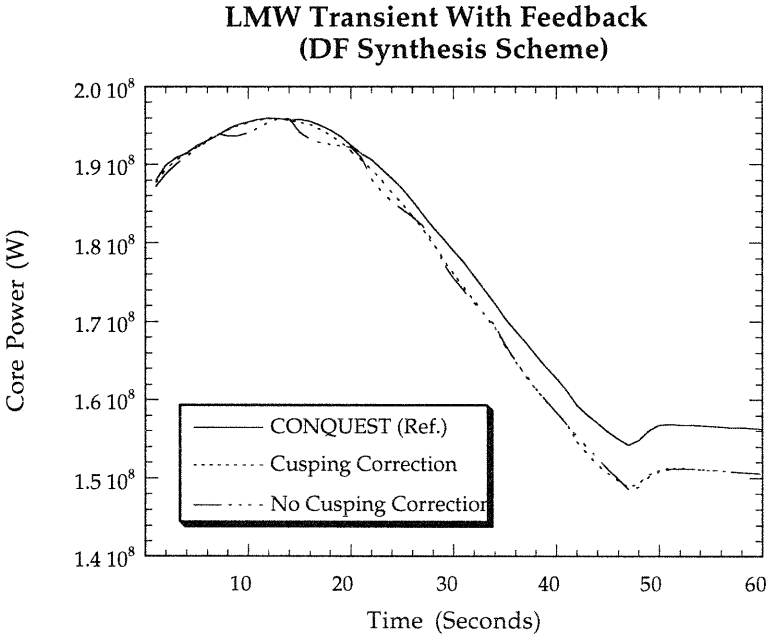

Figure 5.10: Core power vs. time for the LMW transient with feedback demonstrating the effects of cusping correction.

5.4 The PWR Operational Transient

The PWR reactor discussed in this section represents a more realistic reactor model and was introduced by R. Jacqmin [J-1] for analysis of a semi-experimental instrumented nodal synthesis method. The reactor is representative of a Westinghouse pressurized water reactor. The core contains 193 fuel assemblies with dimensions of 21.591 x 21.591 x 360 cm. The radial reflector is explicitly modeled while the axial reflector is represented by infinite reflector albedo boundary conditions. The thermal hydraulic feedback is performed using the WIGL model. The complete description of the reactor model is given in Appendix C.

The reactor is initially critical at 20 % nominal power (667.6 MW_{th}). Control rod bank C and D are partially inserted into the core; C, 120 cm and D, 300 cm. In order to analyze the steady-state and the subsequent transient involving removal of both control rod banks, the expansion functions are obtained from the steady-state CONQUEST calculations for three different reactor conditions. They are: (1) all control rods fully withdrawn (CR Out), (2) control rod bank D fully-inserted (Bank D In) with control rod bank C fully withdrawn and (3) control rod bank C fully-inserted (Bank C In) with control rod bank D fully withdrawn. All CONQUEST calculations were performed at the initial power level (667.6 MW_{th}) and the node spacing of 21.591 x 21.591 x 20 cm was used. The expansion functions employed for both the steady-state and the transient analyses are presented in Table 5.14.

A summary of the steady-state results are presented in Table 5.15. The slower convergence of the non-linear iteration scheme is more pronounced, hence it requires a longer execution time than the reference CONQUEST calculation. Also, huge maximum nodal power errors are observed in both discontinuity factor updating schemes at the axial core boundary. The power density in that node, however, is about 4 % of the average power density. Thus, the huge maximum nodal power errors, shown in percentage, are not a great concern.

The transient is initiated by the removal of control rod bank C and D at a constant speed of 2 cm/s. The control rod bank C reaches the top of the core at t = 60 seconds while the control rod bank D continues its motion. All rod motion ceases at t = 120 seconds leaving the control rod bank D partially inserted (see Appendix C for the figure describing these sequences). The transient is followed until t = 180 seconds when the reactor has nearly reached a new steady-state condition.

The transient results are presented in Figure 5.11. The reference CONQUEST result as well as the point kinetics result is shown. The transient execution times are

Table 5.14: Expansion functions for the PWR steady-state and transient problems. (All expansion functions generated at 667.6 MW_{th})

Axial Plane (k)	Description of Expansion Functions (Axial Plane, k)		
	Expansion Function 1	Expansion Function 2	Expansion Function 3
1	CR Out (1)	Bank D In (1)	Bank C In (1)
2	CR Out (2)	Bank D In (2)	Bank C In (2)
3	CR Out (5)	Bank D In (5)	Bank C In (5)
4	CR Out (5)	Bank D In (5)	Bank C In (5)
5	CR Out (5)	Bank D In (5)	Bank C In (5)
6	CR Out (5)	Bank D In (5)	Bank C In (5)
7	CR Out (5)	Bank D In (5)	Bank C In (5)
8	CR Out (9)	Bank D In (9)	Bank C In (9)
9	CR Out (9)	Bank D In (9)	Bank C In (9)
10	CR Out (9)	Bank D In (9)	Bank C In (9)
11	CR Out (9)	Bank D In (9)	Bank C In (9)
12	CR Out (14)	Bank D In (14)	Bank C In (14)
13	CR Out (14)	Bank D In (14)	Bank C In (14)
14	CR Out (14)	Bank D In (14)	Bank C In (14)
15	CR Out (14)	Bank D In (14)	Bank C In (14)
16	CR Out (14)	Bank D In (14)	Bank C In (14)
17	CR Out (17)	Bank D In (17)	Bank C In (17)
18	CR Out (18)	Bank D In (18)	Bank C In (18)

given in Table 5.16. The point kinetics approximation which assumes the steady-state flux shape for the duration of the transient leads to a large error. Both the radial and axial flux shapes drastically change for this transient and point kinetics approximation inevitably results in an unacceptably poor solution. The CMFD discontinuity factor synthesis scheme replicates the reference result well with about 3 % error in the final core power. Also it is faster than the reference solution by a factor of 3. The non-linear iteration scheme, however, leads to a relatively large error of about 15 % in the final core power. This is a rather puzzling result in that the non-linear iteration scheme should provide a more accurate result and previous examples have demonstrated such to be the case.

Table 5.15: A summary of the results for the PWR steady-state problem with feedback

	CONQUEST (Ref.)	DISCOVER (DF Syn.)	DISCOVER (Non-Lin.)
Eigenvalue	1.045484	1.047720	1.045651
Number of DF Iterations	8	6	14
Number of Outer Iterations	31	25	52
CPU Time (s)	20.8	3.7	25.2
Avg. Nodal Power Error (%)	--	7.93	4.57
Max. Nodal Power Error (%)	--	52.4	29.7
Node (*i,j,k*),		(1,1,18)	(1,1,18)
Ref. Normalized Power Density		0.044	0.044
Error In Max. Power Node (%),	--	2.01	1.36
Node (*i,j,k*),		(1,7,7)	(1,7,7)
Ref. Normalized Power Density		2.38	2.38

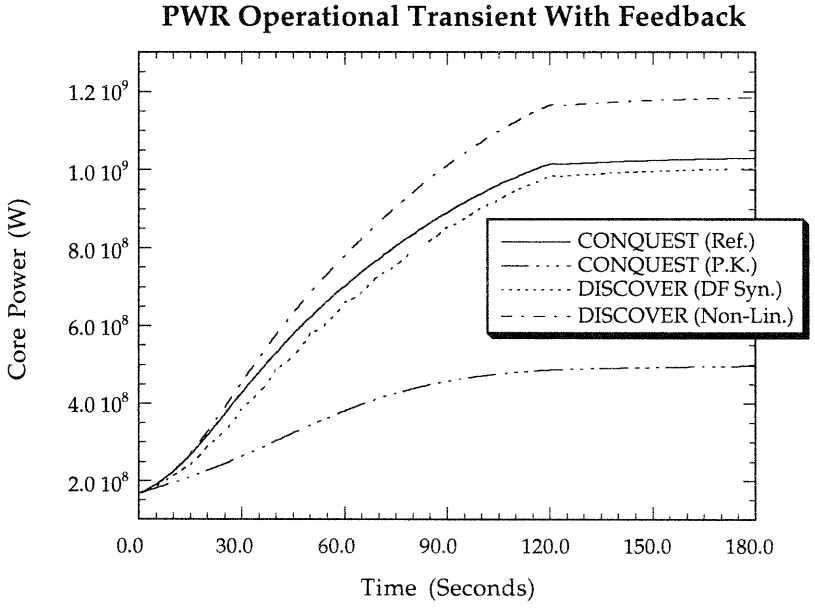

Figure 5.11: Core power vs. time for the PWR operational transient.

Table 5.16 A summary of execution times for the PWR operational transient.

	CPU Time (s)	CPU Time (s)	CPU Time (s)
CONQUEST (Ref.)	906 [a]	906 [a]	906 [a]
CONQUEST (P.K)	274 [a]	274 [a]	274 [a]
DISCOVER (DF Syn.)	281 [b]	271 [c]	209 [d]
DISCOVER (Non-Lin.)	1650 [b]	1126 [c]	636 [d]

[a] Avg. nodal power error convergence criterion = 10^{-3}.
[b] Max. nodal power error convergence criterion = 10^{-3}.
[c] Max. nodal power error convergence criterion = 10^{-2}.
[d] Max. nodal power error convergence criterion = 10^{-1}.

First, a lack of correct expansion functions was hypothesized for the relatively large error in the non-linear iteration result. Only those expansion functions corresponding to the initial power level were used and the space of expansion functions may not have contained the right flux shape for the end of the transient. But, this reasoning does not explain the result obtained from the CMFD synthesis scheme. A lack of proper expansion functions should result in large errors for both schemes. In fact, a subsequent analysis using six expansions, three at the initial power level and three at the final power level, produced essentially the same results shown in Figure 5.11.

A subsequent analysis revealed that the non-linear iteration scheme had grossly mispredicted the axial CMFD discontinuity factors at the boundaries, not only in magnitude and but even in sign. The albedo boundary condition use for the PWR model was thought to be the culprit and another calculation was performed by modeling the axial reflector explicitly. This indeed corrected the misprediction of the axial CMFD discontinuity factors at the boundaries and core/reflector interfaces, but did not correct the overprediction of core power. The power densities in the boundary nodes were so small that even a large error in the axial CMFD discontinuity factors did not lead to a significant change in the final result.

Then, what is causing the large error in the non-linear iteration scheme when, theoretically, it is supposed to be more accurate that the CMFD synthesis scheme? Figures 5.12 through 5.14 give a hint of what may actually be causing the large error shown in Figure 5.11. The non-linear iteration scheme somehow overpredicts the power in the axial plane from which a control rod is being withdrawn. As the control rods traverses the mid-planes, where the power densities are high, the over-prediction amplifies and finally results in a large error shown in Figure 5.11.

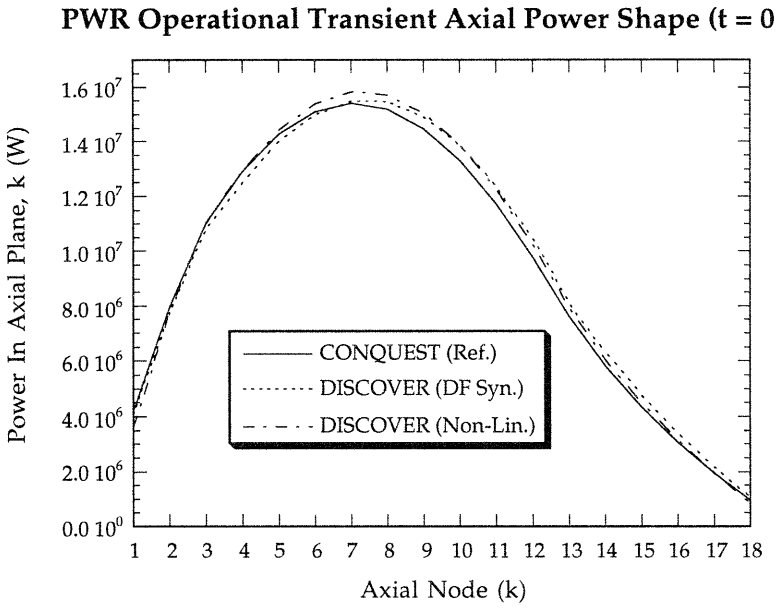

Figure 5.12: Axial power shape for the PWR operational transient (t = 0 s)

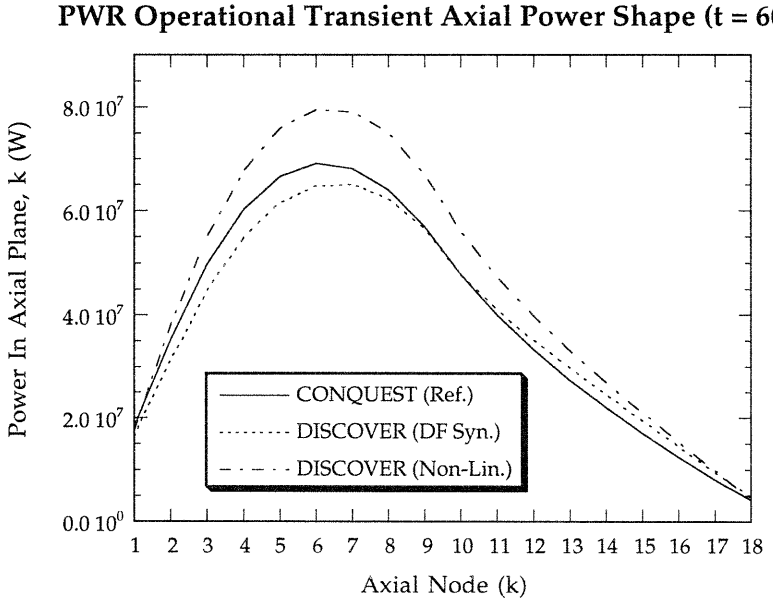

Figure 5.13: Axial power shape for the PWR operational transient (t = 60 s)

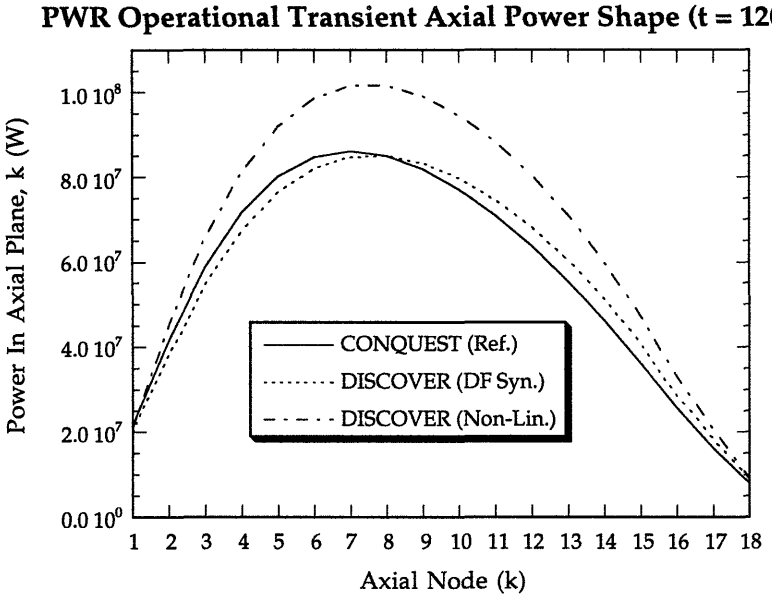

Figure 5.14: Axial power shape for the PWR operational transient (t = 120 s)

A qualitative explanation of this phenomenon is as follows: When only a few expansion functions are used, the synthesis scheme is not well suited to represent a rapid local change in flux shape since the radial flux shape is determined by a linear combination of the expansion functions adopted. Thus, the synthesis scheme tries to approximate a strong local peaking in the flux shape (such as is the case for a control rod removal) by increasing the magnitude of the mixing coefficient more than it should. The non-linear iteration then finds discontinuity factors consistent with the wrong flux shape. On the other hand, the CMFD discontinuity factor synthesis approach uses the weighted average of the precomputed values and therefore somewhat "independently" updates the discontinuity factors. By sheer coincidence, this results in a better prediction of the overall core power than the non-linear iteration scheme.

If this reasoning is valid, the three-dimensional LMW transient considered in Section 5.3.2 should have exhibited the similar trend. However, the error in the LMW transient is compensated by the insertion of control rod group 2. (A similar reasoning should lead to underprediction of power in the axial plane into which a control rod is being inserted.) Also the LMW control rods are not as black as those in the PWR. A new LMW transient involving only control rod group 1 withdrawal should eliminate this compensation in errors. Figure 5.15 shows the result for such a transient and indeed exhibits the same trend shown in Figure 5.11.

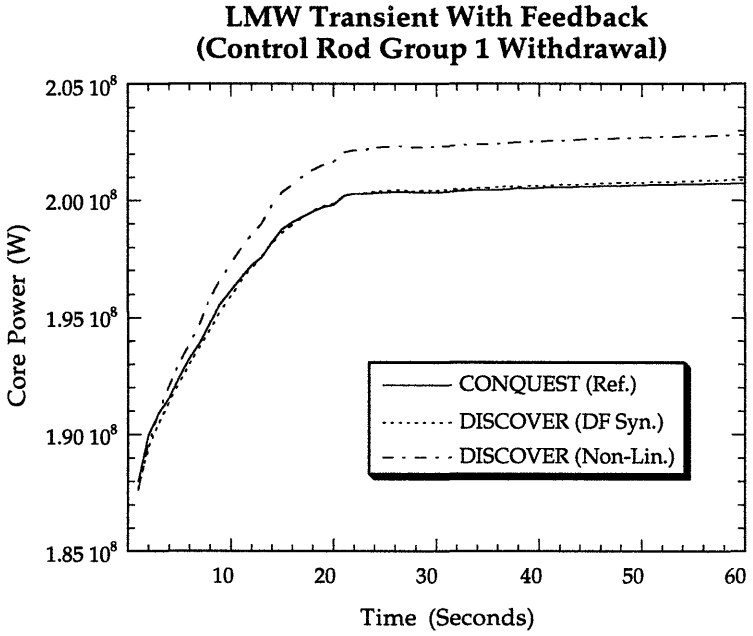

Figure 5.15: Core power vs. time for the LMW transient with feedback. (Control rod group 1 withdrawal)

5.5 The PWR Coolant Inlet Temperature Transient

The transient considered in this section is driven by changing thermal hydraulic conditions of the reactor. The reactor model is the same as the one considered for the PWR operational transient. The reactor is initially in a steady-state, critical condition at nominal power of 3338 MW_{th}. All control rod banks are fully withdrawn. A transient is initiated by a two-second exponential decrease in the coolant inlet temperature, from 555 K to 535 K, followed by an exponential increase to 555 K. The exact form of the perturbation is

$$T_{inlet}(t) = T_{inlet}(0)exp(-t/\tau_1) + T_{inlet}(0)\left[1 - exp(-t/\tau_2)\right], \tag{5.1}$$

where τ_1 = 2.0 s and τ_2 = 2.206 s.

The same expansion functions generated for the PWR operational transient are used for this transient, since it was proven that they are not very sensitive to changes in power level. Further, only one expansion function, namely the control-rod-out shape (CR Out), is used at a given elevation since there is no control rod motion involved. Table 5.17 shows the expansion functions used, and a summary of the steady-state

Table 5.17: Expansion functions for the PWR inlet coolant temperature transient.

Axial Plane (k)	Expansion Function (Axial Plane, k)
1	CR Out (1)
2	CR Out (2)
3	CR Out (5)
4	CR Out (5)
5	CR Out (5)
6	CR Out (5)
7	CR Out (5)
8	CR Out (9)
9	CR Out (9)
10	CR Out (9)
11	CR Out (9)
12	CR Out (14)
13	CR Out (14)
14	CR Out (14)
15	CR Out (14)
16	CR Out (14)
17	CR Out (17)
18	CR Out (18)

results is presented in Table 5.18. Again, a large maximum nodal power errors are observed at the axial core boundary where the power densities are low.

All transient calculations were performed with 1/16 s mixing coefficient time step and the CMFD discontinuity factors were updated every time step. The transient results are shown in Figure 5.16 and the execution times are given in Table 5.19. At peak power, the CMFD discontinuity factor synthesis scheme overpredicts the power by about 3.8 % and the non-linear iteration scheme by about 2.5 %. The point kinetics approximation replicates the reference solution very well since there is no drastic change in flux shape. Because of a minimal number of expansion functions employed, the CMFD discontinuity factor synthesis scheme requires much less execution time than

Table 5.18: A summary of the results for the PWR steady-state problem.

	CONQUEST (Ref.)	DISCOVER (DF Syn.)	DISCOVER (Non-Lin.)
Eigenvalue	1.048782	1.050196	1.050210
Number of DF Iterations	8	10	14
Number of Outer Iterations	23	39	54
CPU Time (s)	18.9	3.8	22.7
Avg. Nodal Power Error (%)	--	5.26	6.38
Max. Nodal Power Error (%)	--	10.8	22.7
Node (*i,j,k*),		(1,7,17)	(6,7,1)
Ref. Normalized Power Density		0.47	0.20
Error In Max. Power Node (%),	--	-1.38	-0.47
Node (*i,j,k*),		(1,7,7)	(1,7,7)
Ref. Normalized Power Density		1.80	1.80

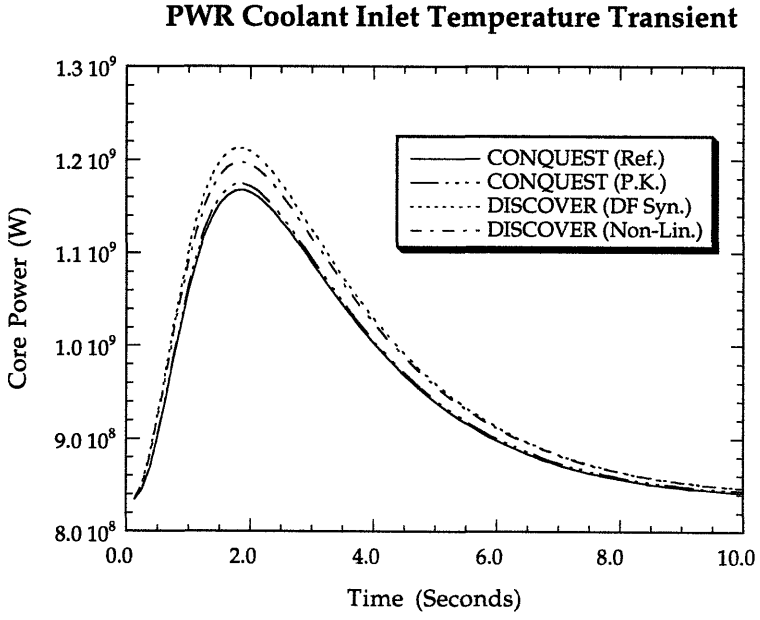

Figure 5.16: Core power vs. time for the PWR coolant inlet temperature transient.

Table 5.19: A summary of execution times for the PWR coolant inlet temp. transient.

	CPU Time (s)	CPU Time (s)	CPU Time (s)
CONQUEST (Ref.)	231 [a]	231 [a]	231 [a]
CONQUEST (P.K)	73 [a]	73 [a]	73 [a]
DISCOVER (DF Syn.)	41 [b]	33 [c]	30 [d]
DISCOVER (Non-Lin.)	281 [b]	183 [c]	146 [d]

[a] Avg. nodal power error convergence criterion = 10^{-3}.
[b] Max. nodal power error convergence criterion = 10^{-3}.
[c] Max. nodal power error convergence criterion = 10^{-2}.
[d] Max. nodal power error convergence criterion = 10^{-1}.

the point kinetics calculation. Also a step doubling adaptive procedure implemented in CONQUEST contributes to a longer execution time for the point kinetics calculation. Compared with the reference calculation there is about a factor of five reduction in execution time. But, even with just one expansion function, the non-linear iteration scheme requires about the same execution time as the reference quasi-static CONQUEST calculation.

5.6 Summary

The space-time dependent nodal synthesis method was applied to the LMW benchmark problem as well as more realistic PWR reactor transients. The accuracy obtainable from the synthesis method is a strong function of the types of expansion functions employed. However, in general, the synthesis method can accurately predict the nodal power to within 5 to 6 percent of the reference solutions. Rather large nodal power errors are observed in some cases, but they generally appear in boundary nodes where power densities are very low. Usually more accurate solutions are obtained from the non-linear iteration scheme rather than the CMFD discontinuity factor synthesis scheme. However, a significant overprediction in core power was observed in the PWR operational transient employing the non-linear iteration scheme. The exact nature of this phenomenon is not well understood, but the lack of flexibility in synthesis method in representing a rapid local flux shape change is believe to the main cause. The CMFD discontinuity factor synthesis approach, which computes discontinuity factors somewhat "independent" of the flux shape, resulted in a better overall core power prediction.

The execution time for the CMFD discontinuity factor synthesis approach was about a factor of five to ten less than that for the reference CONQUEST calculations in steady-state cases. The non-linear iteration scheme, however, did not lead to any reduction in execution time. This lack of reduction in computing time is attributed to the slower convergence of the synthesis method than that of CONQUEST. The polynomial nodal solution routine, which is common in DISCOVER and CONQUEST and is the most time-consuming part of both codes, is another cause. In transient cases, the CMFD discontinuity factor synthesis approach led to about a factor of two to three reduction in execution time. This decrease in execution time reduction is caused by the frequent cross section changes which in turn necessitates the time consuming matrix multiplication and LU factorization. The transient calculation employing the non-linear iteration scheme requires more computing time than the reference solution. The slower convergence rate as well as the factors just mentioned cause this increase in execution time.

A temporally discontinuous application of synthesis was proved to be feasible for the LMW transient without feedback. But, one has to be certain that the expansion functions being replaced do not contribute significantly to the synthesized flux shape. Otherwise, a discontinuous behavior in core power may result. There is no systematic way to predict when and what expansion functions may be replaced. One has to rely on physical intuition based on the particular transient at hand.

CHAPTER 6

CONCLUSIONS AND RECOMMENDATIONS

6.1 Overview and Conclusions

The objective of this study was the development of an efficient, discontinuous space-time dependent nodal synthesis method for the solution of three-dimensional, few-group, steady-state and transient nodal diffusion equations. The synthesis method allows the use of spatially and temporally discontinuous expansion functions to approximate the neutron flux shape of interest.

In Chapter 2, a steady-state, space-dependent synthesis equation was derived by applying a variational procedure to the finite-difference nodal balance equation. Two different approaches were introduced to calculate the CMFD discontinuity factors, which are essential to make the finite-difference nodal balance equations formally exact. The non-linear iteration scheme forces the synthesis solution to match a higher order (quartic) polynomial nodal equations while the CMFD discontinuity factor synthesis scheme uses a weighted averaged of the precomputed values. For the non-linear iteration scheme, it was necessary to modify CONQUEST, a quartic polynomial nodal computer code developed by J. Gehin [G-1], since it only provided the CMFD discontinuity factor ratios.

In Chapter 3, a transient nodal synthesis equation was derived again applying a variational procedure. The use of discontinuous expansion functions combined with the existence of a time derivative necessitated a rather involved mathematical manipulation before a time-dependent nodal synthesis equation as well as a time-continuity equation was derived The introduction of discontinuous expansion functions also forced the use of continuous adjoint weight functions if an over-determined system of equations was to be avoided. Further, a constant number of expansion functions was needed to avoid either an over- or under-determined system of differential equations. The introduction of flux and precursor dynamic frequencies enabled the use of the steady-state non-linear iteration scheme without the need to solve the time-dependent polynomial nodal equations.

The numerical solution methods for the steady-state and time-dependent synthesis equations were discussed in Chapter 4. The properties (or lack of properties) of the steady-state synthesis equation were discussed and a potential convergence problem was indicated. A direct matrix inversion technique, called LU factorization, was introduced and a particular iteration strategy that would optimize the Wielandt's eigenvalue acceleration scheme was discussed. For the transient synthesis solution, the choices of the theta parameter were considered in light of a stability concern, and a fully implicit solution method was adopted. Finally, a temporal solution-advancing strategy was presented that allowed intermittent updates of the CMFD discontinuity factors.

The accuracy and efficiency of the discontinuous space-time dependent nodal synthesis method, incorporated in the DISCOVER code, was demonstrated in Chapter 5. The steady-state and transient results for the LMW benchmark problems and two PWR problems were presented. For most cases, the non-linear iteration scheme proved to be more accurate than the CMFD discontinuity factor synthesis scheme. Average nodal power errors within five to six percents of the reference solutions were achieved with a careful selection of expansion functions. Somewhat large maximum nodal power errors were observed in some cases, but they generally appeared in low power density regions. The feasibility of a temporally discontinuous application was demonstrated on the LMW transient problem. However, distinctive discontinuities were observed if expansion functions were prematurely replaced. There exists no systematic way to predict when and how expansion functions can be replaced. Thus, a continuous temporal application is recommended for transient analysis. An overprediction of core power by about 15 percents was observed for the PWR operational transient when the non-linear iteration scheme was applied. This overprediction is believed to be caused by inaccuracy of the synthesis method.

A substantial reduction in computing time was realized for the steady-state cases when the CMFD discontinuity factor synthesis scheme was applied. A five to tenfold decrease in execution time was consistently observed. The non-linear iteration scheme, however, did not result in any reduction at all. The convergence rate of the non-linear iteration scheme incorporated in DISCOVER was generally slower than that implemented in CONQUEST. Any execution time saving realized by a substantial decrease in the number of unknowns was offset by the degradation in convergence rate. In general, the execution times of the non-linear iteration scheme were comparable to those of the reference calculations.

The reduction in execution time was less pronounced for the transient applications when the CMFD discontinuity factor synthesis scheme was applied. A factor of two to three decrease in computing time was realized. However, again, the non-linear iteration scheme required more computing time (or comparable computing time at best) than CONQUEST calculations. The frequent cross section updates, which in turn necessitated time-consuming matrix multiplication and LU factorization, contributed to the increase in the execution time. The aforementioned degradation in convergence added further execution time.

6.2 Recommendations for Future Work

Several issues arose during this study and following areas are recommended for future investigation.

6.2.1 A Code Allowing Different Number of Expansion Functions Axially

Two competing factors pose difficulties in choosing expansion functions. One wants to employ the expansion functions that closely approximate the physical conditions of a particular axial plane. Practically, this means that many of the expansion functions are very close to each other. A numerical concern, on the other hand, mandates linearly independent expansion functions in order to guarantee a non-singular matrix. Thus, the use of a constant number of expansion function, which is the only option allowed in DISCOVER, forces a user to retain unwanted expansion functions in particular axial planes to accommodate the need of other axial planes. For example, several expansion functions may be needed in axial planes involving control rod motion while just one expansion function may be sufficient for other planes which

do not experience substantial flux shape changes. In this particular situation, one has to include undesirable expansion functions in those axial planes experiencing no flux shape change for other axial planes undergoing substantial flux shape changes. A computer code allowing different number of expansion functions at different axial planes would eliminate this dilemma. Also, more accurate and efficient solutions are possible by excluding undesirable expansion functions and thereby further reducing the number of unknowns.

6.2.2 Further Investigation of Discontinuity Factor Updating Procedures

As the anomaly in Section 5.4 indicates, the effect of the non-linear iteration procedure when combined with synthesis method is not well understood. The synthesis method is an approximate approach with no systematic procedure for predicting error and may result in substantial errors in some cases. Updating the CMFD discontinuity factors by the non-linear iteration procedure may very well positively reinforce the wrong synthesis solution. The CMFD discontinuity factor synthesis approach, on the other hand, produced encouraging results but there is no theoretical explanation of this phenomenon. It is recommended that the two CMFD discontinuity factor updating schemes, incorporated in DISCOVER computer code, be further investigated as to their role in synthesis method.

6.2.3 Non-Iterative Discontinuity Factor Updating During Transient

The fully implicit solution method requires the CMFD discontinuity factor values at t_{n+1} before the solution can be advanced in time. DISCOVER currently employs an iterative approach to update these values and the convergence rate is very slow, especially for the non-linear iteration scheme. A non-iterative discontinuity factor updating scheme would reduce the transient execution time. It is recommended that a sequential updating approach (where the CMFD discontinuity factors at time t_{n+1} are assumed to be same as the current values, but updated before advancing to time t_{n+2}) be investigated for its accuracy and efficiency.

6.2.4 A Quasi-Static Method Using Synthesis As Shape Update

For many transients involving slow flux shape changes, the point kinetics approximation produces adequate results. A quasi-static approach, similar to the one

incorporated in CONQUEST code developed by J. Gehin [G-1], using the synthesis method only for shape updates is recommended for future investigation. This would require less frequent matrix multiplication, which must be carried out in synthesis method whenever there are cross section changes and is the most time-consuming part of the synthesis method.

REFERENCES

[A-1] C. H. Adams and W. M. Stacey, Jr., "An Anomaly Arising in the Collapsed-Group Flux Synthesis Approximation," *Nucl. Sci. Eng.*, **36**, 444 (1969).

[B-1] F. Bennewitz, H. Finnemann, and M. R. Wagner, "Higher Order Corrections in Nodal Reactor Calculations," *Trans. Am. Nucl. Soc.*, **22**, 250 (1975).

[F-1] H. Finnemann, F. Bennewitz, and M. R. Wagner, "Interface Current Techniques for Multidimensional Reactor Calculations," *Atomkernenergie*, **30**, 123 (1977).

[G-1] J. C. Gehin, "A Quasi-Static Polynomial Nodal Method for Nuclear Reactor Analysis," Ph.D. Thesis, Department of Nuclear Engineering, Massachusetts Institute of Technology (September 1992).

[G-2] G. H. Golub and C. F. Van Loan, *Matrix Computations*, Johns Hopkins University Press, Baltimore (1989).

[H-1] J. C. Hughes, "An Experimental Evaluation of the Instrumented Flux Synthesis Method," Ph.D. Thesis, Department of Nuclear Engineering, Massachusetts Institute of Technology (August 1995).

[H-2] A. F. Henry, *Nuclear Reactor Analysis*, MIT Press, Cambridge, Massachusetts (1975).

[H-3] A. F. Henry, "Supplementary Notes on Nodal Methods," Course Notes, 22.213, Department of Nuclear Engineering, Massachusetts Institute of Technology (1993).

[J-1] R. P. Jacqmin, "A Semi-Experimental Nodal Synthesis Method for the On-Line Reconstruction of Three-Dimensional Neutron Flux Shapes and Reactivity," Ph.D. Thesis, Department of Nuclear Engineering, Massachusetts Institute of Technology (September 1991).

[J-2] H. Joo, "Resolution of the Control Rod Cusping Problem for Nodal Methods," Ph.D. Thesis, Department of Nuclear Engineering, Massachusetts Institute of Technology (February 1984).

[K-1] W. S. Kuo, "The General Evaluation of the Nodal Synthesis Method in Nuclear Reactor Transient Analysis," Ph.D. Thesis, Department of Nuclear Engineering, Massachusetts Institute of Technology (June 1994).

[L-1] V. Luco and W. L. Woodruff, "Another Anomaly in Variational Flux Synthesis Method, *Trans. Am. Nucl. Soc.*, **13**, 739 (1970).

[L-2] V. Luco, "On Eigenvalues of the Flux Synthesis Equations," *Trans. Am. Nucl. Soc.*, **14**, 203 (1971).

[L-3] J. D. Lambert, *Computational Methods in Ordinary Differential Equations*, John Wiley & Sons, New York (1973).

[L-4] S. Lagenbuch, W. Mauer, and W. Werner, "Coarse-Mesh Flux Expansion Method for the Analysis of Space-Time Effects in Large Light Water Reactor Cores," *Nucl. Sci. Eng.*, **63**, 437 (1977).

[L-5] K. Lee, "Application of the Point Synthesis Method to Multidimensional Reactor Transient Analysis, Ph.D. Thesis, Department of Nuclear Engineering, Massachusetts Institute of Technology (May 1992).

[N-1] S. Nakamura, Computational Methods in Engineering and Science with Applications to Fluid Dynamics and Nuclear Systems, John Wiley & Sons, New York (1977).

[S-1] W. M. Stacey, Jr., *Space-Time Nuclear Reactor Kinetics*, Academic Press, New York (1969).

[S-2] K. S. Smith, "An Analytic Nodal Method for Solving the Two-Group, Multidimensional, Static and Transient Neutron Diffusion Equations, SM and NE Thesis, Department of Nuclear Engineering, Massachusetts Institute of Technology (March 1979).

[S-3] K. S. Smith, "Nodal Method Storage Reduction by Nonlinear Iteration," *Trans. Am. Nucl. Soc.*, **44**, 265 (1983).

[S-4] W. M. Stacey, Jr., *Variational Methods in Nuclear Reactor Physics*, Academic Press, New York (1974).

[S-5] T. M. Sutton, "Wielandt Iteration as Applied to the Nodal Expansion Method," *Nucl. Sci. Eng.*, **98**, 169 (1988).

[V-1] A. V. Vota, N. J. Curlee, Jr., and A. F. Henry, "WIGL3-A Program for the Steady-State and Transient Solution of the One-Dimensional, Two-Group, Space-Time Diffusion Equations Accounting for Temperature, Xenon, and Control Feedback," WAPD-TM-788, Bettis Atomic Power Laboratory (February 1969).

[W-1] E. L. Wachspress, *Iterative Solution of Elliptic Systems and Applications to the Neutron Diffusion Equations of Reactor Physics*, Prentice-Hall, Eanglewood Cliffs, New Jersey (1966).

[Y-1] J. B. Yasinsky and S. Kaplan, "Synthesis of Three-Dimensional Flux Shapes Using Discontinuous Sets of Trial Functions," *Nucl. Sci. Eng.*, **28**, 426 (1967).

[Y-2] J. B. Yasinsky, "The Solution of the Space-Time Neutron Group Diffusion Equations by a Time-Discontinuous Synthesis Method," *Nucl. Sci. Eng.*, **29**, 381 (1967).

[Y-3] J. B. Yasinsky, " Numerical Studies of Combined Space-Time Synthesis," *Nucl. Sci. Eng.*, **34**, 158 (1968).

[Y-4] J. B. Yasinsky and S. Kaplan, "Anomalies Arising from the Use of Adjoint Weighting in a Collapsed Group Space Synthesis Model," *Nucl. Sci. Eng.*, **31**, 354 (1968).

[Z-1] M. L. Zerkle, "Development of a Polynomial Nodal Method with Flux and Current Discontinuity Factors," Ph.D. Thesis, Department of Nuclear Engineering, Massachusetts Institute of Technology (June 1992).

APPENDIX A

THE QUADRATIC TRANSVERSE LEAKAGE MOMENTS AND COEFFICIENTS

Since the same non-linear iteration scheme used in the CONQUEST computer code is incorporated in the DISCOVER computer program, this appendix is copied from J. Gehin's Ph.D. thesis [G-1].

In this appendix the transverse-leakage coefficients and moments required by the weighted residual equations will be derived. The transverse leakage moments for node (l,m,n) in the u-direction is defined by

$$S_{gup}^{lmn} \equiv \int_{u_l}^{u_{l+1}} w_p(u) S_{gu}^{mn}(u) du, \tag{A.1}$$

where $w_p(u)$ is the weight function. For moments weighting we use the first and second order expansion functions given by

$$w_1(u) = \left(\frac{u - u_l}{h_u^l} \right) - \frac{1}{2}, \tag{A.2a}$$

$$w_2(u) = 3\left(\frac{u - u_l}{h_u^l} \right)^2 - 3\left(\frac{u - u_l}{h_u^l} \right) + \frac{1}{2}. \tag{A.2b}$$

The transverse leakage moments are determined by assuming that its shape in the u-direction can be represented by a quadratic polynomial. The coefficients of the polynomial are obtained by requiring the quadratic approximation to preserve the transverse leakage in three adjacent nodes. Within the core interior, the quadratic transverse leakage which is fitted to the three adjacent nodes is used only for the central node. Nodes located on the reactor boundary, however, do not have nodes on both sides requiring that a biased quadratic fit be used. In addition, a flat transverse leakage approximation may be used at the reactor surface.

A.1 The Quadratic Transverse Leakage Approximation

For the quadratic transverse leakage approximation, we represent the transverse leakage by

$$S_{gu}^{mn}(u) = \bar{S}_{gu}^{lmn} + \left(\bar{S}_{gu}^{l-1,mn} - \bar{S}_{gu}^{lmn}\right)\rho_{u_l}^{l-1}(u) + \left(\bar{S}_{gu}^{l+1,mn} - \bar{S}_{gu}^{lmn}\right)\rho_{u_l}^{l+1}(u)\,, \tag{A.3}$$

where the u-direction node-averaged transverse leakage for node (l,m,n) is given by

$$\bar{S}_{gu}^{lmn} = \frac{1}{h_u^l}\int_{u_l}^{u_{l+1}} S_{gu}^{mn}(u)du\,,$$

and the quadratic polynomials are

$$\rho_{u_l}^{l-1}(u) = a_{u_l}^{-} + b_{u_l}^{-}\left(\frac{u-u_l}{h_u^l}\right) + c_{u_l}^{-}\left(\frac{u-u_l}{h_u^l}\right)^2\,, \tag{A.4a}$$

$$\rho_{u_l}^{l+1}(u) = a_{u_l}^{+} + b_{u_l}^{+}\left(\frac{u-u_l}{h_u^l}\right) + c_{u_l}^{+}\left(\frac{u-u_l}{h_u^l}\right)^2\,. \tag{A.4b}$$

Substituting the transverse leakage approximation, Eq. (A.3), into Eq. (A.1) and performing the required integration gives the following equations for the transverse leakage moments

$$S_{gu1}^{lmn} = \frac{1}{12}\left[(b_{u_l}^{-} + c_{u_l}^{-})\bar{S}_{gu}^{l-1,mn} - (b_{u_l}^{-} + b_{u_l}^{+} + c_{u_l}^{-} + c_{u_l}^{+})\bar{S}_{gu}^{lmn} + (b_{u_l}^{+} + c_{u_l}^{+})\bar{S}_{gu}^{l+1,mn}\right], \tag{A.5a}$$

$$S_{gu2}^{lmn} = \frac{1}{60}\left[c_{u_l}^{-}\bar{S}_{gu}^{l-1,mn} - (c_{u_l}^{-} + c_{u_l}^{+})\bar{S}_{gu}^{lmn} + c_{u_l}^{+}\bar{S}_{gu}^{l+1,mn}\right]. \tag{A.5b}$$

The quadratic polynomial coefficients are obtained by requiring the transverse leakage approximation to preserve the average transverse leakages in each of three

adjacent nodes. This results in the following constraints on the quadratic polynomial coefficients

$$\frac{1}{h_u^{l-1}}\int_{u_{l-1}}^{u_l}\rho_{u_l}^{l-1}(u)du=1,$$
$$\frac{1}{h_u^{l}}\int_{u_l}^{u_{l+1}}\rho_{u_l}^{l-1}(u)du=0,$$
$$\frac{1}{h_u^{l+1}}\int_{u_{l+1}}^{u_{l+2}}\rho_{u_l}^{l-1}(u)du=0,$$
$$\frac{1}{h_u^{l-1}}\int_{u_{l-1}}^{u_l}\rho_{u_l}^{l+1}(u)du=0,$$
$$\frac{1}{h_u^{l}}\int_{u_l}^{u_{l+1}}\rho_{u_l}^{l+1}(u)du=0,$$
$$\frac{1}{h_u^{l+1}}\int_{u_{l+1}}^{u_{l+2}}\rho_{u_l}^{l+1}(u)du=1.$$

Substituting Eqs. (A.4a) and (A.4b) into above constraints and performing necessary integration give the quadratic coefficients

$$a_{u_l}^{-}=\frac{h(h+h_p)}{(h_m+h+h_p)(h_m+h)},$$
$$b_{u_l}^{-}=-\frac{2h(2h+h_p)}{(h_m+h+h_p)(h_m+h)},$$
$$c_{u_l}^{-}=\frac{3h^2}{(h_m+h+h_p)(h_m+h)},$$
$$a_{u_l}^{+}=-\frac{h_m h}{(h_m+h+h_p)(h+h_p)},$$
$$b_{u_l}^{+}=\frac{2h(h_m-h)}{(h_m+h+h_p)(h+h_p)},$$
$$c_{u_l}^{+}=\frac{3h^2}{(h_m+h+h_p)(h+h_p)},$$

where

$$h_m=h_u^{l-1},$$
$$h=h_u^{l},$$
$$h_p=h_u^{l+1}.$$

The transverse leakage coefficients are functions only of the reactor geometry.

A.2 LHS-Biased Quadratic Transverse Leakage Approximation

For nodes adjacent to the external reactor surface, M. Zerkle [Z-1] introduced a biased quadratic transverse leakage approximation. The transverse leakage in the u-direction in node (l,m,n), which is on the Left-Hand-Side (LHS) reactor surface is given by

$$S_{gu}^{mn}(u) = \bar{S}_{gu}^{lmn} + \left(\bar{S}_{gu}^{l+1,mn} - \bar{S}_{gu}^{lmn}\right)\rho_{u_l}^{l+1}(u) + \left(\bar{S}_{gu}^{l+2,mn} - \bar{S}_{gu}^{lmn}\right)\rho_{u_l}^{l+2}(u)\,, \tag{A.6}$$

where

$$\rho_{u_l}^{l+1}(u) = a_{u_l}^{+} + b_{u_l}^{+}\left(\frac{u-u_l}{h_u^l}\right) + c_{u_l}^{+}\left(\frac{u-u_l}{h_u^l}\right)^2\,, \tag{A.7a}$$

$$\rho_{u_l}^{l+2}(u) = a_{u_l}^{++} + b_{u_l}^{++}\left(\frac{u-u_l}{h_u^l}\right) + c_{u_l}^{++}\left(\frac{u-u_l}{h_u^l}\right)^2\,. \tag{A.7b}$$

Substituting the transverse leakage approximation, Eq. (A.6), into Eq. (A.1) and performing the required integration gives the following equations for the transverse leakage moments

$$S_{gu1}^{lmn} = \frac{1}{12}\left[(b_{u_l}^{+} + c_{u_l}^{+})\bar{S}_{gu}^{l+1,mn} - (b_{u_l}^{+} + b_{u_l}^{++} + c_{u_l}^{+} + c_{u_l}^{++})\bar{S}_{gu}^{lmn} + (b_{u_l}^{++} + c_{u_l}^{++})\bar{S}_{gu}^{l+2,mn}\right], \tag{A.8a}$$

$$S_{gu2}^{lmn} = \frac{1}{60}\left[c_{u_l}^{+}\bar{S}_{gu}^{l+1,mn} - (c_{u_l}^{+} + c_{u_l}^{++})\bar{S}_{gu}^{lmn} + c_{u_l}^{++}\bar{S}_{gu}^{l+2,mn}\right]. \tag{A.8b}$$

The quadratic polynomial coefficients are obtained by requiring the transverse leakage approximation, Eq. (A.6), to preserve the average transverse leakage in each of three nodes (l,m,n), $(l+1,m,n)$ and $(l+2,m,n)$. This results in the following constrains on the quadratic polynomial coefficients

$$\frac{1}{h_u^l}\int_{u_l}^{u_{l+1}} \rho_{u_l}^{l+1}(u)du = 0,$$

$$\frac{1}{h_u^{l+1}}\int_{u_{l+1}}^{u_{l+2}} \rho_{u_l}^{l+1}(u)du = 1,$$

$$\frac{1}{h_u^{l+2}}\int_{u_{l+2}}^{u_{l+3}} \rho_{u_l}^{l+1}(u)du = 0,$$

$$\frac{1}{h_u^{l}}\int_{u_l}^{u_{l+1}} \rho_{u_l}^{l+2}(u)du = 0,$$

$$\frac{1}{h_u^{l+1}}\int_{u_{l+1}}^{u_{l+2}} \rho_{u_l}^{l+2}(u)du = 0,$$

$$\frac{1}{h_u^{l+2}}\int_{u_{l+2}}^{u_{l+3}}\rho_{u_l}^{l+2}(u)du = 1.$$

Substituting Eqs. (A.7a) and (A.7b) into above constraints and performing necessary integration give the quadratic coefficients

$$a_{u_l}^{+} = -\frac{h\left[h(h+4h_p+2h_{pp})+3h_p(h_p+h_{pp})+{h_{pp}}^2\right]}{(h+h_p+h_{pp})(h+h_p)(h_p+h_{pp})},$$

$$b_{u_l}^{+} = \frac{2h\left[h(2h+6h_p+3h_{pp})+3h_p(h_p+h_{pp})+{h_{pp}}^2\right]}{(h+h_p+h_{pp})(h+h_p)(h_p+h_{pp})},$$

$$c_{u_l}^{+} = -\frac{3h^2(h+2h_p+h_{pp})}{(h+h_p+h_{pp})(h+h_p)(h_p+h_{pp})},$$

$$a_{u_l}^{++} = \frac{h(h+h_p)}{(h+h_p+h_{pp})(h_p+h_{pp})},$$

$$b_{u_l}^{++} = -\frac{2h(2h+h_p)}{(h+h_p+h_{pp})(h_p+h_{pp})},$$

$$c_{u_l}^{++} = \frac{3h^2}{(h+h_p+h_{pp})(h_p+h_{pp})},$$

where

$$h = h_u^l,$$
$$h_p = h_u^{l+1},$$
$$h_{pp} = h_u^{l+2}.$$

The transverse leakage coefficients are functions only of the reactor geometry.

A.3 RHS-Biased Quadratic Transverse Leakage Approximation

Similarly, the transverse leakage in the u-direction in node (l,m,n), which is on the Right-Hand-Side (LHS) reactor surface is given by

$$S_{gu}^{mn}(u) = \bar{S}_{gu}^{lmn} + \left(\bar{S}_{gu}^{l-1,mn} - \bar{S}_{gu}^{lmn}\right)\rho_{u_l}^{l-1}(u) + \left(\bar{S}_{gu}^{l-2,mn} - \bar{S}_{gu}^{lmn}\right)\rho_{u_l}^{l-2}(u), \qquad \text{(A.9)}$$

where

$$\rho_{u_l}^{l-1}(u) = a_{u_l}^{-} + b_{u_l}^{-}\left(\frac{u-u_l}{h_u^l}\right) + c_{u_l}^{-}\left(\frac{u-u_l}{h_u^l}\right)^2, \qquad \text{(A.10a)}$$

$$\rho_{u_l}^{l-2}(u) = a_{u_l}^{--} + b_{u_l}^{--}\left(\frac{u-u_l}{h_u^l}\right) + c_{u_l}^{--}\left(\frac{u-u_l}{h_u^l}\right)^2. \qquad \text{(A.10b)}$$

Substituting the transverse leakage approximation, Eq. (A.9), into Eq. (A.1) and performing the required integration gives the following equations for the transverse leakage moments

$$S_{gu1}^{lmn} = \frac{1}{12}\left[(b_{u_l}^{-} + c_{u_l}^{-})\bar{S}_{gu}^{l-1,mn} - (b_{u_l}^{-} + b_{u_l}^{--} + c_{u_l}^{-} + c_{u_l}^{--})\bar{S}_{gu}^{lmn} + (b_{u_l}^{--} + c_{u_l}^{--})\bar{S}_{gu}^{l-2,mn}\right], \qquad \text{(A.11a)}$$

$$S_{gu2}^{lmn} = \frac{1}{60}\left[c_{u_l}^{-}\bar{S}_{gu}^{l-1,mn} - (c_{u_l}^{-} + c_{u_l}^{--})\bar{S}_{gu}^{lmn} + c_{u_l}^{--}\bar{S}_{gu}^{l-2,mn}\right]. \qquad \text{(A.11b)}$$

The quadratic polynomial coefficients are obtained by requiring the transverse leakage approximation, Eq. (A.9), to preserve the average transverse leakage in each of three nodes (l,m,n), (l-1,m,n) and (l-2,m,n). This results in the following constrains on the quadratic polynomial coefficients

$$\frac{1}{h_u^l}\int_{u_l}^{u_{l+1}} \rho_{u_l}^{l-1}(u)du = 0,$$
$$\frac{1}{h_u^{l-1}}\int_{u_{l-1}}^{u_l} \rho_{u_l}^{l-1}(u)du = 1,$$
$$\frac{1}{h_u^{l-2}}\int_{u_{l-2}}^{u_{l-1}} \rho_{u_l}^{l-1}(u)du = 0,$$
$$\frac{1}{h_u^{l}}\int_{u_l}^{u_{l+1}} \rho_{u_l}^{l-2}(u)du = 0,$$
$$\frac{1}{h_u^{l-1}}\int_{u_{l-1}}^{u_l} \rho_{u_l}^{l-2}(u)du = 0,$$
$$\frac{1}{h_u^{l-2}}\int_{u_{l-2}}^{u_{l-1}} \rho_{u_l}^{l-2}(u)du = 1.$$

Substituting Eqs. (A.10a) and (A.10b) into above constraints and performing necessary integration give the quadratic coefficients

$$a_{u_l}^{-} = \frac{h\left[h_{mm}(h_{mm}+3h_m+h)+h_m(3h_m+2h)\right]}{(h_{mm}+h_m+h)(h_m+h)(h_{mm}+h_m)},$$
$$b_{u_l}^{-} = -\frac{2h\left[h_{mm}(h_{mm}+3h_m)+3h_m{}^2-h^2\right]}{(h_{mm}+h_m+h)(h_m+h)(h_{mm}+h_m)},$$
$$c_{u_l}^{-} = -\frac{3h^2(h_{mm}+2h_m+h)}{(h_{mm}+h_m+h)(h_m+h)(h_{mm}+h_m)},$$

$$a_{u_l}^{--} = -\frac{hh_{mm}}{(h_{mm}+h_m+h)(h_{mm}+h_m)},$$
$$b_{u_l}^{--} = \frac{2h(h_m-h)}{(h_{mm}+h_m+h)(h_{mm}+h_m)},$$
$$c_{u_l}^{--} = \frac{3h^2}{(h_{mm}+h_m+h)(h_{mm}+h_m)}.$$

where

$$h_{mm} = h_u^{l-2},$$
$$h_m = h_u^{l-1},$$
$$h = h_u^l.$$

The transverse leakage coefficients are functions only of the reactor geometry.

A.4 Flat Transverse Leakage Approximation

In the flat transverse leakage approximation, the transverse leakage in the u-direction is assumed to be constant and equal to the node-averaged u-direction transverse leakage

$$S_{gu}^{mn} = \bar{S}_{gu}^{lmn}. \tag{A.12}$$

Substituting the flat transverse leakage approximation into Eq. (A.1) and performing the required integration reveal that for this approximation the transverse leakage moments are zero

$$S_{gup}^{lmn} = 0, \qquad p = 1,2. \tag{A.13}$$

APPENDIX B

NUMERICAL STUDY OF THERMAL HYDRAULIC MODELS

This appendix presents a numerical study of two thermal hydraulic difference approaches, namely an Implicit Donor Cell (IDC) and an Implicit WIGL model. This numerical study is intended to identify unusual charateristics, if any, of the WIGL model. If we neglect boiling and turbulence effects and also assume that there is no heat transfer, the one-dimensional energy balance equation can be written as

$$\frac{\partial H}{\partial t} + u\frac{\partial H}{\partial z} = 0, \tag{B.1}$$

where H and u are enthalpy and velocity of the coolant, respectively. The difference between IDC and WIGL models lies in the space-time discretization. The discretization schemes used for IDC and WIGL models are given in Figures B.1 and B.2, respectively.

The space-time discretization of Eq. (B.1), assuming a constant node spacing and step size, using the IDC model results in the following finite-difference equation

$$\frac{H_k^{n+1} - H_k^n}{\Delta t} + u\frac{H_k^{n+1} - H_{k-1}^{n+1}}{\Delta z} = 0, \tag{B.2}$$

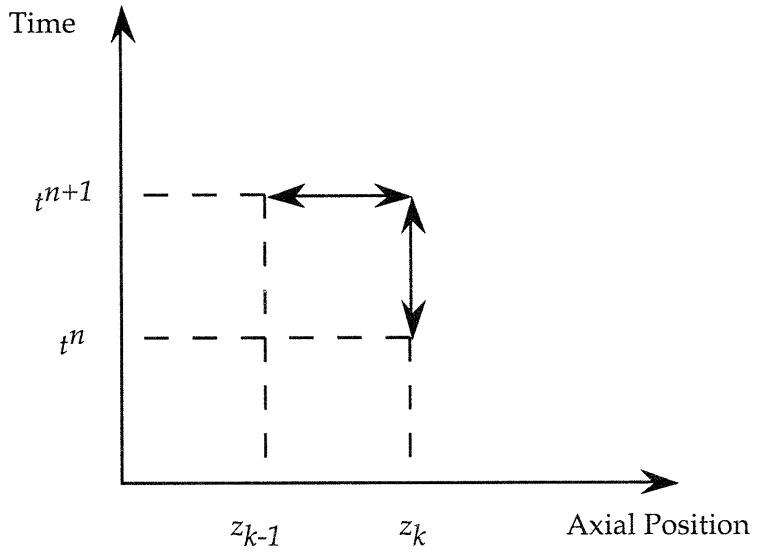

Figure B.1: Space-time discretization used for IDC model.

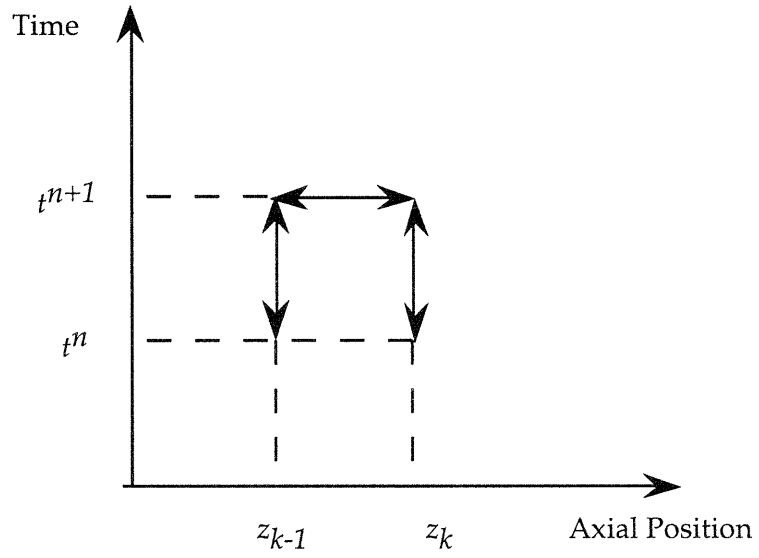

Figure B.2: Space-time discretization used for WIGL model.

where H_k^n represent the coolant enthalpy at axial position k and time step n. Rearranging Eq. (B.2) leads to

$$H_k^{n+1} = \frac{rH_{k-1}^{n+1} + H_k^n}{1+r}, \qquad r \equiv \frac{u\Delta t}{\Delta z}. \tag{B.3}$$

Similarly, the space-time discretization of Eq. (B.1), assuming a constant node spacing and time step size, using the Implicit WIGL model results in the following finite-difference equation

$$\frac{1}{2}\left(\frac{H_k^{n+1} - H_k^n}{\Delta t}\right) + \frac{1}{2}\left(\frac{H_{k-1}^{n+1} - H_{k-1}^n}{\Delta t}\right) + u\frac{H_k^{n+1} - H_{k-1}^{n+1}}{\Delta z} = 0. \tag{B.4}$$

Rearranging Eq. (B.4) gives

$$H_k^{n+1} = \frac{(2r-1)}{(2r+1)}H_{k-1}^{n+1} + \frac{H_k^n + H_{k-1}^n}{2r+1}, \qquad r \equiv \frac{u\Delta t}{\Delta z}. \tag{B.5}$$

Eqs. (B.3) and (B.5) along with the following expression of the node-averaged enthalpy

$$\overline{H}_k = \frac{1}{2}(H_k + H_{k+1}), \tag{B.6}$$

are applied to a very simple two-node problem with several different values of r. Figure B.3 shows the schematic diagram of the two-node problem considered to compare the numerical properties of the IDC and the Implicit WIGL models. The transient involves a step change in the coolant enthalpy from $H_{inlet} = 0$ to $H_{inlet} = 1$ at time $t = 0$. Figures B.4 through B.7 show the average enthalpy of node 2 versus time steps. We are interested mainly in the average enthalpy because the cross section feedback model uses the average temperature of the coolant in a node.

Both the IDC and the Implicit WIGL models converge to the true solution and there exists hardly any difference between the two models for $r > 0.5$. If anything, the Implicit WIGL model converges faster to the true solution than the IDC model. For $r =$ 0.1, there exists a phase mismatch for the Implicit WIGL model (the node-averaged enthalpy decreases when it should increase), but it is difficult to say even in this situation that the IDC model approximates the true solution better than the Implicit WIGL model. Furthermore, this phase mismatch is rarely encountered in reactor analysis because for most cases considered, the values of r are usually larger than 1.

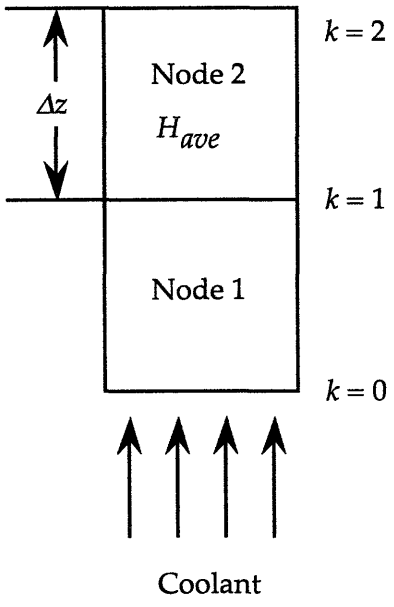

Figure B.3: Two-node problem used to test thermal hydraulic models.

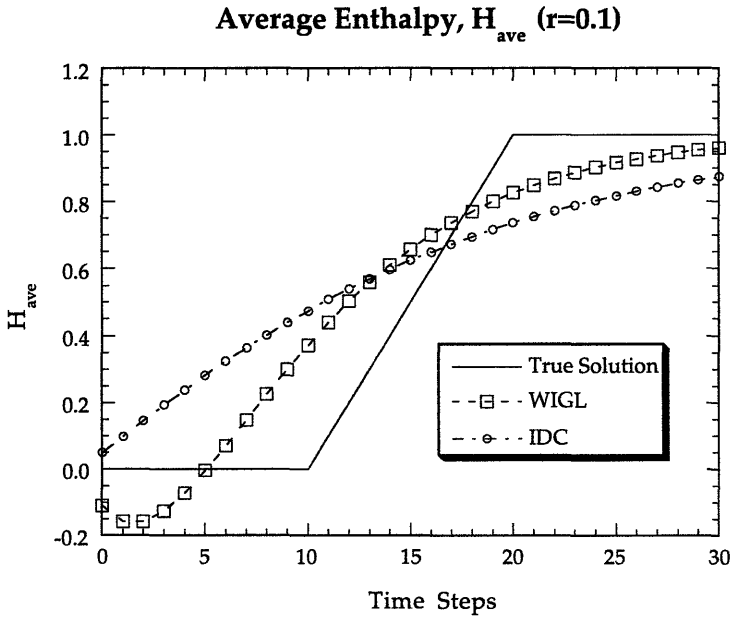

Figure B.4: Average enthalpy vs. time steps for $r = 0.1$.

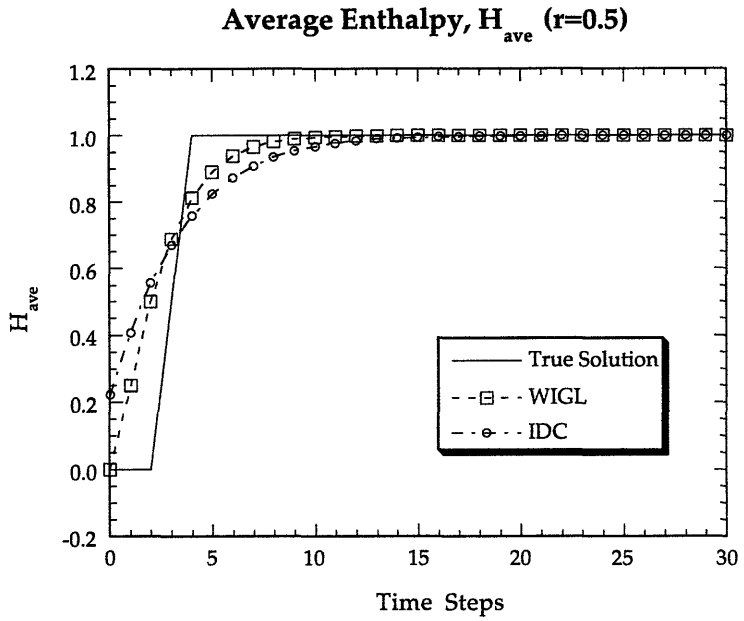

Figure B.5: Average enthalpy vs. time steps for $r = 0.5$.

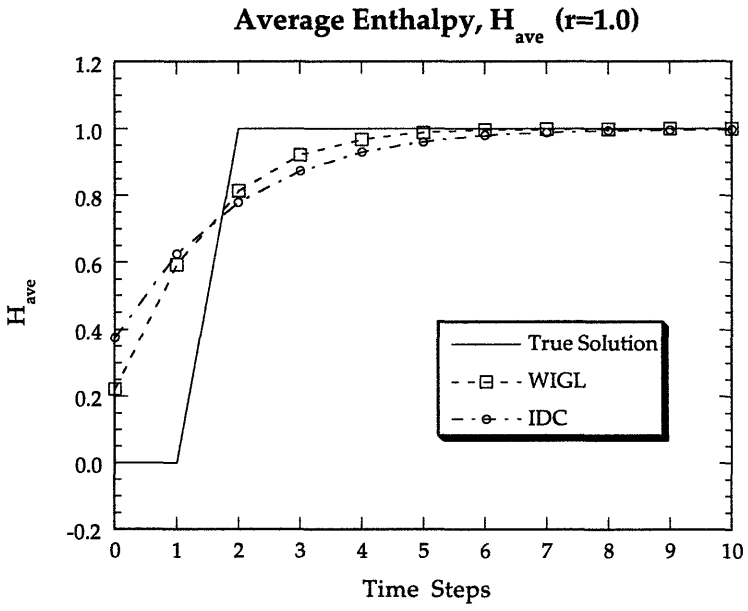

Figure B.6: Average enthalpy vs. time steps for $r = 1.0$

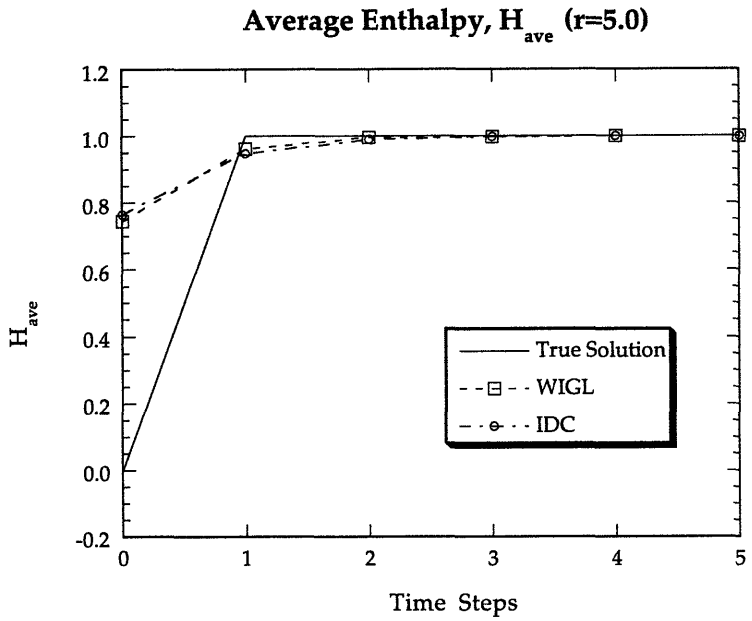

Figure B.7: Average enthalpy vs. time steps for $r = 5.0$.

The results presented in this appendix show that the WIGL model exhibits no unusual behavior compared with the donor cell model. For all practical purposes, both the models lead to similar results. For comparison purpose, however, the WIGL model was incorporated in DISCOVER.

APPENDIX C

PROBLEM SPECIFICATIONS

C.1 The LMW LWR Transient Problem

Geometry:

Quadrant of Reactor Horizontal Section

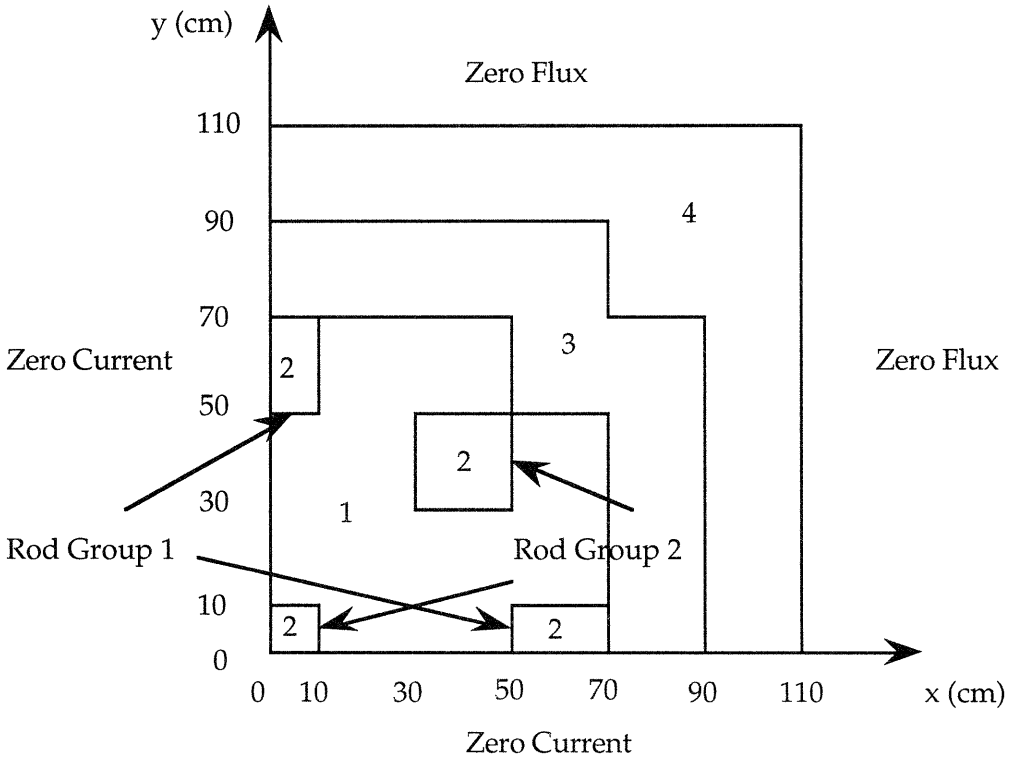

Reactor Vertical Section

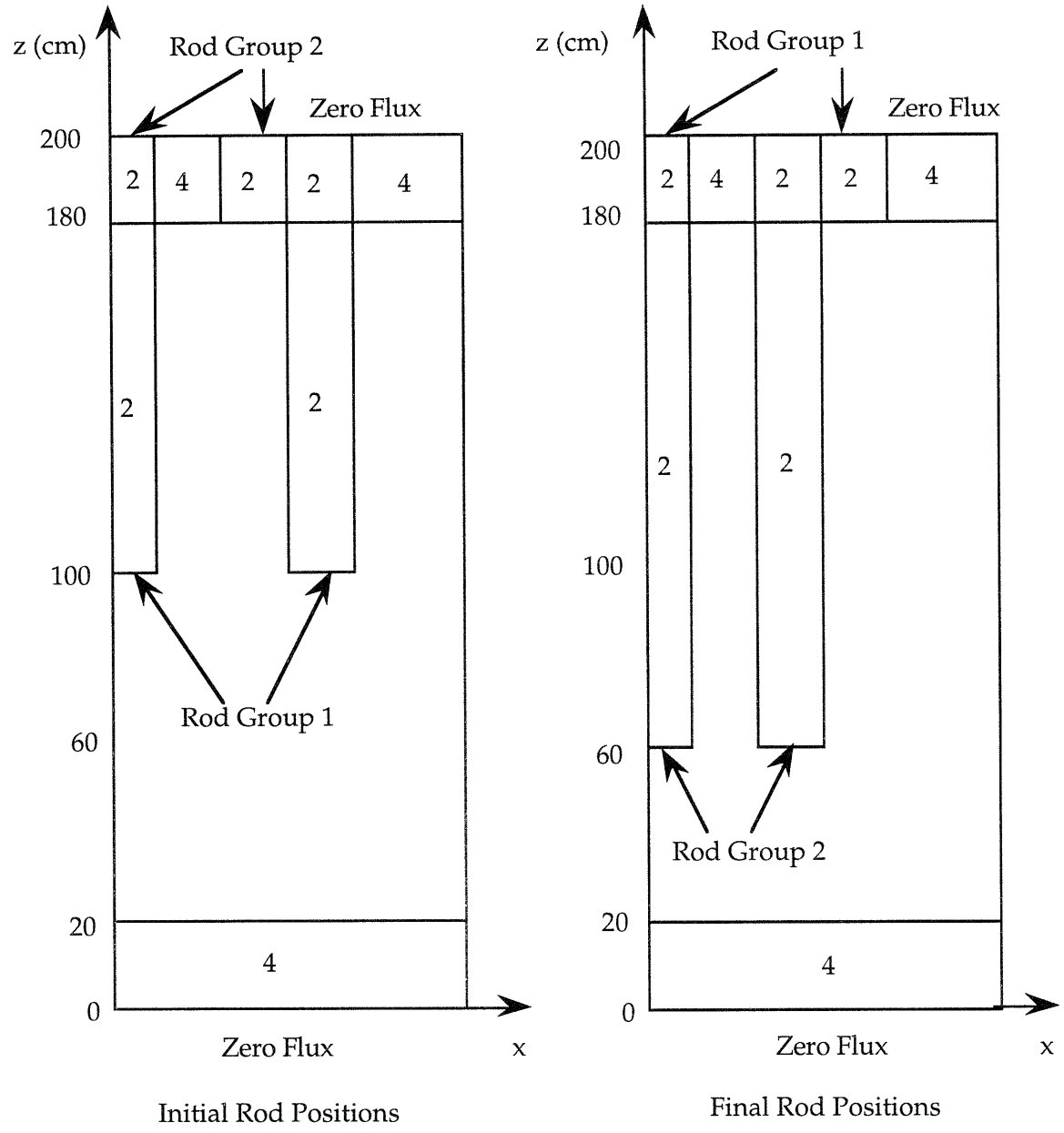

Material Properties:

Composition	Group, g	D_g (cm)	Σ_{ag} (cm^{-1})	$\upsilon\Sigma_{fg}$ (cm^{-1})	Σ_{21} (cm^{-1})
1	1	1.423913	0.01040206	0.006477691	0.0175555
	2	0.356306	0.08766217	0.1127328	
2	1	1.423913	0.01095206	0.006477691	0.0175555
	2	0.356306	0.08766217	0.1127328	
3	1	1.425611	0.01099263	0.007503284	0.01717768
	2	0.350574	0.09925634	0.1378004	
4	1	1.634227	0.002660573	0.0	0.02759693
	2	0.264002	0.04936351	0.0	

χ_1 = 1.0
χ_2 = 0.0
υ = 2.5
v_1 = 2.25 x 10^7 cm/s
v_2 = 2.5 x 10^5 cm/s

Delayed Neutron Data:

Family, d	β_d	λ_d (s^{-1})
1	0.000247	0.0127
2	0.0013845	0.0317
3	0.001222	0.115
4	0.0026455	0.311
5	0.000832	1.40
6	0.000169	3.87

χ_{d1} = 1.0
χ_{d2} = 0.0, d = 1,2, ..., 6

Energy Conversion Factor: 3.204 x 10^{-11} J/fission

Perturbation:

Control Rod Group 1 removed at 3.0 cm/s, $0 \le t \le 26.666$ s
Control Rod Group 2 inserted at 3.0 cm/s, $7.5 \le t \le 47.5$ s

WIGL Thermal Hydraulic Parameters:

C_f = 2.46×10^6 ergs/g/K
C_c = 5.43×10^7 ergs/g/K
ρ_f = 10.3 g/cm^3
W_o = 2.2×10^6 g/s
h_o = 2.71×10^7 ergs/cm^2/s/K
A_H = 2.59 cm^{-1}
U = 2.2×10^6 ergs/cm^2/s/K
$V_c/(V_c+V_f)$ = 0.559
$\left(\frac{\partial \rho_c H}{\partial \bar{T}_c}\right)$ = 1.60×10^7 ergs/cm^3/K
Pressure = 1.53×10^7 Pa
Coolant Inlet Temperature = 533 K
Initial Power = 184.8 MW_{th} (Quarter Core)

Macroscopic Cross Section Derivatives:

Parameter, Σ	$\frac{\partial \Sigma}{\partial \rho_c}$	$\frac{\partial \Sigma}{\partial \bar{T}_c}$	$\frac{\partial \Sigma}{\partial \bar{T}_f}$
D_1^{-1}	+0.41	-8.0×10^{-5}	-6.6×10^{-6}
D_2^{-1}	+2.7	-1.3×10^{-3}	-2.6×10^{-6}
Σ_{c1}	$+2.83 \times 10^{-3}$	$+3.0 \times 10^{-6}$	$+3.3 \times 10^{-7}$
Σ_{c2}	$+1.4 \times 10^{-2}$	-8.2×10^{-6}	-3.7×10^{-7}
$\upsilon\Sigma_{f1}$	+0.0	+0.0	+0.0
$\upsilon\Sigma_{f2}$*	$+4.132 \times 10^{-2}$	-2.075×10^{-5}	-2.5×10^{-6}
Σ_{f1}	+0.0	+0.0	+0.0
Σ_{f2}*	$+1.7 \times 10^{-2}$	-8.3×10^{-6}	-1.0×10^{-6}
Σ_{21}	$+2.4 \times 10^{-2}$	-1.5×10^{-6}	$+8.5 \times 10^{-8}$

* Zero for reflector material (composition #4)

Reference Coolant Density = 0.7961 g/cm3
Reference Coolant Temperature = 533 K
Reference Fuel Temperature = 533 K

C.2 The PWR Transient Problems

Geometry:

Quadrant of the Reactor, Assembly dimensions 21.591 cm x 21.591 cm. In unrodded planes, composition #16 is replaced by composition #1.

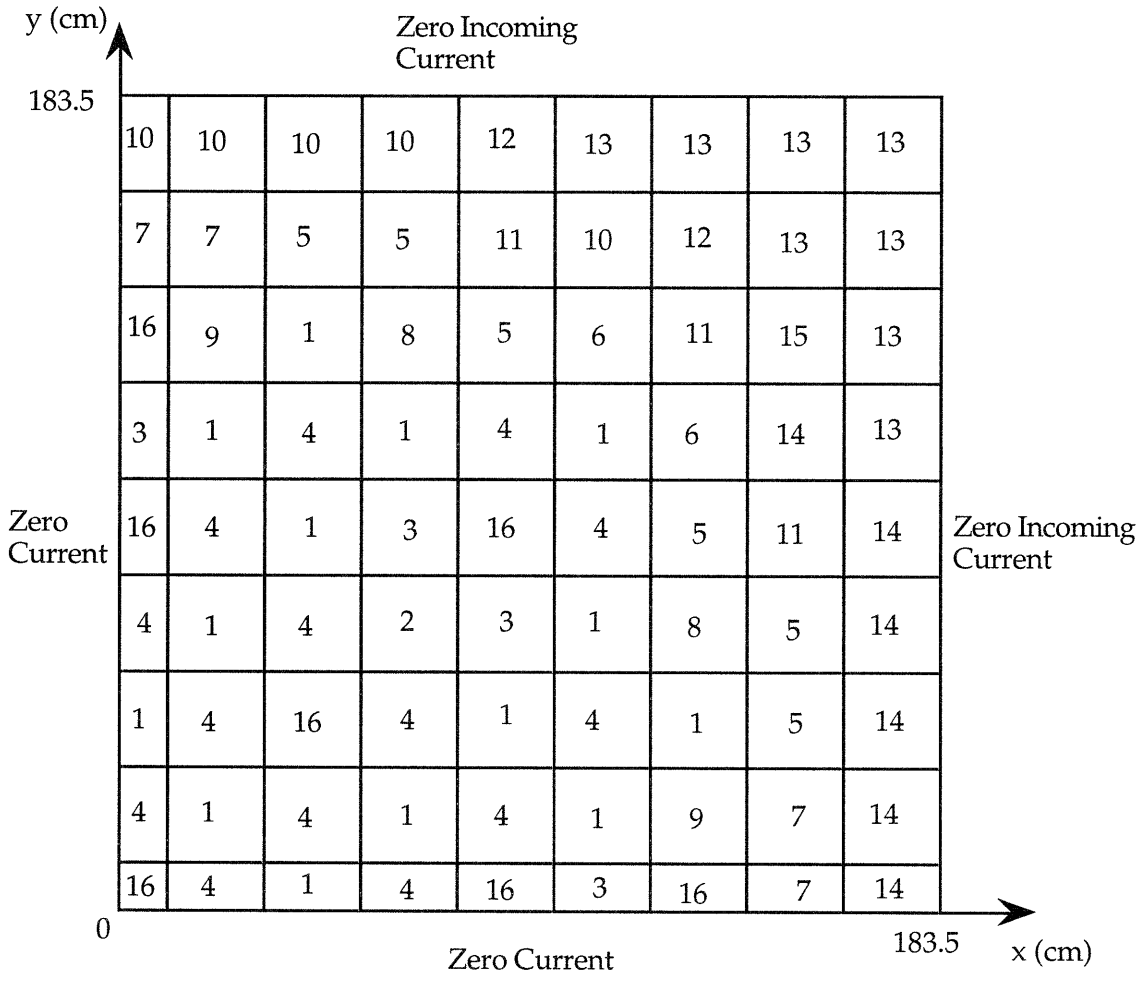

10	10	10	10	12	13	13	13	13
7	7	5	5	11	10	12	13	13
16	9	1	8	5	6	11	15	13
3	1	4	1	4	1	6	14	13
16	4	1	3	16	4	5	11	14
4	1	4	2	3	1	8	5	14
1	4	16	4	1	4	1	5	14
4	1	4	1	4	1	9	7	14
16	4	1	4	16	3	16	7	14

Control Rod Bank D & C Locations and Reactor Vertical Section

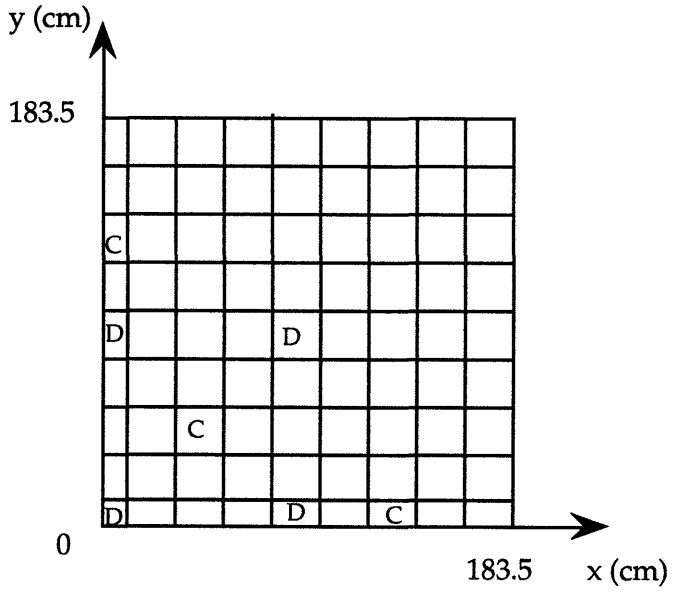

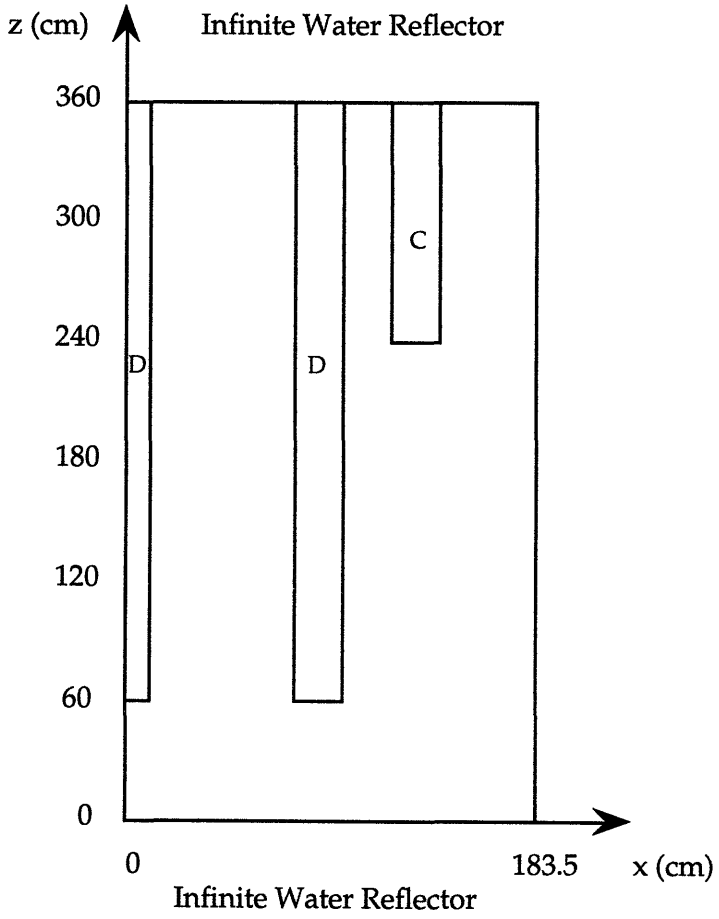

Material Properties:

Composition	Group, g	D_g (cm)	Σ_{ag} (cm^{-1})	$\upsilon\Sigma_{fg}$ (cm^{-1})	Σ_{21} (cm^{-1})
1	1	1.3648	0.008887	0.005550	0.017245
	2	0.4826	0.130772	0.185823	
2	1	1.3603	0.009661	0.006267	0.015942
	2	0.4776	0.169403	0.229195	
3	1	1.3596	0.009957	0.006267	0.015398
	2	0.4798	0.181915	0.230258	
4	1	1.3592	0.10104	0.006269	0.015128
	2	0.4810	0.188426	0.230923	
5	1	1.3594	0.009509	0.006890	0.016386
	2	0.4673	0.169073	0.264760	
6	1	1.35898	0.0096925	0.0068905	0.0160495
	2	0.46853	0.1762888	0.2653975	
7	1	1.35890	0.009730	0.006890	0.015981
	2	0.46875	0.177654	0.265512	
8	1	1.3576	0.010252	0.006892	0.015022
	2	0.4728	0.200287	0.267778	
9	1	1,3572	0.010399	0.006894	0.014752
	2	0.4740	0.206951	0.268552	
10, 14	1	1.4957	0.002683	0.0	0.022923
	2	0.3637	0.051595	0.0	
11	1	1.3933	0.003541	0.0	0.017943
	2	0.3659	0.068149	0.0	
12, 15	1	1.6701	0.001220	0.0	0.031408
	2	0.3621	0.039330	0.0	
13	1	1.7446	0.000596	0.0	0.035032
	2	0.3614	0.034208	0.0	
16	1	1.321964	0.013482	0.055670	0.015178
	2	0.486198	0.161003	0.194976	

$\chi_1 = 1.0, \quad \chi_2 = 0.0, \quad \upsilon = 2.5,$

$v_1 = 2.25 \times 10^7$ cm/s, $\quad v_2 = 2.5 \times 10^5$ cm/s.

Axial Albedo Boundary Conditions:

Γ_{11}	Γ_{12}	Γ_{21}	Γ_{22}
4.011	0.0	2.805	8.993

Delayed Neutron Data:

Family, d	β_d	λ_d (s^{-1})
1	0.000247	0.0127
2	0.0013845	0.0317
3	0.001222	0.115
4	0.0026455	0.311
5	0.000832	1.40
6	0.000169	3.87

$\chi_{d1} = 1.0$
$\chi_{d2} = 0.0, \quad d = 1,2, ..., 6$

Macroscopic Cross Section Derivatives:

Parameter, Σ	$\frac{\partial \Sigma}{\partial \rho_c}$	$\frac{\partial \Sigma}{\partial \bar{T}_c}$	$\frac{\partial \Sigma}{\partial \bar{T}_f}$
D_1^{-1}	0	-8.0×10^{-5}	-6.6×10^{-6}
D_2^{-1}	0	-1.3×10^{-3}	-2.6×10^{-6}
Σ_{c1}	0	$+3.0 \times 10^{-6}$	$+3.3 \times 10^{-7}$
Σ_{c2}	0	-8.2×10^{-6}	-3.8×10^{-7}
$\upsilon\Sigma_{f1}$	0	+0.0	+0.0
$\upsilon\Sigma_{f2}$*	0	-2.075×10^{-5}	-2.5×10^{-6}
Σ_{f1}	0	+0.0	+0.0
Σ_{f2}*	0	-8.3×10^{-6}	-1.0×10^{-6}
Σ_{21}	0	-1.5×10^{-6}	-8.5×10^{-8}

* Zero for reflector material (composition #10 ~ 15)

Reference Coolant Density = 0.79755 g/cm3
Reference Coolant Temperature = 533 K
Reference Fuel Temperature = 533 K

WIGL Thermal Hydraulic Parameters:

C_f = 2.46 x 10^6 ergs/g/K

C_c = 5.43 x 10^7 ergs/g/K

ρ_f = 10.3 g/cm^3

W_o = 3.868 x 10^6 g/s

h_o = 3.293 x 10^7 ergs/cm^2/s/K

A_H = 3.097 cm^{-1}

U = 2.2 x 10^6 ergs/cm^2/s/K

$V_C/(V_C+V_f)$ = 0.542

$\left(\frac{\partial \rho_c H}{\partial \overline{T}_c}\right)$ = 1.60 x 10^7 ergs/cm^3/K

Pressure = 1.551 x 10^7 Pa

Coolant Inlet Temperature = 555 K

Initial Power = 166.9 MW_{th} (Quarter Core)

Transient #1: Rod Motion Transient Perturbation

Rod Bank C & D are removed at a velocity of 2 cm/s

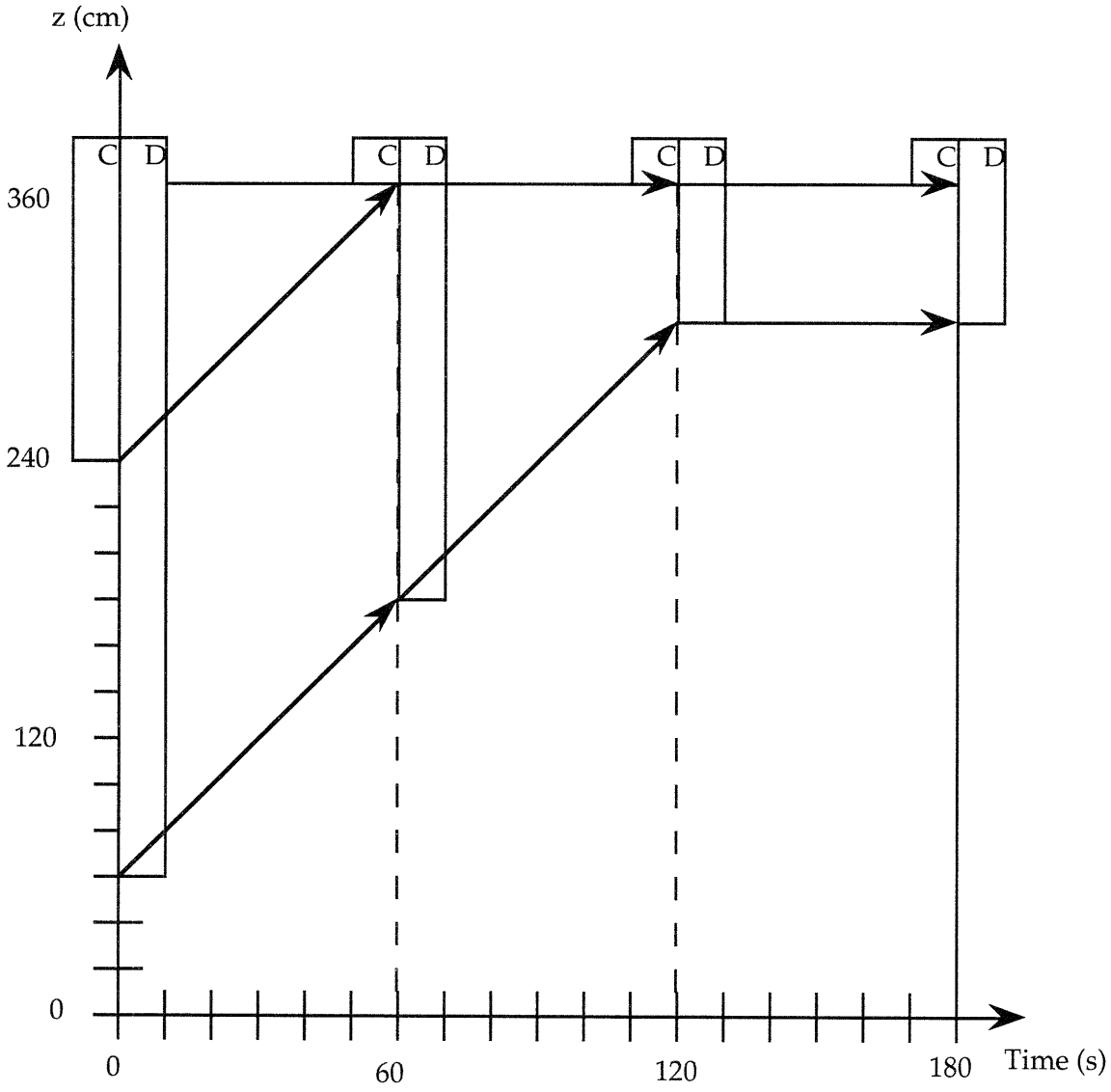

Transient #2: Coolant Inlet Temperature Perturbation

The coolant inlet temperature is varied according to

$$T_{inlet}(t) = T_{inlet}(0)\,exp(-t/\tau_1) + T_{inlet}(0)\left[1 - exp(-t/\tau_2)\right],$$

where

τ_1 = 2.0 s
τ_2 = 2.206 s.

Initial Power = 834.5 MW_{th} (Quarter Core)
All control rods are at completely withdrawn positions.